Mississippi State University
Scholars Junction

Theses and Dissertations | Theses and Dissertations

1-1-2011

Assessing the effects of toxic synthetic organic compounds on activated sludge communities

Kristopher Michael Lightsey

Follow this and additional works at: https://scholarsjunction.msstate.edu/td

Recommended Citation
Lightsey, Kristopher Michael, "Assessing the effects of toxic synthetic organic compounds on activated sludge communities" (2011). *Theses and Dissertations*. 754.
https://scholarsjunction.msstate.edu/td/754

This Dissertation - Open Access is brought to you for free and open access by the Theses and Dissertations at Scholars Junction. It has been accepted for inclusion in Theses and Dissertations by an authorized administrator of Scholars Junction. For more information, please contact scholcomm@msstate.libanswers.com.

www.manaraa.com

ASSESSING THE EFFECTS OF TOXIC SYNTHETIC ORGANIC COMPOUNDS ON ACTIVATED SLUDGE COMMUNITIES

By

Kristopher Michael Lightsey

A Dissertation
Submitted to the Faculty of
Mississippi State University
in Partial Fulfillment of the Requirements
for the Degree of Doctor of Philosophy
in Civil and Environmental Engineering
in the Department of Civil and Environmental Engineering

Mississippi State, Mississippi

December 2011

www.manaraa.com

ASSESSING THE EFFECTS OF TOXIC SYNTHETIC ORGANIC COMPOUNDS ON ACTIVATED SLUDGE COMMUNITIES

By

Kristopher Michael Lightsey

Approved:

Benjamin S. Magbanua, Jr. Associate Professor of Civil and Environmental Engineering (Dissertation Director)	Dennis D. Truax Professor of Civil and Environmental Engineering (Committee Member)
James L. Martin Professor of Civil and Environmental Engineering (Committee Member and Graduate Program Coordinator)	Hossein Toghiani Associate Professor of Chemical Engineering (Committee Member)
Sarah A. Rajala Dean of the James Worth Bagley College of Engineering	

www.manaraa.com

Name: Kristopher Michael Lightsey

Date of Degree: December 9, 2011

Institution: Mississippi State University

Major Field: Civil and Environmental Engineering

Major Advisor: Dr. Benjamin S. Magbanua, Jr.

Title of Study: ASSESSING THE EFFECTS OF TOXIC SYNTHETIC ORGANIC COMPOUNDS ON ACTIVATED SLUDGE COMMUNITIES

Pages in Study: 175

Candidate for Degree of Doctor of Philosophy

The recent technological advances in environmental monitoring coupled with the increasingly stringent effluent requirements being placed on waste treatment systems makes it vital to have a more complete understanding of how specific compounds in waste streams can impact wastewater treatment processes. Since activated sludge processes are recognized as one of the most often applied technologies in wastewater treatment, this study assesses the impacts of select toxic synthetic organic compounds (SOCs) on the activated sludge communities in two types of wastewater treatment reactors: a completely-mixed activated sludge reactor (CMAS) and a sequencing batch reactor (SBR). Commonly applied activated sludge monitoring parameters, such as solids analysis and substrate removal, are collected and correlated to the results of microscopic image analysis (IA) and direct gradient gel electrophoresis (DGGE) to

www.manaraa.com

monitor the response of the activated sludge communities to variations in operational conditions, including the incorporation of SOCs in the influent feed and varying the solids retention time.

The results of this research indicate that the response of the activated community is highly dependent on the reactor configuration. The CMAS settling performance was more strongly correlated to the shape parameters, and the SBR settling performance was more strongly correlated to the size parameters, which is qualitatively supported by particle settling theory when considering that SBR flocs were found to be larger than the CMAS flocs. The SBR began to exhibit larger floc sizes and had a higher sludge volume index with the incorporation of SOCs, while the CMAS flocs became more spherical after SOCs were incorporated and exhibited more discrete settling. The molecular analysis results revealed that the community structure within the activated sludge system was transient in response to environmental variations. Banding patterns indicated that samples were more similar to other samples taken from the same reactor under the same operational conditions. Thus, as operational conditions were varied, sample banding patterns would also change, indicating transitions in the genetic composition, and ultimately the dominant species present, in response to environmental changes.

www.manaraa.com

DEDICATION

This work is dedicated to my wonderful wife, Brandy, and my two precious boys, Karsen and Kooper. I would have never been able to get to this point without your continuous, unconditional love and support.

www.manaraa.com

ACKNOWLEDGEMENTS

The author would like to express his sincere gratitude to a number of people without whom this work could not have been completed. First and foremost, I would like to thank my primary advisor, Dr. Ben Magbanua, for his continuous vision and support of my efforts and for the numerous reviews and insights that he gave in regards to the work. I would also like to thank my committee members, Dr. Dennis Truax, Dr. James Martin and Dr. Hossein Toghiani, for their support of this work. I would also like to extend my sincere gratitude to Dr. Song Zhang and Peter Rush, from the Department of Computer Science and Engineering at Mississippi State University, for their contributions to the initial development of the image processing software. I would like to thank Mr. Bill Holmes for his help in developing the GC/MS procedures and for allowing the use of the equipment in the Mississippi State Chemical Laboratory. Finally, I would like to thank the many undergraduate workers for their valuable work in the day-to-day operations of this research study, including Chandler Pace, Sarah Duffy, Keith Ferguson, Will Dendinger, Mathew Horton, and Jennifer Sloan.

www.manaraa.com

TABLE OF CONTENTS

www.manaraa.com

www.manaraa.com

LIST OF TABLES

TABLE

www.manaraa.com

LIST OF FIGURES

FIGURE

www.manaraa.com

www.manaraa.com

www.manaraa.com

www.manaraa.com

CHAPTER I

INTRODUCTION

1.1 Motivation

Advancements in environmental monitoring and assessment technologies allow for the quantification of specific contaminants with increasing sensitivity and accuracy. Furthermore, the impacts of toxic synthetic organic compounds (SOCs) are becoming a high priority for regulatory agencies in terms of monitoring and control. For these reasons, environmental laws and permits are being mandated with limits on effluent concentrations set at very low quantities for specific organic constituents. Due to increasing detection capabilities and more stringent effluent standards, the demand arises for a more complete understanding of how these SOCs affect the microbial population dynamics and the capability of SOC removal within an activated sludge (AS) reactor.

For several decades, models have been developed and utilized to predict the degradation of oxygen-demanding materials and nutrient removal. However, these models currently do not accurately account for the inhibitory nature of toxic organic waste on the bioprocesses and degradation pathways in the AS system. The problem arises in that the models typically lump all degradable organic matter into the biochemical oxygen demand (BOD), while many of the SOCs are only degradable by portions of the population (Magbanua et al., 1994; Magbanua et al., 1998).

www.manaraa.com

Even in models that incorporate inhibitory parameters, such as the Andrews Model (1968), there will be discrepancies between predicted and measured values due to biodegradation of the SOCs by only a fraction of the biomass community that actually degrades target SOCs (Magbanua et al., 1998). A better understanding of the effects that certain SOCs have on the biological system can potentially provide an opportunity for more precise prediction of the biodegradation of these organic chemicals through the AS treatment process.

1.2 Research Goals and Questions

The main goals of this study are to utilize microscopic image analysis coupled with molecular biology techniques in order to assess the variations of the activated sludge community when it is subjected to toxic SOCs in the influent feed. The study will attempt to develop a more complete understanding of the effects that SOCs have on the microbial population in an AS system through answering the following:

- How does the genetic makeup of the microbial population change as influent SOC concentrations and reactor design parameters are varied? What are the impacts of these microbial variations on the process performance?
- How does the diversity of the population fluctuate with changing influent conditions and reactor regimes? What relationships can be developed between the varying diversity and the AS system performance?
- How do the variations in SOC concentrations and design parameters affect the floc size and floc size distribution in the AS system? How do these changes affect the overall treatment capabilities?

www.manaraa.com

- Can the resulting variations in microbial diversity and floc size and size distribution be quantitatively related? What insights can be obtained from the resulting variations in relation to bioprocess uncertainty?

1.3 Research Hypothesis

The overall diversity of the microbial community and the floc sizes and size distribution all play an important role in the AS system's ability to treat SOCs in wastewater. Through understanding the significance of these parameters, the uncertainty associated with SOC treatment could be minimized and more economical treatment strategies could be implemented.

www.manaraa.com

CHAPTER II

LITERATURE REVIEW

2.1 Synthetic Organic Compounds

Synthetic organic compounds (SOCs) are becoming more prevalent in industrial waste streams, especially those emanating from the chemical manufacturing and pharmaceutical industries. Regulatory agencies, such as the Environmental Protection Agency (USEPA), recognize the potential hazards of these pollutants and have begun limiting the concentrations of specific chemicals in waste streams. The USEPA (1979a) has developed a priority pollutant list of 129 contaminants, of which 115 are SOCs. Table 2.1 provides a list of the synthetic organic priority pollutants, as defined by the USEPA, and recognized as a significant threat to public health and the environment.

Some SOCs have been detected in surface waters and WWTP effluents in the $ng \cdot L^{-1}$ to $\mu g \cdot L^{-1}$ range (Kümmerer, 2004). Because the techniques for quantifying SOCs have become accurate at such low concentrations, regulations are being imposed on the levels of specific SOCs in waste streams that must be met. Although they are often found at very low concentrations, many SOCs impose a significant risk to the environment and to public health. SOCs refer to any organic compound that is industrially synthesized, and as such they are an extremely diverse group of chemicals. Figure 2.1 presents a general classification according to volatility and polarity (Crittenden et al., 2005).

www.manaraa.com

Table 2.1

Synthetic organic priority pollutants.

Acenaphthene	1,2-trans-Dichloroethylene	2,4-Dinitrophenol	Vinyl Chloride
Acrolein	2,4-Dichlorophenol	4,6-Dinitro-o-cresol	Aldrin
Acrylonitrile	1,2-Dichloropropane	N-Nitrosodimethylamine	Dieldrin
Benzene	1,3-Dichloropropene (trans)	N-Nitrosodiphenylamine	Chlordane
Benzidine	2,4-Dimethylphenol	N-Nitrosodi-n-propyl-amine	4,4-DDT
Carbon Tetrachloride	2,4-Dinitrotoluene	Pentachlorophenol	4,4-DDE
Chlorobenzene	2,6-Dinitrotoluene	Phenol	4,4-DDD
1,2,4-Trichlorobenzene	1,2-Diphenylhydrazine	Bis (2-ethylhexyl) Phthalate	alpha-Endosulfan
Hexachlorobenzene	Ethylbenzene	Butyl benzyl phthalate	beta-Endosulfan
1,2-Dichloroethane	Fluoranthene	Di-n-butyl phthalate	Endosulfan sulfate
1,1,1-Trichloroethane	4-Chlorophenyl phenyl ether	Di-n-octyl phthalate	Endrin
Hexachloroethane	4-Bromophenyl phenyl ether	Diethyl phthalate	Endrin aldehyde
1,1-Dichloroethane	Bis (2-chloroisopropyl) ether	Dimethyl phthalate	Heptachlor
1,1,2-Trichloroethane	Bis (2-chloroethoxy) methane	Benzo[a]anthracene	Heptachlor epoxide
1,1,2,2-Tetrachloroethane	Methylene Chloride	Benzo[a]pyrene	alpha-BHC
Chloroethane	Methyl chloride	3,4-Benzofluoranthene	beta-BHC
Bis(chloromethyl) ether	Methyl Bromide	Benzo[k]fluoranthene	gamma-BHC
Bis(2-chloroethyl) ether	Bromoform	Chrysene	delta-BHC
2-Chloroethyl vinyl ether	Dichlorobromomethane	Acenaphthylene	PCB-1242
2-Chloronaphthalene	Trichlorofluoromethane	Anthracene	PCB-1254
2,4,6-Trichlorophenol	Dichlorodifluoromethane	Benzo[g,h,i]perylene	PCB-1221
p-Chloro-m-cresol	Chlorodibromomethane	Fluorene	PCB-1232
Chloroform	Hexachlorobutadiene	Phenanthrene	PCB-1248
2-Chlorophenol	Hexachlorocyclopentadiene	Dibenzo[a,h]anthracene	PCB-1260
1,2-Dichlorobenzene	Isophorone	Indeno[1,2,3-c,d]pyrene	PCB-1016
1,3-Dichlorobenzene	Naphthalene	Pyrene	Toxaphene
1,4-Dichlorobenzene	Nitrobenzene	Tetrachloroethylene	Asbestos
3,3-Dichlorobenzidine	2-Nitrophenol	Toluene	2,3,7,8- (TCDD)
1,1-Dichloroethylene	4-Nitrophenol	Trichloroethylene	

Source: USEPA, 1979a.

www.manaraa.com

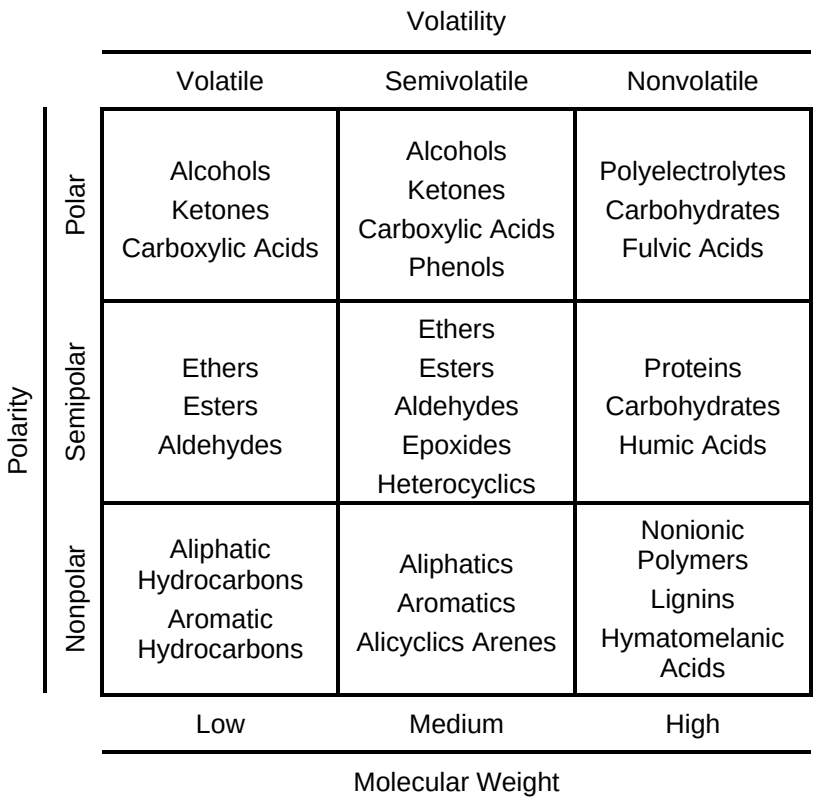

Figure 2.1 Schematic classification of SOCs found in water (Adapted from Crittenden et al., 2005).

2.1.1 Important Physicochemical Properties of SOCs

In order to accurately assess the fate of specific organic chemicals, whether within a treatment process or in the transfer phenomena in the environment, several important properties must be determined and understood. When studying SOCs, problems arise in that the list of priority pollutants is highly diverse, and each specific chemical will likely have unique properties associated with its transport and degradation (Kümmerer, 2004). The problem is compounded further because these chemicals are designed with inherent activities. This is especially true of pesticides which are specifically developed to be toxic to the target organisms (Schnoor, 1992) and in the case of pharmaceuticals which

www.manaraa.com

are designed for therapeutic purposes such as antibiotics, analgesics, and anti-inflammatory agents (Kümmerer, 2004). Since more stringent regulations are being imposed on specific chemicals, it is important to determine which properties of a given contaminant will have a significant impact on the ultimate environmental fate of that chemical. Equilibrium distribution of chemicals into different environmental compartments is one of the common methods used in determining expected behavior patterns of specific chemicals in the environment (Bloemen & Burn, 1993). According to Klimiuk and Kulikowska (2004), the removal efficiency of individual SOCs as it relates to AS treatment is highly diverse and mainly depends on the physicochemical properties of the compounds, especially their solubility, vapor pressure, partitioning between phases and polarity.

2.1.1.1 Henry's Law Coefficient

Many SOCs express high volatility which allow for the chemicals to be directly stripped into the atmosphere and escape further treatment. Therefore, it is important to determine the partitioning between the air-water phases for a given chemical that is undergoing treatment. Henry's law constant is a physical property of a specific chemical that characterizes its partitioning in an air-water binary system at equilibrium (Bloemen & Burn, 1993). Henry's law states that under equilibrium conditions, the partial pressure of a gas above a liquid is proportional to the chemical concentration in the liquid:

$$P_g = H_{La} C_L \tag{2-1}$$

where, P_g = partial pressure of the gas [atm]; C_L = concentration of chemical in liquid [$mol \cdot L^{-3}$]; H_{La} = Henry's constant [$(atm \cdot L^3) \cdot mol^{-1}$] (LaGrega et al., 2001). Henry's law

www.manaraa.com

constants are necessary in order to predict how organic chemicals will behave in the environment and to assess the environmental risks caused by the chemicals. Generally, higher Henry's law constants suggest that chemicals are likely to move into the gas phase while lower constants suggest they will remain in solution (Bloemen & Burn, 1993).

2.1.1.2 Octanol-Water Distribution Coefficient

The octanol-water distribution coefficient is another phase partitioning coefficient that is important in monitoring the transport of chemicals in the environment. It represents the equilibrium concentration ratio of a specific chemical between *n*-octanol and water as given by:

$$K_{ow} = \frac{C_o}{C_w} \tag{2-2}$$

where, C_o = concentration of chemical in *n*-octanol; C_w = concentration of chemical in water; K_{ow} = dimensionless octanol-water distribution coefficient (Bloemen & Burn, 1993). This ratio gives an indication of a specific chemical's accumulation behavior and also is used to estimate other parameters, such as solubility, adsorption coefficients, and bioconcentration factors (Kümmerer, 2004). Kümmerer further suggests that the octanol-water distribution coefficient gives an indication of an organic chemical's tendency to partition into lipids, sorb to particulates or biomass, and distribute among the different environmental compartments. Typically, chemicals with higher K_{ow} values will be more hydrophobic and sorb to organic particulates, lipids, and soil particles, while lower K_{ow} values indicate that a chemical will be more hydrophilic and will generally remain in the aqueous phase (LaGrega et al., 2001).

www.manaraa.com

2.1.1.3 Sludge Sorption-Desorption Coefficient

The sludge sorption-desorption coefficient is similar to the octanol-water coefficient in relating the equilibrium concentration between liquid phase and solid phase, but in this case the solid phase is biomass or sludge. This is an important factor in discussing SOCs because many organic chemicals are treated by biological wastewater treatment plants (Kümmerer. 2004). The sorption process can be a controlling factor in the removal of organic pollutants through biological wastewater treatment, and may influence the biodegradation rates within the treatment process (Carballa et al., 2008). Simply stated, the biomass sorption coefficient ($K_{biomass}$) is given by:

$$K_{biomass} = \frac{C_{biomass}}{C_w} \qquad (2\text{-}3)$$

where, $C_{biomass}$ = concentration of chemical sorbed to the biomass. However, Kümmerer (2004) suggests that although this coefficient can be approximated through studies with typical biomass concentrations, it more often estimated from the octanol-water coefficient or the organic carbon-based coefficient K_{oc}. Carballa et al. (2008) found that K_{ow} and K_{oc} based approaches work sufficiently for simple hydrophobic interactions, but they are significantly inaccurate when used to describe polar and ionic compounds. Due to the inherent diversity among the physicochemical properties of SOCs, it may be necessary to determine the specific chemicals being treated and conduct appropriate studies to determine a better estimate of the ratio being sorbed to biomass. The sorbtion dynamics have also been found to be greatly influenced by environmental conditions, such as temperature, pH, particle size distribution, salinity, and solids concentration (LaGrega et al., 2001).

www.manaraa.com

2.1.2 Biological Treatment of SOCs

Large amounts of SOCs are typically recalcitrant to biodegradation, but specific reactor regimes and operational strategies are actually capable of reliably removing many of the SOC contaminants (Hu et al., 2005). Advanced oxidation processes (AOPs), such as the Fenton oxidation, have been the subject of numerous studies on the degradation and mineralization of recalcitrant organics. Also, more advanced techniques including the photofenton process under UV-vis irradiation have been used to treat SOC-containing waste (Jeong & Yoon, 2004). Biological treatment, however, is more efficient in many cases and results in more economical, onsite treatment, as opposed to physical treatment which utilizes separate evaporation and filtration steps or to chemical treatment which often demands strong and expensive oxidizers (Håkansson et al., 2005). Other researchers indicate that, even when using biological treatment, mixed cultures are often required to degrade toxic materials, and independent degradation pathways may require reactor conditions that are not desirable to other organisms in the culture, often resulting in arranging sequential bioreactors (Campos et al., 2003; Perron & Welander, 2004). The principal removal mechanisms of SOCs in typical biological treatment systems include sorption onto the AS sludge, volatilization, stripping due to forced air injection, and biodegradation (Klimiuk & Kulikowska, 2004). Although biological treatment is recognized by USEPA as the most effective treatment option for SOC-containing waste, the modeling approaches currently implemented have significant uncertainty associated with them (Magbanua et al., 2004). In order to assure compliance, however, most treatment processes are engineered with larger, less economical safety factors to account for the process uncertainty associated with SOC removal.

www.manaraa.com

2.2 The Activated Sludge Process

The activated sludge process is a biological wastewater treatment process that is generally comprised of three basic components (Metcalf & Eddy, 2003):

- An aeration basin for suspending the microorganisms and supplying oxygen
- A separation phase in which the solids and liquids are separated
- A recycle system to maintain a desired activated sludge population

Figure 2.2 provides a simple schematic for the typical AS process using different types of reactors. Within the AS treatment process, the active microorganisms that are used to treat the wastewater are commonly referred to as activated sludge flocs, due to their inherent tendencies to bind together through extracellular networks. Dissolved waste contaminants and other constituents that cannot be removed by physical means must be biologically converted so that they can be removed from the waste stream. It has been estimated that roughly two-thirds of the influent organic substrate is incorporated into cellular material and one-third is utilized as energy for cell synthesis and maintenance (Bisogni et al., 1971).

www.manaraa.com

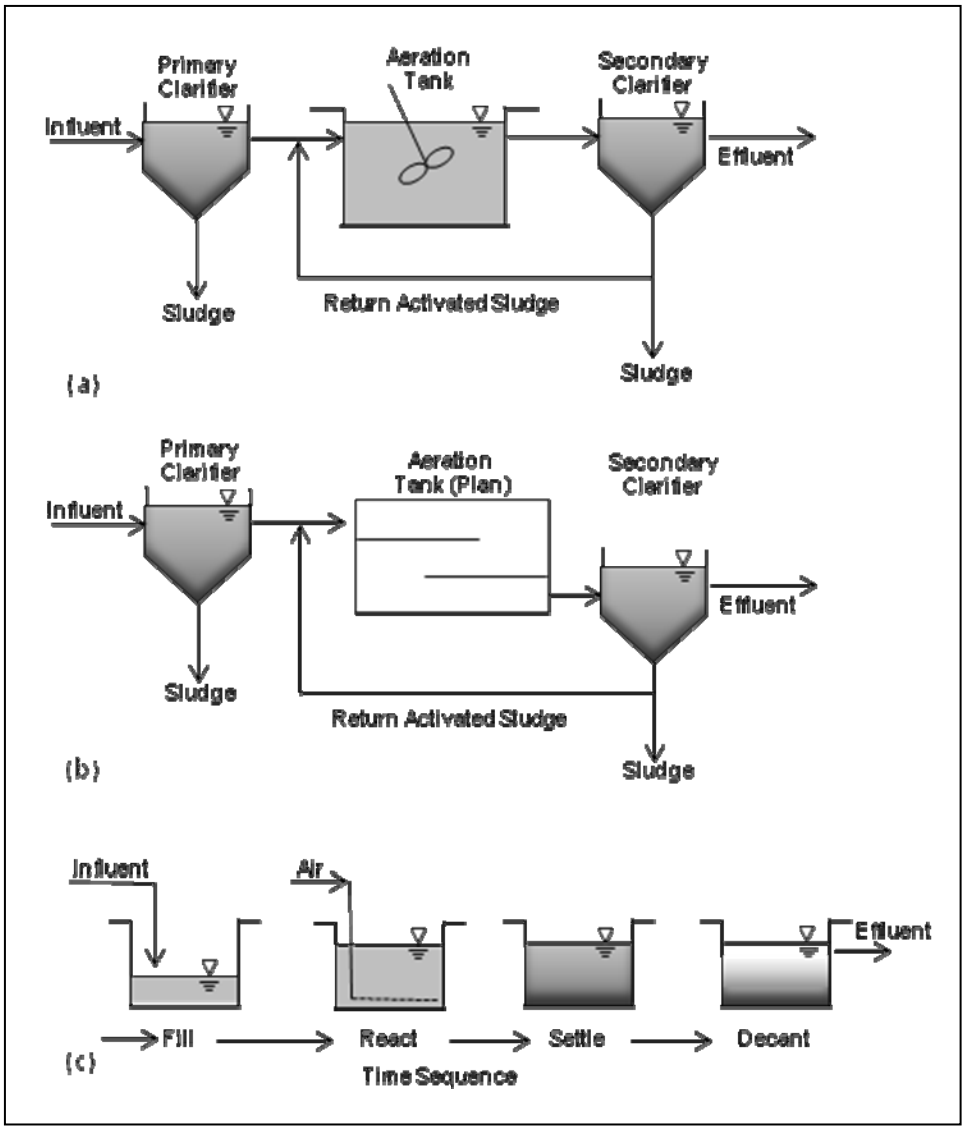

Figure 2.2 Typical activated sludge reactor configurations: (a) Completely mixed activated sludge (CMAS) process, (b) plug- flow process, and (c) sequencing batch reactor (SBR) process. (From Metcalf & Eddy, 2003).

www.manaraa.com

2.2.1 Activated Sludge Flocs

Activated sludge flocs are comprised of intricate matrices of microorganisms, extracellular polymers, organic and inorganic molecules, incorporated substrate, and biological waste material (Wilén et al., 2003). The physical, chemical, and morphological compositions of an AS floc are each heavily influenced by environmental conditions (Jin et al., 2004). These environmental factors include, but are not limited to, the dissolved oxygen level, the type and quantity of substrate provided, temperature, pH, reactor configuration, and the velocity gradient within the reactor (Alagappan & Cowen, 2001; Jin et al., 2004; Kilander et al., 2006). The interactions between the operating conditions of a treatment reactor, the physiological state of the biomass, and the sludge characteristics within the reactor are complex (Massé et al., 2006), and the physicochemical characteristics of the AS floc will influence many aspects of the biological treatment process including: "substrate transfer and utilization, floc formation and breakup, supernatant filtration, biosolids thickening via sedimentation and/or floatation, and biosolids dewatering" (Guan et al., 1998).

The specific materials that make up the sludge flocs, as well as the surface phenomena that they invoke, have been investigated for decades and are still the focus of numerous studies on the AS process. Variations in the AS floc ultimately affect the overall performance of the reactor because they influence both the kinetics of the microbial community (Grady et al., 1996) and the flocculation properties of the sludge (Wilén et al., 2003). The performance of the clarifier or sedimentation basin is essential to maintaining an effective AS sludge plant with suitable effluent quality, which must meet increasingly stringent standards (Grijspeerdt & Verstraete, 1997). The clarifier

www.manaraa.com

efficiency is highly dependent on the nature and settling characteristics of the sludge (Jin et al., 2004). Although the precise reason for variations in settling characteristics is yet unknown, it is believed that they are most likely a result of changes in the nutritional balance of the system and the dominant microbial population (Forster, 1985a; Goodwin & Forster, 1985; Lovett et al., 1983).

A main focus of current and past research studies investigate the composition of the extracellular polymeric substances (EPS) and seek to understand the role of EPS in gravity separation of the AS floc (Sponza, 2004). The EPS constitutes 50-60% of the organic fraction of AS and is a complex matrix mainly composed of excreted polymers, lysis and hydrolysis products, and adsorbed organic matter (Wilén et al., 2003). The EPS also incorporates ionogenic biopolymers (Morgan et al., 1990) and polyvalent metal ions (Forster, 1985b) which contribute to the surface charges of the flocs. Earlier studies concluded that surface charges do not necessarily have to be suppressed in order to flocculate and indicated that electrostatic forces are important to AS floc stability (Liao et al., 2001). Other studies indicated a strong correlation between the hydrophobicity of the cell surface and the adhesion to the AS floc (Zita & Hermansson, 1997). Although the exact role of the EPS is not completely understood, it is accepted that the composition of the EPS, along with other surface properties including surface charge and hydrophobicity, govern the settleability of the sludge and are important in controlling the sludge volume index (SVI) (Jin et al., 2004; Sponza, 2004; Zita & Hermansson, 1997).

www.manaraa.com

2.2.2 Activated Sludge Reactor Parameters

Several characteristics and measureable parameters of the AS treatment reactor can be used to gage the performance of the reactor. Through the quantification of key reactor parameters, the treatment efficiency can be monitored for the AS system. Current modeling approaches allow for simulation of the AS system performance once specific parameters are determined (Afonso & Cunha, 2002). Reactor parameters can also be correlated to other parameters in order to study the effects that variations in the operational strategies will have on the AS system.

2.2.2.1 Solids Analysis

The solids concentration is a key component of the treatment system that can be used to approximate the amount of biomass in the reactor. As indicated in Figure 2.3, the total solids within a reactor can be subdivided into several categories based on their susceptibility to physical separation and to volatilization. The specific techniques for completing the solids analysis are detailed in the standard methods (APHA et al., 2005); however, a brief overview of the process is provided here. The total solids account for all solids that remain after all moisture from the sample is evaporated off. The wet sample can also be subjected to a filter process that separates the suspended solids – those that are retained on the filter pad, from the dissolved solids – those that pass through the filter. The solids can be further separated by utilizing a furnace which heats the samples to 550°C and burns off all volatile components, leaving mainly inorganic byproducts. Results from the solids analysis are used in several other calculations that assess and/or

www.manaraa.com

control reactor performance, including the sludge volume index and the solids retention time.

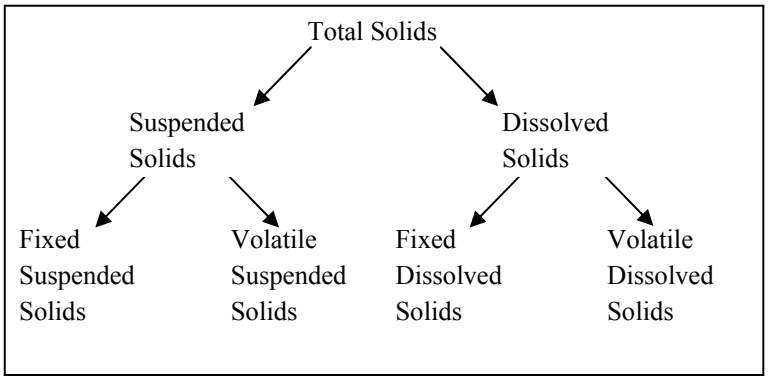

Figure 2.3 Components of wastewater solids analysis.

2.2.2.2 Sludge Volume Index

The sludge volume index (SVI) gives a representation of the sludge's ability to settle out during the clarification process. The separation of the sludge from the effluent stream is vital to maintaining an acceptable effluent product and to returning activated sludge back to the reactor (Lee et al., 1983). The SVI is determined first by settling the sludge for 30 minutes, often in a graduated cylinder or Imhoff cone, in order to determine the ratio of sludge volume to sample volume. Then, the SVI [$L^3_{sludge} \cdot M^{-3}_{sludge}$] is calculated as follows:

$$SVI = \frac{V_S}{X_T} \tag{2-4}$$

where, V_s = volume of settled sludge per volume of sample [$L^3_{sludge} \cdot L^{-3}_{sample}$] and X_T = total suspended solids [$M_{sludge} \cdot L^{-3}$] (APHA et al., 2005). Activated sludge settling behavior has four stages- reflocculation, initial settling, transition, and compression, and

www.manaraa.com

the time at which these stages may occur varies depending on the unique sludge properties (Lee et al., 1983). Although it is preferred that the sludge be in the compression phase when the volume is recorded, often the sludge is still in transition at the 30 minute mark of the SVI test. According to Lee et al. (1983), a diluted SVI (dSVI) can be conducted instead to assure that suspended solids concentration is not sufficiently high as to cause an artificial SVI boundary.

Several studies have been conducted to determine the correlation of SVI and other system parameters. Also, variations in the SVI have been linked to the variations in floc properties of the AS system. The morphology of the AS floc, specifically the increased irregularity of the floc shape, has been correlated to an increased SVI (Grijspeerdt & Verstraete, 1997). Also, variations in solids retention time (SRT) have been shown to influence the SVI and the amount of suspended solids lost in the effluent (Liao et al., 2006). At lower SRTs, the flocs became more irregular and more variable with size which leads to a higher SVI. However, other studies indicated that if the sludge age is plotted versus SVI, the relationship is highly dependent on the substrate being used, although good agreement was demonstrated for similar substrates (Lovett et al., 1983).

2.2.2.3 Solids Retention Time

The solids retention time (SRT), also known as the mean cell residence time, is another key element used to assess and control reactor performance. The SRT is calculated by performing a microorganism mass balance on the reactor, taking into account the influent, effluent, and any wastage streams. The typical calculation for SRT [t^{-1}] is:

www.manaraa.com

$$SRT = \frac{VX}{X_w Q_w + X_e Q_e} \tag{2-5}$$

where, V = volume of the reactor [L^3], X = volatile suspended solids [$M_{biomass} \cdot L^{-3}$], Q = volumetric flow rate [$L^3 \cdot t^{-1}$], and the subscripts w and e denote wastage stream and effluent stream, respectively (Metcalf & Eddy, 2003). In the typical constant volume system, the flow rates can be adjusted accordingly to maintain a desired SRT. The SRT is possibly the most critical parameter of an activated sludge wastewater treatment plant because it affects the overall treatment performance, including the amount of sludge produced and the oxygen requirements for the system (Metcalf & Eddy, 2003). As mentioned in the preceding discussion on SVI, varying the SRT has been shown to directly affect the biomass characteristics and the SVI (Liao et al., 2006).

2.2.2.4 Microbial Kinetics

Knowledge of the microbial kinetics is essential in biological treatment via the AS process (Contreras et al., 2001). Accurate modeling approaches for the AS process allow for predicting the effluent quality with reasonable certainty. Initial attempts to model the AS process involved the use of reaction engineering techniques combined with microbial kinetics from the Monod (1949) microbial growth model which incorporates saturation kinetics:

$$r_g = \mu X = \mu_m \frac{S_S}{K_S + S_S} X \tag{2-6}$$

and, a linear biomass decay model:

$$r_d = bX_B \tag{2-7}$$

www.manaraa.com

where, r_g = microbial growth rate [$M_{biomass} \cdot L^{-3} \cdot t^{-1}$], μ = specific growth rate [t^{-1}], X = volatile suspended solids concentration [$M_{biomass} \cdot L^{-3}$], μ_m = maximum specific growth rate [t^{-1}], S_S = substrate concentration [$M_{substrate} \cdot L^{-3}$], K_S = half-saturation constant [$M_{substrate} \cdot L^{-3}$], r_d = microbial decay rate [$M_{biomass} \cdot L^{-3} \cdot t^{-1}$], and b = decay coefficient [t^{-1}]. The Monod-type kinetics have been utilized in numerous studies, as noted by Vavilin and Lokshina (1996) and Kovarova-Kovar and Elgi (1998). Also, software packages have been developed to simulate AS biotreatment systems based on Monod kinetics in AS models developed, i.e. ASM 1 (Henze et al., 1987), ASM 2 (Henze et al., 1999), and ASM 3 (Gujer et al., 1999). These modeling approaches consider the hydrolysis of particulate/polymeric substrate into soluble substrate and are commonly applied to predict the biodegradation of organic substrate (Nakhla et al., 2006).

Although these modeling techniques allow for fairly accurate prediction for biogenic substrate removal, SOCs incorporated in the waste stream can lead to inaccurate results. Since it is recognized that many SOCs inhibit their own biodegradation, the Andrews (1968) model is one approach that has been applied to account for the inhibitory nature of SOCs (Vavilin & Lokshina, 1996). In this case, an inhibition coefficient, K_I, is introduced into the microbial growth model:

$$r_g = \mu_m \frac{S_S}{K_S + S_S + \frac{S_S}{K_I}} X_B \qquad (2\text{-}8)$$

The Andrews model has been widely used to model high strength inhibitory wastewaters (Nakhla et al., 2006). In many cases, however, the typical approaches using either the Monod or Andrews model when applied to SOC-containing wastewaters would lead to inaccurate or non-conservative results (Alagappan & Cowan, 2001). Alagappan

www.manaraa.com

and Cowan note the example of solvents which are known to be toxic and can cause microbial cell death at levels below their solubility limits. In the case of these solvents, there is the potential for inhibition of microbial activity, even for the biomass associated with the degradation of the inhibitory contaminants.

Accurate estimation of the kinetic parameters incorporated in the correct model structure will allow for predicting the fate of SOCs through the AS process with less uncertainty and more reliable results. Estimating the kinetics of biodegradation can be accomplished through a number of research techniques (Contreras et al., 2001). Accurate estimates, however, are necessary in order to accurately model SOC removal in an AS system. The method of determining kinetic parameters, specifically in modeling SOC removal, directly affects the prediction capabilities of the model used (Magbanua et al., 2003). Variability in the kinetic parameter estimates also stem from a number of inherent factors of the microbial community. The physiological state and microbial diversity within a culture are found to directly affect the kinetic parameters that describe the AS community (Grady et al., 1996). Following this logic, relationships could potentially be found between the microbial diversity and the kinetic parameters of the community.

In order to estimate the kinetic parameters of an AS system, a mass balance can be applied to the reactor for both biomass growth and substrate utilization. The typical mass balance could be written as follows:

$$Accumulation = Mass\ In - Mass\ Out + Generation \tag{2-9}$$

For the biomass mass balance, substitution of the appropriate terms yields:

$$\frac{d(XV)}{dt} = Q_o X_o - Q_e X_e - Q_w X_w + r_g V - r_d V \tag{2-10}$$

www.manaraa.com

For the substrate mass balance, substitution of the appropriate terms yields:

$$\frac{d(S_s V)}{dt} = Q_o S_o - Q_e S_e - Q_w S_w - r_{bio} - r_{vol} - r_{ads} \quad (2\text{-}11)$$

where r_{bio} is the rate of biodegradation, r_{vol} is the rate of volatilization, and r_{ads} is the rate of adsorption, each with units of $[M_{substrate} \cdot t^{-1}]$. The rate of biodegradation, r_{bio}, can be related to the Monod growth rate, r_g, by multiplying r_g by the inverse of the true growth yield, Y:

$$r_{bio} = -\frac{1}{Y} r_g V \quad (2\text{-}12)$$

where the units of Y are $M_{biomass} \cdot M_{substrate}^{-1}$ and recognizing that the negative sign is already incorporated into the mass balance presented in Eq. 2-11. The rate of volatilization and the rate of adsorption can often be neglected for typical wastewater constituents. However, when attempting to estimate volatile SOC kinetic parameters, it is important to estimate the contribution of these mechanisms to the overall removal of the substrate (Grady et al., 1997; Hsieh, 2000). Additionally, an approximation of the competent biomass actively involved in the SOC degradation is important to develop more accurate estimates of kinetic parameters (Magbanua et al., 1998).

Partitioning of SOCs into multiple phases in the AS reactor affects the available concentration for biodegradation by the biomass and not accounting for the portions of substrate removed via abiotic processes will lead to inaccurate, non-conservative estimates of the ability of the biomass to degrade the substrate of interest. The rate of volatilization is indicative of the mass transfer of SOCs into the rising air bubbles, which is often referred to as a stripping rate. The mass transfer equation for stripping of an SOC is often presented similar to that of Chao et al. (2008) as:

www.manaraa.com

$$r_{vol} = K_L a(S^* - S)V \tag{2-13}$$

where K_La is the mass transfer coefficient [t^{-1}] and S^* is the bulk gas-phase concentration [$M_{substate} \cdot L^{-3}$], which is often assumed to be zero in the case of SOCs. This results in a first-order equation to account for the removal of SOCs by volatilization (Grady et al., 1997). K_La for SOCs can be related to the K_La for oxygen transfer based on the ratio of diffusion coefficients (Bielefeldt & Stensel, 1999):

$$K_L a_{SOC} = K_L a_{O_2} \left(\frac{D_{SOC}}{D_{O_2}} \right)^n \tag{2-14}$$

where D_{SOC} and D_{O2} are the diffusion coefficient of the SOC and oxygen, respectively, in water [$L^2 \cdot t^{-1}$] and n is a constant which is based on the type of aeration system used. The constant is typically assumed to be 0.5 for mechanical surface aerators and 1 for diffused air systems.

Adsorption of the substrate to the biomass in the system is also a method of removal when the solids are wasted from the reactor or they escape in the effluent. In the same manner as stripping of SOCs, neglecting the contribution of this removal mechanism can potentially lead to a non-conservative estimate of the biodegradation capabilities of the biomass. The rate of adsorption for a steady-state CMAS is a function of the waste flow rate, the biomass concentration and the amount of SOC sorbed to the biomass at equilibrium (Grady et al., 1997; Hsieh, 2000):

$$r_{ads} = Q_w X_w k_p S \tag{2-15}$$

where k_p is the partition coefficient [$L^3 \cdot M_{biomass}^{-1}$]. The partition coefficient can be approximated based on the octanol-water coefficient, K_{ow}, and the fraction of organic

www.manaraa.com

carbon in the solids, f_{oc}, which is approximated to be 0.53 for biological cells (Hsieh, 2000):

$$k_p = (6.3 \times 10^{-7}) f_{oc} K_{ow} \quad (2\text{-}16)$$

Utilizing these mass balance terms and making certain assumptions regarding a CMAS, such as constant volume and steady-state performance, kinetic parameters can be approximated from experimental time-concentration data. It should be noted that although the principles of this analysis can be applied to batch systems, due to the sequential nature of SBRs, the differential equations over the react period often cannot be simplified using steady-state assumptions.

2.2.2.5 Floc Size and Size Distribution

Knowledge of the floc size and size distribution is an essential part of understanding the AS process. Insight in to the particle size distribution of an activated sludge system has been shown to be a cornerstone in studying flocculation and sedimentation, substrate transfer and utilization, gravity separation and thickening of sludge, and in the mathematical modeling of the AS process (Li & Ganczarczyk, 1991). Determining the size of a particle with a homogenous, regular shape only requires a single dimension, such as the diameter of a sphere or the side of a cube; however, in practice particles are often irregular and have an infinite number of linear dimensions (Allen, 1997). Therefore, relevant shape factors or size equivalents are required to compare irregular particles. Grijspeerdt and Verstraete (1997) selected several important parameters to compare different flocs. For correlating the size of the flocs, the authors used the equivalent circle diameter (D_e), calculated from the projected area:

www.manaraa.com

$$D_e = 2 \cdot \sqrt{\frac{Area}{\pi}} \tag{2-17}$$

Other parameters that the authors implemented were used to attempt to relate the shape of flocs to their settling properties. These parameters included:

- The form factor (FF) determines the shape of the object boundary relative to a circle, which would have a FF of one:

$$FF = \frac{4 \cdot \pi \cdot Area}{Perimeter^2} \tag{2-18}$$

- The aspect ratio (AR) determines how elongated an object is along the major axis. Again, a circle will have an AR of one:

$$AR = 1.0 + \frac{4}{\pi}\left(\frac{Length}{Width} - 1.0\right) \tag{2-19}$$

- The roundness (RD) is another parameter that relates the elongation of the particle to that of a circle. In this case, RD ranges from 0 to 1, where one indicates a circle:

$$RD = \frac{4 \cdot Area}{\pi \cdot Length^2} \tag{2-20}$$

The authors assert that these parameters were verified to be reproducible, provided that the biomass concentration remains between 0.5 and 4 $g \cdot L^{-1}$.

Along with some of the parameters used by Grijspeerdt and Verstraete, Contreras et al. (2004) also utilized the reduced radius of gyration (R_g) as a comparative parameter for the AS flocs:

$$R_g = \frac{\sqrt{M_{x2} + M_{y2}}}{\sqrt{Area/\pi}} \tag{2-21}$$

www.manaraa.com

where, M_{x2} and M_{y2} are the central second moments with respect to the x-axis and y-axis of the image, respectively. R_g equals 0.707 for a circle and it decreases the more an object is elongated. In terms of a pixilated computer image, M_{x2} and M_{y2} are calculated as follows:

$$M_{x2} = \frac{1}{N}\sum_{i=1}^{N}\left(x_i - M_{x1}\right)^2 \tag{2-22}$$

$$M_{y2} = \frac{1}{N}\sum_{i=1}^{N}\left(y_i - M_{y1}\right)^2 \tag{2-23}$$

with,

$$M_{x1} = 1/N\sum_{i=1}^{N} x_i^2 \tag{2-24}$$

$$M_{y1} = 1/N\sum_{i=1}^{N} y_i^2 \tag{2-25}$$

where, (x_i,y_i) is the position of each pixel that belongs to the analyzed particle and N is the number of pixels in the particle. Other research has indicated that R_g can be directly related to both the mass and density of microbial flocs (Guan et al., 1998).

Once relevant particle sizes have been defined, the frequency of occurrence of each size can be determined by microscopy, electrical and light sensing zone methods, surface distributions by photo-sedimentation and mass distributions by sieving and x-ray sedimentation (Allen, 1997). To graphically present the frequency distribution, the relationship between size and frequency may be written:

$$f(x) = \frac{dF(x)}{dx} \text{ so that } \int_0^x F(x) = \int_0^x f(x)dx \tag{2-26}$$

Li and Ganczarczyk (1991) suggest that although frequency of occurrence, number concentration, or count are traditionally used to give size distributions, they may also be

www.manaraa.com

expressed as surface area, volume, and mass. The authors also claim that when studying the AS process the latter distributions are often of equal or greater importance.

2.3 Research Techniques

Several advanced research techniques will be required during this study. This study will incorporate molecular methods to assess bacterial diversity and variations throughout the time of the research. It will also incorporate microscopic image analysis to investigate any changes in the flocculation characteristics of the activated sludge flocs. Another aspect of this study will be to quantify the effluent contaminants at extremely low levels which will incorporate gas chromatography. Each of these separate research methods were reviewed prior to conducting the study.

2.3.1 Molecular Methods

Molecular techniques were investigated to determine which methods would be utilized to characterize the genetic makeup of the microbial community being studied. These methods typically include three key steps: nucleic acid extraction, amplification via polymerase chain reactions (PCR), and analysis of the diversity of the amplified molecules through either genetic fingerprinting or sequencing (Widada et al., 2002). Numerous molecular studies have been conducted on environmental samples in order to determine which microorganisms are dominant in the system and to monitor changes in the system in response to environmental variations. DNA analysis is an increasingly reliable method for monitoring the diversity of microbial communities. A DNA strand will denature to a certain extent as determined by its specific nucleotide sequence

www.manaraa.com

composition. DNA fingerprints can be compared between different communities to determine the microbial diversity present (Nakatsu et al., 2000).

One method used to directly determine the genetic diversity of complex microbial populations is to use denaturing gradient gel electrophoresis (DGGE). Muyzer et al. (1993) present an approach in which DGGE is used to analyze the structure and species composition of microbial communities. In their study, PCR was used to amplify rDNA, and DGGE separated the PCR amplicons based on the electrophoretic mobility of a partially melted DNA molecule in polyacrylamide gels with a linearly increasing gradient of denaturants. Denaturants used in the polyacrylamide gel are urea and formamide. A 100% denaturant solution consists of 7 M urea and 40% formamide in water. In order to obtain a gradient, a lower denaturant solution and a higher denaturant solution are prepared and are poured using a gradient former. DGGE separates PCR amplicons of the same size based on their specific sequences because different sequences can be separated according to differential denaturation, or melting, profiles (Ercolini, 2004). DGGE bands can be revealed through traditional staining techniques including ethidium bromide (Gillan et al., 1998; Xia et al., 2005). More advanced staining procedures allow for more sensitive detection of low concentrations of DNA fragments, examples include silver staining (Felske et al., 1996), SYBR Green staining (Henckel et al., 2000), and SYBR Gold staining (Watanabe et al., 2001). Cost is often a prohibitive factor in utilizing more advanced stains over ethidium bromide, while toxicity considerations favor some of the more expensive stains. The resulting DGGE fingerprint provides a series of bands that are relative to the microbial species present in the sample. To carry the process further, identification of the species can be accomplished by excising, purifying, and sequencing

www.manaraa.com

the individual bands from DGGE profile (Ercolini, 2004). Figure 2.4 presents a flow chart for the molecular approaches used to directly monitor the microbial diversity of an environmental sample.

It has also been noted from studies that bacterial populations found in the environment are much more diverse than those isolated in laboratory work, and many microorganisms that are responsible for SOC biodegradation in natural environments have not been isolated in the laboratory yet (Watanabe et al., 1998). Direct extraction of DNA from an environmental sample has been shown to account for greater than 90% of the microorganisms present, which are not readily cultured in the laboratory, but may be responsible for the majority of the biodegradation activity of interest (Widada et al., 2002). The newer approach of DNA extraction from an environmental sample provides a better characterization of the microbial population because it does not carry the selective inhibition of the synthetic media used in more conventional culture methods (Amann et al., 1995).

www.manaraa.com

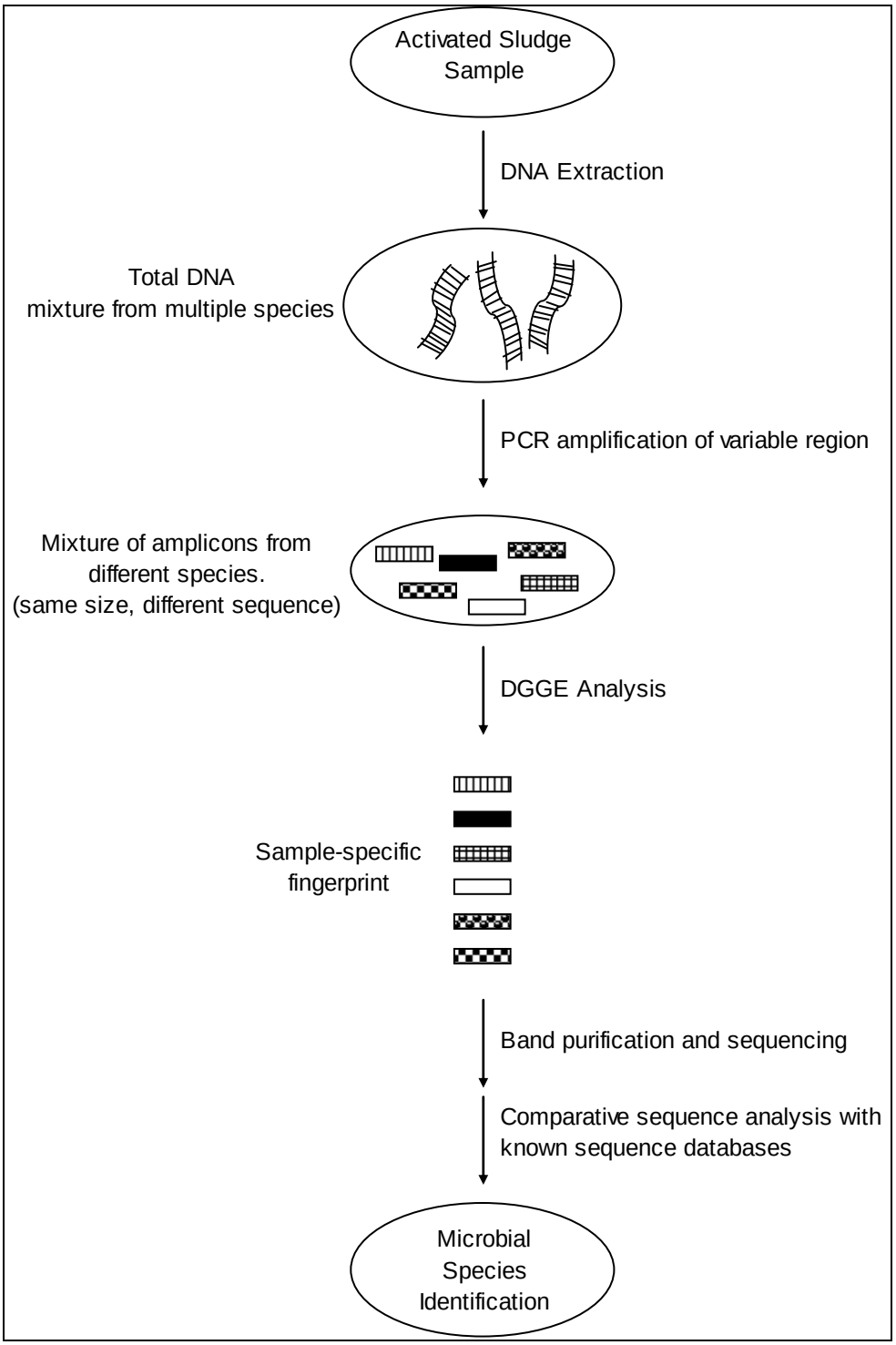

Figure 2.4 Flow diagram of the application of PCR-DGGE to an environmental sample (Ercolini, 2004).

www.manaraa.com

Although the approach has proved successful in multiple environments, extraction from AS systems has the added difficulty of disrupting bacterial cells regardless of the biochemical composition or their localization within the AS floc (Bourrain et al., 1999). The DNA extraction technique itself may introduce bias when it is applied to a mixed culture where the same extraction efficiency is difficult to achieve across all species (Ercolini, 2004). Bourrain et al.(1999) further suggest that the extraction procedure must be optimized to efficiently release the nucleic acids from complex microbial environments, and the extraction efficiency determines the quantity, quality, and diversity of the extracted nucleic acids. Therefore, optimization of the DNA extraction procedure is essential in order to assess the microbial diversity of the AS floc.

The extracted nucleic acids must also be compatible with PCR and other downstream processes. Studies also suggest that the PCR process itself can also introduce bias in the community analysis procedure. PCR amplification has resulted in differential or preferential amplification of rDNA genes, which may be a result of reannealing of the template DNA (Reysenbach et al., 1992; Suzuki & Giovannoni, 1996). Ribosomal DNA (rDNA) is most often targeted for PCR amplification because it is a highly conserved region of the genome that also contains variable regions (Ercolini, 2004). For bacterial populations, the most commonly amplified regions for bacterial community analysis are the variable regions in the 16S rDNA (Ercolini, 2004; Muyzer et al., 1993; Muyzer, 1999). Different bacterial species will have different base pair compositions within the variable regions of the 16S rDNA (Ercolini, 2004). Table 2.2 reports several of the primer sets found in the literature which are used to study environmental communities.

www.manaraa.com

Table 2.2

Primer sequences for environmental samples.

Primer[a]	Sequence[b,c]	Position[d]	Environmental Source	Authors
fD1	AGA GTT TGA TCC TGG CTC AG	8-27	activated sludge	Bourrain et al., 1999
rD1	AAG GAG GTG ATC CAG CC	1524-1540		
fU1	TGA CTG ACT GAG TGC CAG CMG CCG CGG	515-541[f]	soil, water samples, urine	Chaudhuri et al., 2006
rU1	TGA CTG ACT GAG AGC TCT ACC TTG TTA CGM YTT	1477-1509[f]		
27F	AGA GTT TGA TCA TGG CTC AG	8-27	marine biofilm	Gillan et al., 1998
1492R	GGT ACC TTG TTA CGA CTT	1492-1509		
GM5F[e]	CCT ACG GGA GGC AGC AG	341-357	biofilm; California estuaries; mixed microbial communities	Gillan et al., 1998; Murray et al., 1996; Muyzer et al., 1993
518R	ATT ACC GCG GCT GCT GG	518-534		
fU2	ATG GCT GTC GTC AGC T	1055-1070	microbial mat from hot springs	Ferris et al., 1996
rU2[e]	ACG GGC GGT GTG TAC	1392-1406		
PRBA338F[e]	AC TCC TAC GGG AG CAG CAG	338-358	soil samples	Nakatsu et al., 2000
PRUN518R	ATT ACC GCG GCT GCT GG	518-534		
PRBA968F[e]	AA CGC GAA GAA CCT TAC	968-983	soil samples	Nakatsu et al., 2000
PRBA1406R	ACG GGC GGT GTG TAC	1392-1406		
fU3	TTC CGG TTG ATC CYG CCG GA	2-21	mixture of purified DNA	Reysenbach et al., 1992
rU3	GGT TAC CTT GTT ACG ACT T	1492-1510		

[a]Primers not named in source are named fU for forward universal and rU for reverse universal.
[b]Primers are orientated from the 5' to 3' end.
[c]M = A/C; Y = C/T.
[d]Numbering based on the 16S rRNA of *E. coli.*
[e]GC-clamp was attached to 5' end.
[f]Position approximated from other given regions.

www.manaraa.com

DGGE is considered the most commonly used culture-independent fingerprinting method when assessing diversity of complex microbial communities directly from environmental samples (Ercolini, 2004). DGGE has been found to be a highly effective method for identifying microorganisms found in the environment that are difficult to isolate in cultures (Watts et al., 2001). Watts et al. (2001) further conclude that DGGE provides a means to rapidly screen for the absence or presence of selected species in response to changes in environmental conditions. DGGE coupled with the appropriate PCR primer set is also capable of assessing the diversity of specific catabolic genes. Henckel et al. (2000) utilized this technique in a study to assess the diversity of specific methanotrophic populations in soil. Similar techniques have been applied to assess SOC-specific catabolic gene diversity, including organisms that actively degrade BTEX in contaminated soils (Junca & Pieper, 2003; Junca & Pieper, 2004). Several molecular methods are currently being applied to assess microbial community structure and to investigate the diversity of catabolic genes in environmental samples (Widada et al., 2002).

Using these or similar techniques, several studies have investigated the microbial diversity of complex communities. The techniques have been employed with success in both aquatic environments (Ferris et al., 1996; Lyautey et al., 2005) and soil communities (Nakatsu et al., 2000). The specific environment under investigation typically dictates the precise method of nucleic acid extraction, however recent studies claim to have obtained a uniform method of DNA extraction from different types of environmental samples, both soil and water (Chaudhuri et al., 2006). Once the DGGE rDNA profiles are obtained, the banding patterns are considered to be a genetic fingerprint of the whole

www.manaraa.com

bacterial community, and the discrete bands are assumed to represent a unique bacterial population (Fromin et al., 2002). Also, the intensities of specific bands are assumed to directly indicate the relative density of the corresponding bacteria with the given sequence (Murray et al., 1996).

Analysis of microbial community DNA profiles have been historically accomplished through visually investigating the variations in the gel images from sample to sample (Fromin et al., 2002). These variations can include the appearance or disappearance of specific bands or changes in the intensities over time. More recently, techniques have been developed, which utilize more sophisticated statistical approaches and incorporate image-analysis software. Specific populations could also be identified by excising specific gel fractions and sequencing the rDNA (Xia et al., 2005). The obtained sequences can be compared to available sequence libraries, which can potentially identify the species present by similarity comparisons.

Xia et al. also applied statistical analysis to calculate the Shannon biodiversity index, S:

$$S = -\sum_{i=1}^{N} P_i * \log P_i \qquad (2\text{-}27)$$

where, P_i is the ratio of one specific group of bacteria to the total microorganisms in the sample, and N is the total number of microbial species in the samples. Another technique used to statistically analyze the DGGE profile of multiple environmental samples was to use the pairwise similarity coefficient, C_s (Gillan et al., 1998). This coefficient is calculated based on the similarities between two separate lanes on the DGGE gel:

$$C_s = \frac{2j}{(a+b)} \times 100 \qquad (2\text{-}28)$$

www.manaraa.com

where, a is the number of DGGE bands in one sample, b is the number of DGGE bands in another sample, and j is the number of common DGGE bands. A C_s of 100% means that the two samples are identical and a C_s of 0% means that the two profiles are completely different.

Although visual analysis has been successfully applied in numerous studies, Datta & Datta (2003) report that it is a labor intensive and highly subjective process. The authors suggest that hierarchical clustering is an important tool commonly applied in the fields of genetics and molecular biology. Eisen et al. (1998) report the use of pairwise average-linkage clustering analysis to develop relational trees, or dendrograms, that reflect the level of similarity between objects based on branch length. Numerous clustering methods are available, but Datta & Datta (2003) suggest that using unweighted pair group method average (UPGMA) based on correlation distances to develop the hierarchical cluster is one of the simplest and most commonly applied techniques for assessing similarities between profiles. In the UPGMA method, the 'distances' between clusters is taken as the average of the 'distances' between the points in each cluster (Datta and Datta, 2003). This method can be applied based on any number of statistical coefficients used to generate the correlation distance between the points.

Through the discussed analysis techniques, the microbial diversity should be able to be quantified and compared throughout the experimental period to determine the effects of SOCs on the diversity of the population.

www.manaraa.com

2.3.2 Microscopic Image Analysis

Another focus of the proposed research is to monitor the changes in the morphology of the microbial flocs throughout the process in relation to the operational strategy variations. It is understood that AS flocs are made of a complex and heterogeneous composition, and the size and size distribution of the flocs will depend heavily on the environment, including influent composition (Jin et al., 2004). It has also been shown that the floc size-density-structure relationship is vital to optimizing phase separation (Jorand et al., 1995). Knowledge concerning the size and morphology of AS flocs leads to a better understanding of the AS process and to better control of the AS system (Li & Ganczarczyk, 1991).

Several technologies are currently available for analyzing floc size and morphology, which typically combine microscopic techniques, image-analysis software, and statistical methods. Allen (1997) claims that a microscopic examination should always be used to conduct a particle size analysis. Lopez et al. (2005) suggest that the images of AS flocs can be obtained using wide-field epifluorescence microscopy, confocal laser scanning microscopy (CLSM), or two-photon excitation laser scanning microscopy (TPE-LSM). The images produced from these methods allow for varying degrees of quantitative analysis. However, other authors suggest alternative approaches including phase contrast illumination systems (Contreras et al., 2004; Araya-Kroff et al., 2004) or light-scattering detection devices, such as the Malvern Mastersizer, which are specifically developed for floc size analysis (Jin et al., 2004; Massé et al., 2006). Guan et al. (1998) conclude that, with the scattering of light, information on the floc structure can be divulged from the variation of light intensity with the angle of scatter. Araya-Kroff et

www.manaraa.com

al. (2004) found that phase contrast microscopy can be an equally useful tool in floc image analysis. In their study, phase contrast microscopy was coupled with specially developed software to allow quantitative monitoring of the dynamic changes of the AS flocs, which is similar to the goals of the current research project.

2.3.2.1 Sample Preparation for Image Analysis

Several steps must be taken to utilize microscopic image analysis to monitor the size and morphology of AS flocs. Care must be taken during the initial sample preparation and handling in order to prevent undesired forces on the flocs from distorting the fragile floc morphology of larger flocs (Li & Ganczarczyk, 1991). Care must also be exercised in the initial sample preparation because the measurement sample is so small in relation to the studied environment that it is difficult to make it representative of the bulk (Allen, 1997). Research has suggested that any extraction of the particles from the system will influence the particle size distributions, and large shear forces will break up flocs (Kilander et al., 2006). Although automatic, in-situ, non-intrusive measurements are ideal for investigating floc parameters, several studies make use of manual or automatic sampling and microscopy to study floc morphology (Araya-Kroff et al., 2004; Contreras et al., 2004; Grijspeerdt & Verstraete, 1997; Pons et al., 1993). However, in the case of manual sampling, delicate manipulation is required. Grijspeerdt and Verstraete (1997) suggest that the sample be sufficiently diluted to avoid saturation of the image and that the liquid layer must be thin enough to use high magnification. The authors accomplished this by dispersing the sample into a petri dish and diluting it 5:1 with effluent. Contreras et al. (2004), however, placed 10 µl samples directly on

www.manaraa.com

microscope slides. Studies have concluded that determination of floc size and other morphological parameters are independent of the dilution of the sludge sample, provided the biomass concentration is between 0.5 and 4 $g \cdot L^{-1}$ (Grijspeerdt & Verstraete, 1997). This indicates that the major purpose of dilution is for visibility of the majority of flocs, and not to increase accuracy of individual measurements. However, the authors do suggest that changing magnification will highly influence the measurements for a given sample, so all work that is to be compared must be conducted at a constant magnification.

2.3.2.2 Microscopic Image Capture and Image Processing

When using microscopic techniques, images must be captured and saved in a mode compatible for further processing. Typically, a video camera is mounted on the microscope, and the image is captured and digitized through a frame grabbing software program (Grijspeerdt & Verstraete, 1997; Pons et al., 1993). In most cases, the microscope must be focused manually to determine the 'best' view of the flocs, since the three dimensional nature of the flocs makes it difficult to have the entire floc in focus at one time. After saving the image, grid correction may be necessary depending on the aspect ratios of the camera, image capture software, and the computer pixels. The grid correction is accomplished by using a scale slide to measure the field of view and relate it to the number of pixels in the image. Further image processing is used to improve the image and make it more available to computer-automated measurements, but at the same time, try to maintain the accuracy of the image.

The first step in further image processing is usually binarization in order to convert the grey-scale images to black and white images (Pons et al., 1993). During the

www.manaraa.com

binarization process, images are assigned a threshold value at which the floc particles are clearly separated from any background colors and pixels are reassigned a grey-level value of either zero (black) or one (white) (Grijspeerdt & Verstraete, 1997). At this point, pixels are clearly defined as being associated with the floc (a value of zero) or background (a value of one). In order to assign the flocs a one value for counting purposes, the image properties must be inverted, so that the pixels that are ones become zeros and zeros become ones.

Next, a series of processes is applied to differentiate individual flocs. These processes include erosion processes, to disconnect touching particles that should be separated, and dilation processes, to apply a peripheral layer of pixels to the new non-touching images (Allen, 1997). After the individual flocs are differentiated, the flocs are labeled so that all pixels associated with a unique floc will have a separate label (Kilander et al., 2006). Once flocs are labeled, the user has the ability to count the number of pixels in each floc, and if the pixel size is known, the particle sizes can be estimated. In many instances, prior to labeling the flocs it may be necessary to clean up the image by placing an artificial border around the image so all flocs that are touching the edge of the image are not seen as connected, and it may be desirable to remove smaller flocs below a certain threshold that may be artifacts, debris, or broken pieces from larger flocs (Araya-Kroff et al., 2004; Contreras et al., 2004; Pons et al., 1993). The floc size and size distribution can then be computed using an appropriate software program. In some cases, the total projected surface area may be desired, which requires an additional step of removing the inner holes of the aggregates prior to labeling and counting pixels (Araya-Kroff et al., 2004).

www.manaraa.com

The image processing becomes more complicated when there are large amounts of filamentous organisms, which will create significant porosity within the floc or make separate flocs appear connected. When filaments are present in a mixed culture, manual classification of filaments and floc-forming bacteria may be required (Contreras et al., 2004). A bottom hat filter can also be applied to enhance the filaments and other small aggregates that have lower grey levels (Araya-Kroff et al., 2004). Araya-Kroff et al. utilize several steps to isolate filaments from the aggregates and characterize them separately. The filaments are isolated through using a segmentation program coupled with a logic subtraction of the mask binary image that contains the larger aggregates. Then, smaller aggregates are removed based on a pixel area and radius of gyration threshold. Finally, the filaments are skeletonized and pruned and the lengths are determined by:

$$L = 1.122 \cdot N \cdot F_{cal} \tag{2-29}$$

where, N = the number of pixels in the skeletonized image; F_{cal} = the calibration factor [$\mu m \cdot pixel^{-1}$]; and 1.122 is a correction factor used to homogenize filaments at various angles.

www.manaraa.com

CHAPTER III

METHODOLOGY

3.1 SOC Selection

An important step in this project was determining which SOCs would be selected as candidates for study. Three major criteria had to be satisfied in order for an SOC to be used:

- Industrial and environmental significance,
- Available biodegradation pathway information, and
- Chemical properties conducive to aqueous biological treatment.

Primarily, test SOCs were taken from the USEPA priority pollutant list since these compounds have been identified as having industrial significance and as posing an imminent threat to public health and the environment. However, some additional chemicals were also initially selected primarily due to similar research studies using them, which provides important information as to the chemical properties and a basis for comparison of results between studies.

Once a large preliminary list was established representing many SOCs that were both industrially and environmentally significant, those chemicals were cross-referenced with the University of Minnesota's Biocatalyst/Biodegradation Database (UMBBD). This database compiles a list of chemicals for which the biodegradation pathways have been

www.manaraa.com

studied and the intermediate enzymes within the process of biodegradation are given. This information is critical for developing primers for specific enzymes involved in the degradation of a given chemical. By using this information, a much more manageable list was established for study, which includes only SOCs that have known degradation pathways. In many cases, this database provides the actual organisms involved in the biodegradation, which is also useful in the molecular analysis of the biodiversity of the activated sludge system.

The next step in the selection process was to determine which of the given chemicals are most suitable for activated sludge treatment. This involves looking at the important physicochemical properties listed previously. The SOCs must be biodegradable, but the amount removed through abiotic processes must be minimized, such as sorption to the biomass or volatilization due to aeration, so that accurate estimates can be obtained for the biological removal efficiency. In order to quickly access this information for the SOCs, the Estimation Programs Interface (EPI) Suite™ was used as a screening tool to aid in determining which chemicals possess the appropriate properties (USEPA-SRC). This software package was developed by the USEPA's Office of Pollution Prevention Toxics and the Syracuse Research Corporation. All preliminary SOCs that met the other two criteria were input into the EPI Suite™ and the chemical information was copied into a spreadsheet to sort and compare the properties of the SOC, including Henry's law coefficient and the octanol-water coefficient. Actual experimental values from the program's database were used when possible, but if they were not available the estimated values generated by the program were used.

www.manaraa.com

After these cross-analyzing procedures were applied, the list of available SOCs for study was significantly reduced. To determine which of these chemicals would be most appropriate for study, several additional criteria would be applied. The chemicals would ideally represent a broad range of functional groups and be readily quantifiable at low concentrations. Also, the number of available DNA sequences for specific enzymes in the biodegradation pathway had to be within a manageable range for the primer development process. The number of sequences available was determined by doing a search for the given enzyme using the Core Nucleotide database from the National Center for Biotechnology Information (NCBI). After all of these criteria had been considered, four chemicals were selected as test SOCs for this study: Acrylonitrile, Chlorobenzene, Methyl-tert-butyl-ether (MTBE), and Phenol.

3.1.1 Acrylonitrile

Acrylonitrile (CAS 107-13-1) is a commonly produced industrial chemical that is primarily used in the manufacturing of copolymers for the production of acrylic fibers, nitrile rubber and plastic resins (USEPA, 1998; 1994; 1979b). However, acrylonitrile poses serious health and environmental concerns, as it is explosive, flammable, and highly toxic (ACC, 1959), and it is a known carcinogen (USEPA, 1994). There are several synonyms for acrylonitrile, including 2-propenenitrile, acrylon, carbacryl, cyanoethene, cyanoethylene, Acritet, Fumigrain, propenenitrile, VCN, Ventox, and vinyl cyanide (USEPA, 1998). The chemical formula is C_3H_3N and the structure of acrylonitrile, presented in Figure 3.1**,** is a planar molecule with an assumed bond length, α, of 120° (ACC, 1959).

www.manaraa.com

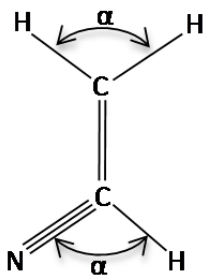

Figure 3.1 Structure of acrylonitrile (ACC, 1959).

According to the USEPA (1994), volatilization is a potential transport mechanism for acrylonitrile, but probably proceeds slowly based on Henry's law constant (1.38×10^{-4} $atm \cdot m^3 \cdot mole^{-1}$ from EPI Suite). Furthermore, the USEPA suggest that the low log K_{ow} (0.25 from EPI Suite) and high solubility make acrylonitrile minimally susceptible to adsorption to sediment or suspended particles. Therefore, the majority of removal from a biological wastewater reactor, if any is discovered, would most likely be a result biodegradation and not physical removal processes. Acrylonitrile undergoes biodegradation via the pathway presented in Figure 3.2. From this information, primers may be developed based on the sequences of the initial enzymes from both pathways, aliphatic nitrilase and nitrile hydratase/amidase. The toxicological information provided in the Material Safety Data Sheet (MSDS) for acrylonitrile indicates a LD50 for oral ingestion in a rat ($LD50_{oral,rat}$) is 0.15 $g \cdot kg^{-1}$.

www.manaraa.com

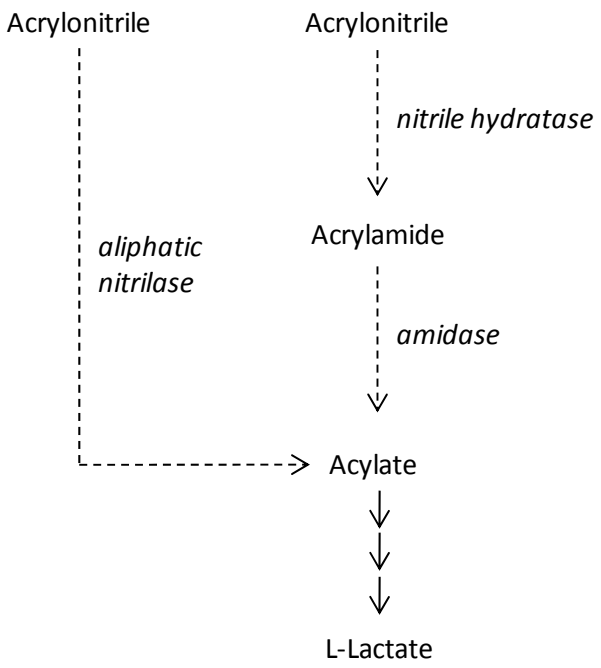

Figure 3.2 Acrylonitrile biodegradation pathway (Adapted from: UMBBD).

3.1.2 Chlorobenzene

Chlorobenzene (CAS 108-90-7), a halogenated aromatic hydrocarbon, has several industrial uses both as an intermediate and as a solvent in chemical manufacturing processes (USEPA, 1995). Chlorobenzene is used as an intermediate in the production of rubber chemicals, agricultural chemicals, antioxidants, and dyes and pigments. It has also been used in the production of phenol and aniline, and as a solvent in the production of paints, adhesives, pharmaceuticals, and waxes. Chlorobezene is not a known carcinogen, but according to the USEPA, it has been shown to cause acute and chronic problems with the liver, kidneys, and the central nervous system. There are several synonyms for chlorobenzene, including monochlorobenzene, chlorobenzol, phenyl

www.manaraa.com

chloride, and benzene chloride. Chlorobenzene's chemical formula is C_6H_5Cl and its structure, presented in Figure 3.3, is a benzene ring with a substituted chlorine.

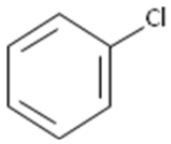

Figure 3.3 Structure of chlorobenzene (McMurry, 1984).

According to the USEPA (1995), volatilization is a major transport mechanism for chlorobenzene based on Henry's law constant (31.1 x 10^{-4} atm·m^3·$mole^{-1}$ from EPI Suite). Furthermore, the log K_{ow} value (2.84 from EPI Suite) and lower solubility suggest that chlorobenzene has the potential for adsorption to AS particles in the wastewater treatment process. The major removal mechanisms for chlorobenzene in the AS system would be evaporation and biodegradation, with a smaller portion attributed to adsorption (USEPA, 1995). Since evaporation is a significant factor, the % removal must be estimated using K_H and the known aeration rates in the reactors. Chlorobenzene biodegrades via the pathway presented in Figure 3.4. Primers could be developed based on the nucleic acid sequence of the initial enzyme chlorobenzene dioxygenase, which is specific to chlorobenzene. Another possible enzyme that could be used from the pathway is catechol-1,2-dioxygenase used to metabolize catechol, which is a common intermediate in several aromatic biodegradation pathways and has the added benefit of being studied in previous research (Rudolph & Grady, 2002; Mesearch et al., 2000). The $LD50_{oral,rat}$ for ingestion of chlorobenzene is 1.1 g·kg^{-1} as reported in the MSDS.

www.manaraa.com

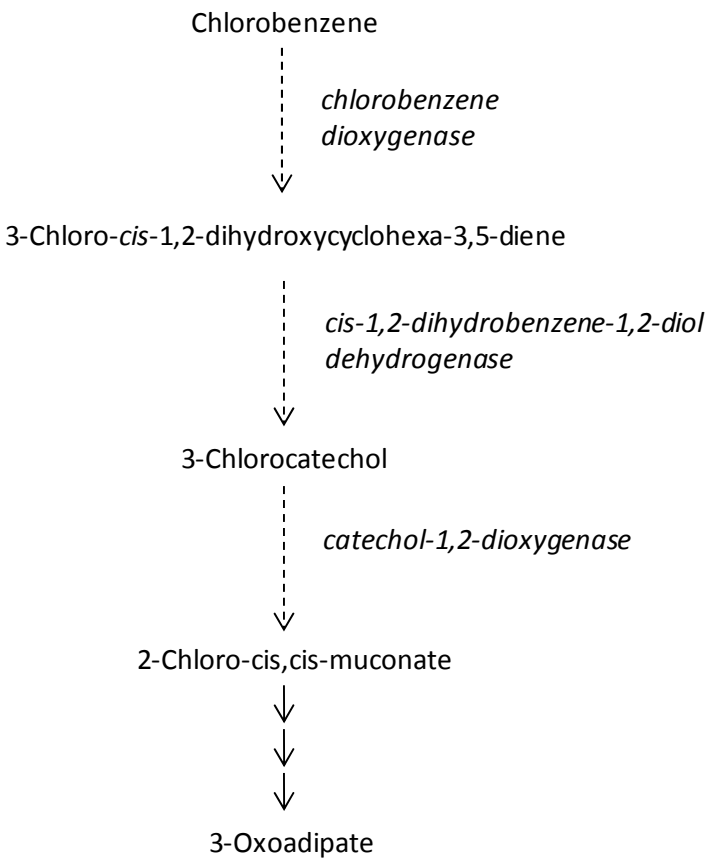

Figure 3.4 Chlorobenzene biodegradation pathway (Adapted from: UMBBD).

www.manaraa.com

3.1.3 Methyl-tert-butyl-ether

Methyl-tert-butyl-ether, MTBE, (CAS 1634-04-4) is a synthetic compound primarily used as a fuel additive designed to increase combustion efficiency and reduce harmful emissions such as ozone and carbon monoxide. MTBE is reported as a possible carcinogen which can target the kidneys and the central nervous system, however all toxicological properties have not been thoroughly investigated (Jacobs et al., 2001). Synonyms for MTBE include tert-butyl-methyl-ether and 2-methyl-2-methoxy-propane. MTBE is an aliphatic ether with the chemical formula $C_5H_{12}O$, as shown in the structure presented in Figure 3.5 with α equaling 122 degrees.

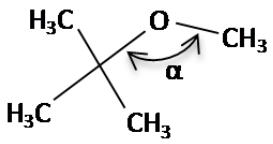

Figure 3.5 Structure of MTBE (Jacobs, 2001).

MTBE exhibits a relatively high solubility (51 $g \cdot L^{-1}$ from EPI Suite) and low Henry's law constant (5.87 x 10^{-4} $atm \cdot m^3 \cdot mole^{-1}$ from EPI Suite) compared with other VOCs, which suggests it preferentially partitions into the water phase when introduced into the environment. Diaz & Drogos (2002) further suggest that MTBE's low adsorption potential, as evidenced by the log K_{ow} value (0.94 from EPI Suite), and low biodegradability make it a significant environmental concern since it will travel with the groundwater and surface water flows, causing serious impacts on water quality. MTBE is both recalcitrant and toxic to natural microorganisms, and as such it not only resists

www.manaraa.com

biodegradation but it may inhibit the degradation of other SOCs (Jacobs et al., 2001). MTBE undergoes biodegradation via the pathway presented in Figure 3.6. From this information, primers can be developed based on the nucleic acid sequence of either initial enzyme, alkane-1-monooxygenase or the unspecific monooxygenase. It is also an interested note that alkane-1-monooxygenase is present again later in the biodegradation pathway. MTBE has a $LD50_{oral,rat}$ of 4 $g \cdot kg^{-1}$ reported in the MSDS.

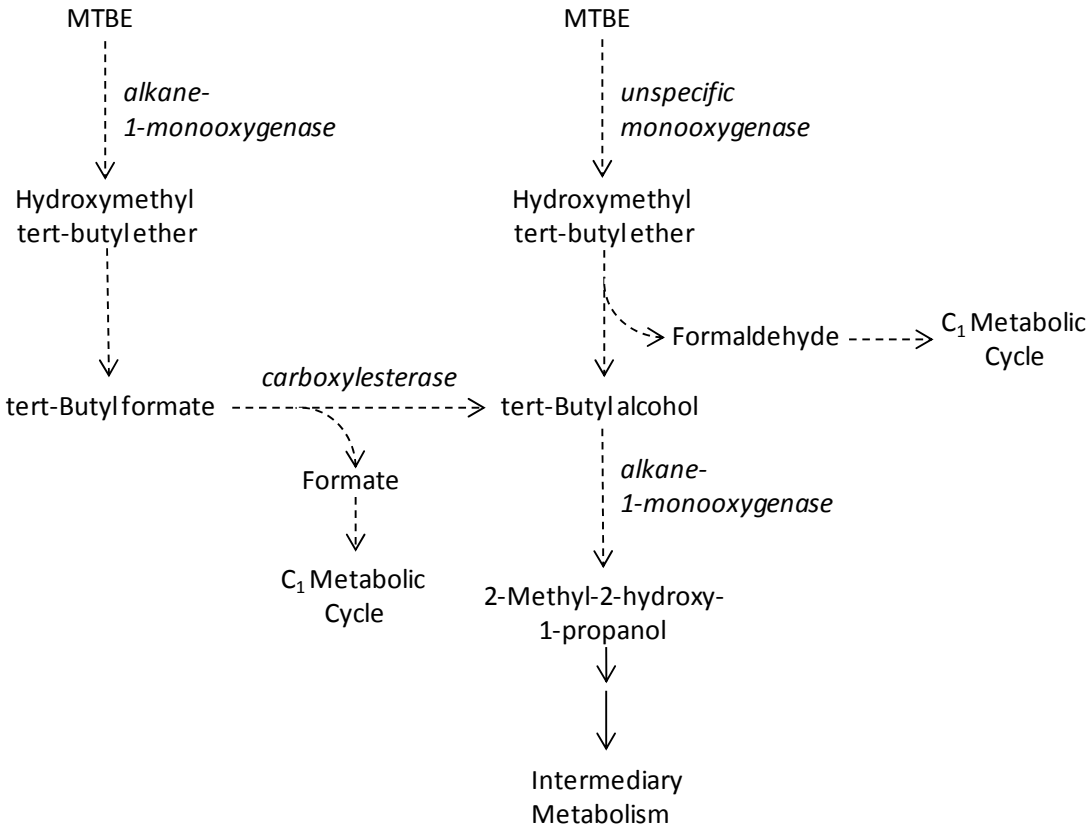

Figure 3.6 MTBE biodegradation pathway (Adapted from: UMBBD).

www.manaraa.com

3.1.4 Phenol

Phenol (CAS 108-95-2), a naturally occurring compound found in coal tar, is industrially synthesized due its high demand for use in the manufacturing of an array of products, including antiseptics, resins, adhesives, disinfectants and explosives (McMurry, 1984). The largest use of phenol is as in intermediate in the production of phenolic resins (USEPA, 2002). According to the USEPA, the toxicological effects associated with phenol include lung, liver, and kidney problems; tremors and other central nervous system effects; and at high doses it can be fatal. Synonyms for phenol are benzenol, hydroxybenzene, monophenol, oxybenzene, phenyl alcohol, phenyl hydrate, and phenyl hydroxide. The structure of phenol, illustrated in Figure 3.7, is a benzene ring with a substituted hydroxyl group, having the chemical formula C_6H_6O.

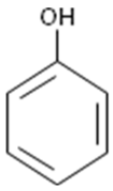

Figure 3.7 Structure of phenol (McMurry, 1984).

Based on the low Henry's law constant (0.00333×10^{-4} atm·m^3·mole^{-1} from EPI Suite) and moderate solubility (87 g·L^{-1} from USEPA, 2002), phenol is not likely to evaporate from the aqueous system and should remain in solution at the lower concentrations expected in this study. Also, phenol's log K_{ow} (1.46 from EPI Suite) suggests that it is somewhat hydrophobic, but should not significantly adsorb to the activated sludge particles. Phenol undergoes biodegradation via the pathway presented in

www.manaraa.com

Figure 3.8. Primers could be developed from this information based on the phenol-specific enzyme phenol-2-monooxygenase early in the pathway or based on the enzymes used for the intermediate catechol biodegradation, either catechol 2,3-dioxgenase or catechol 1,2-dioxygenase. Since, as mentioned previously, catechol is an intermediate for several aromatic compounds, using these enzymes could give a broader assessment on the AS population and the phenol-specific enzyme could look directly at those bacteria responsible for its biodegradation. The specific population directly utilized in phenol removal during AS treatment has been analyzed in several studies, using microbiological enumeration techniques (Magbanua et al., 1998) and genetic techniques (Watanabe et al., 1998). Phenol has a $LD50_{oral,rat}$ of 0.32 to 0.51 $g \cdot kg^{-1}$ reported in the MSDS.

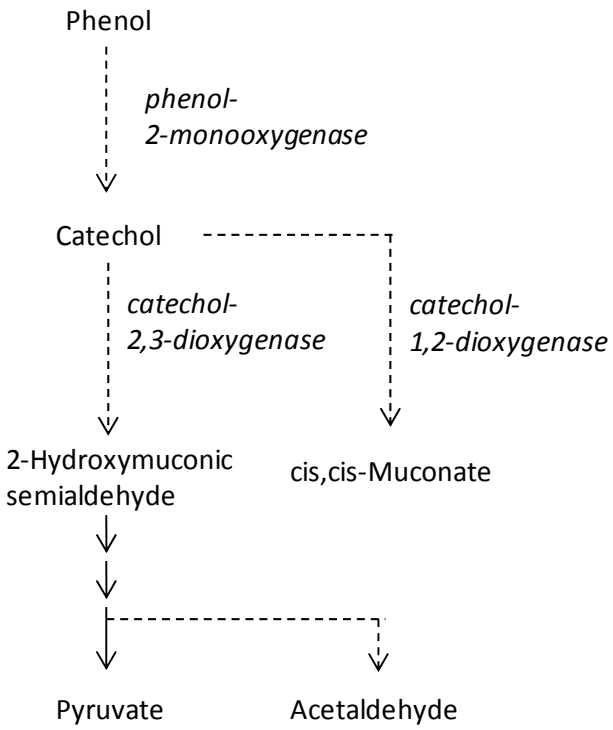

Figure 3.8 Phenol biodegradation pathway (Adapted from: UMBBD).

www.manaraa.com

3.1.5 SOC Quantification

Influent SOCs were precisely dosed using syringe pumps, and effluent samples were collected and analyzed to determine SOC removal in each reactor. Effluent samples were collected directly from the discharge lines of each reactor during their normal operations, such that reactor operation was not interrupted during the sampling process. Samples were collected in 40 ml glass sample vials with Teflon-lined caps and stored at 4 ºC in accordance with the appropriate EPA sampling methods for each compound (Keith, 1996). SOC analysis was performed using a purge and trap extraction system and gas chromatography with mass spectrometry detection (GC/MS). Samples were diluted with DI water to ensure that the SOCs were in an appropriate range for GC/MS detection, which was less than 500 $\mu g \cdot L^{-1}$ based on the calibration curves developed, and 10 mL of diluted sample was loaded into a gas tight syringe and injected.

The samples were first concentrated using a Tekmar 3000 purge and trap system (Tekmar, Cincinnati, OH, USA) equipped with a Vocarb 3000 K trap (Supelco, Bellefont, PA, USA). The purge and trap sampler was programmed as follows: purge ready temperature, 30 °C; preheat temperature, 80 °C; preheat time, 10 min; purge time, 20 min; line temperature, 200 °C; MCS line temperature, 200 °C; desorb preheat temperature, 245 °C; trap desorb temperature, 250 °C; trap desorb time, 5 min; trap bake temperature, 260 °C; trap bake time, 10 min.

The concentrated samples were then injected into a Varian Saturn II GC/MS (Varian Instruments, Inc., Palo Alto, CA, USA) fitted with a fused silica Rtx-Volatiles column (60 m×0.32 mm×1.5 μm df) (Restek, Bellefont, PA, USA). Chromatography conditions were as follows: injector temperature 250 °C; oven temperature, 35 °C for 3

www.manaraa.com

min, increased to 200 °C at a rate of 10 °C·min^{-1}, then maintained at 200 °C for 5.5 min. MS data was collected and analyzed to determine SOC concentrations using Varian Mass Spectrometry Workstation Version 6.3 (Varian Instruments, Inc., Palo Alto, CA, USA).

3.2 Activated Sludge Reactors

This research attempted to study the effects that SOCs have on the activated sludge process through developing and maintaining lab scale wastewater treatment reactors. These reactors were stabilized and acclimated to a biogenic feed, originally, and then were subjected to a specified amount of SOCs and monitored for changes in the biomass properties. In order to assess any influence of the reactor flow regime, two different types of reactors were constructed: a sequencing batch reactor (SBR) and a completely mixed activated sludge reactor (CMAS). The reactors were designed with similar volumes, feed concentrations, flow rates, aeration rates and mixing power, such that the only significant difference is the flow regime between the two reactors. Table 3.1 presents the feed recipe for the synthetic wastewater influent. The feed was autoclaved and sealed to inhibit any biodegradation prior to introduction into reactors.

www.manaraa.com

Table 3.1

Reactor feed composition.

Component	Concentration[a] (mg/L)	Concentration[a,b] (mg/L as COD)
Biogenic Substrates[c]		720
Peptone	321.43	450
Glucose	119.05	127
Sodium Acetate	285.71	143
Inorganic Nutrients[c]		
$(NH_4)_2SO_4$	142.86	
$MgSO_4$	4.76	
$CaCl_2 \cdot 2\ H_2O$	9.52	
$FeCl_3 \cdot 6\ H_2O$	1.19	
KH_2PO_4	71.43	
SOCs		60
Acrylonitrile	8.30	15
Chlorobenzene	7.28	15
Methyl-tert-butyl-ether	8.26	15
Phenol	6.30	15
	TOTAL COD:	780

[a] Concentrations are final influent concentration supplied to reactors.

[b] Theoretical COD based on chemical formulas.

[c] Feed prepared with deionized water and autoclaved at 121 °C.

www.manaraa.com

Two plexiglass lab scale wastewater treatment reactors were constructed with dimensions of 30.5 cm x 25.4 cm x 30.5 cm (L x W x H), with the actual water depth maintained at a working volume of 15 L plus freeboard for potential overfilling. The reactors were supplied with air at a reported rate 0.261 cfm through two dual-port aquarium pumps. Mixing was applied via a Barndstead dual-shaft mixer, using the high torque shaft and the control module set to an eight. Both reactors were initially seeded with 15 L of return sludge from the Ernest E. Jones Wastewater Treatment Plant operated by the City of Starkville, MS. The reactors were maintained at room temperature (23 ± 2 °C) and the fine bubble air diffusers maintained the dissolved oxygen at a concentration above 2 $mg \cdot L^{-1}$. The SBR operated at four cycles per day. Each cycle consisted of a fill cycle of approximately 5 min, which varied slightly based on pump flow rates. The concentrated feed solution was pumped at a rate of 0.75 L per cycle, or 3 $L \cdot d^{-1}$, and the dilution water was pumped at a rate of 6.75 L per cycle, or 27 $L \cdot d^{-1}$, in order to have a 10:1 dilution of the concentrated feed and a 0.5 d hydraulic residence time (HRT). The SBR then began the reaction phase, which lasted five hours. After the react phase, the reactor entered the settling phase where all aeration and mixing was shut down and the solids were allowed to settle out for 1 h. Finally, half of the reactor volume was decanted and the next cycle initiated. The CMAS was continuously mixed and aerated. The concentrated feed solution and dilution water cycled on every 30 min for approximately 7 min, which varied slightly based on pump flow rates. The concentrated feed solution was supplied to the CMAS at a rate of 62.5 mL per cycle, or 3 $L \cdot d^{-1}$, and the dilution water was pumped at a rate of 562.5 mL per cycle, or 27 $L \cdot d^{-1}$, to maintain a 10:1 dilution. The CMAS overflowed directly into a 3 L conical clarifier which had a continuous underflow

www.manaraa.com

that was returned to the reactor. The clarifier incorporated a low-speed mixer that was operated intermittently in order to enhance flocculation and settling. The mixer was turned on for 10 seconds every hour during the time period when no pumps were on and there was no outflow, to reduce solids loss in the effluent. In both reactors, sludge was wasted directly from the reactor chamber to maintain the appropriate SRT. In the CMAS, the wastage pump cycled on every 2 h, while the SBR cycled on every 6 h just prior to the settling phase. The wastage rate from each reactor was varied based on the MLVSS concentration, but the average daily wastage over the 5d SRT was 1.76 $L \cdot d^{-1}$ and 2.35 $L \cdot d^{-1}$ for the CMAS and SBR, respectively. For the 10 d SRT, the average wastage was 0.66 $L \cdot d^{-1}$ for the CMAS and 1.21 $L \cdot d^{-1}$ for the SBR.

Both reactors were routinely tested to verify and maintain steady operating conditions. The total (TSS) and volatile suspended solids (VSS) were monitored in the mixed liquor and effluent, and the SVI and effluent COD were measured, all in accordance with the Standard Methods (APHA et al., 2005). The effluent was not filtered prior to COD determination, however the effluent soluble COD was estimated by correcting for the COD content of the effluent VSS. The VSS was assumed to contain 1.42 $mgCOD \cdot mgVSS^{-1}$, in accordance with the literature (Rittmann and McCarty, 2001); that stoichiometric factor was validated by comparison of filtered and non-filtered effluent samples (data not shown). The influent and effluent flow rates, pH, and dissolved oxygen concentration in the reactors were also monitored. In addition, the initial settling velocity (ISV) of the sludge interface was determined by pouring 1 L of mixed liquor, taken directly from the reactor, into a 1 L graduated cylinder and measuring the distance traveled by the sludge interface after 3 min. The 3-min time interval was

www.manaraa.com

selected solely based on experimental trials, and was sufficient to permit the establishment of a distinct sludge blanket underlying a clarified zone, but not for hindered settling to be perceptible.

3.2.1 CMAS Kinetic Parameter Estimation

Estimation of kinetic parameters provides quantitative analysis based on experimental results which can be used as a means to assess the treatment capabilities of a biological community or as potential predictive tools for simulations and modeling. The kinetic parameters are not typically estimated from full scale in-situ measurements, but instead, researchers often utilize respirometric techniques in which oxygen uptake data is coupled with substrate utilization (Goudar & Ellis, 2001). The Monod kinetic parameters can then be approximated through the use of regression analysis. Viessman and Hammer (2004) outline a previously developed procedure for estimating kinetic parameters from a CMAS reactor. Using the mass balance presented as Eq. 2-10 and incorporating the assumptions that X_o is zero and the system is at steady-state with constant volume, Eq. 2-10 can be rewritten as follows:

$$\frac{Q_w X_w - Q_e X_e}{V} = r_g - r_d \tag{3-1}$$

Substituting Eq. 2-6 and Eq. 2-7 for r_g and r_d, respectively, and dividing by X results in:

$$\frac{Q_w X_w - Q_e X_e}{VX} = \mu_m \frac{S_S}{K_S + S_S} - b \tag{3-2}$$

Further recognition that the left side of the Eq. 3-2 is the inverse of Eq. 2-5, Eq. 3-2 can be rewritten as:

www.manaraa.com

$$\frac{1}{\theta_C} = \mu_m \frac{S_S}{K_S + S_S} - b \tag{3-3}$$

where θ_C is the SRT. Finally, letting k equal μ_m/Y, the resulting linear equation takes the form of:

$$\frac{1}{\theta_C} = Y \frac{kS_S}{K_S + S_S} - b \tag{3-4}$$

Veissman and Hammer (2004) point out that the specific substrate utilization rate, U $[t^{-1}]$, can be determined from experimental data as:

$$U_{meas} = \frac{(S_O - S_S)}{\tau X} = \frac{kS_S}{K_S + S_S} \tag{3-5}$$

where τ is the HRT [t], or simply the flowrate through the system divided by the reactor volume. Therefore, Eq. 3-4 is simplified to the common y = mx + b linear form by substituting U, with the slope being equal to the growth yield, Y, and the y-intercept is then equal to the decay coefficient, b. Experimental data for the initial and final substrate concentration was then used to calculate the experimental U_{meas}. Linear regression was performed on the data to calculate Y and b based on the plot of $1 \cdot \theta_C^{-1}$ versus U_{meas}. Inverting Eq. 3-5 results in another linear form that allows for the estimation of k and Ks. The values for k and Y can then be used to calculate μ_m for the biogenic substrate.

$$\frac{1}{U_{meas}} = \frac{K_S}{k}\frac{1}{S_s} + \frac{1}{k} \tag{3-6}$$

For the SOC specific kinetic parameters, a similar approach was used, except the abiotic removal mechanisms and the competent biomass had to be approximated. Grady et al. (1997) present a simplified method for estimating the contribution of abiotic mechanisms to the removal of SOCs by determining a dimensionless abiotic loss

www.manaraa.com

coefficient which is based on the theoretical ratio of the reduction in capable biomass due to abiotic mechanisms to the concentration of capable biomass that would result from SOC biodegradation if there was no abiotic removal. The resulting equation developed by Grady et al. (1997) took the form:

$$\gamma = \frac{K_L a \cdot S_S + \frac{k_p \cdot S_S \cdot X_T}{\theta_C}}{\frac{1}{\tau}(S_O - S)} \tag{3-7}$$

where γ is the fraction of SOC removal attributable to abiotic losses. The authors further simplify the equation by substituting α, the dimensionless abiotic loss coefficient.

$$\alpha = \alpha_V + \alpha_S \tag{3-8}$$

where

$$\alpha_V = K_L a \cdot \tau \tag{3-9}$$

and

$$\alpha_S = \frac{k_p \cdot X_T}{\theta_C} \cdot \tau \tag{3-10}$$

Substituting α into Eq. 3-7 and rearranging the equation gives:

$$\gamma = \frac{\alpha\left(\frac{S_S}{S_O}\right)}{\left(1 - \frac{S_S}{S_O}\right)} \tag{3-11}$$

Since γ represents the fraction of SOC attributable to abiotic removal, it can be substituted into the specific substrate utilization rate equation as follows:

$$U_{meas} = \frac{Q_O(S_O - S)(1-\gamma)}{VX} \tag{3-12}$$

www.manaraa.com

Using Eq. 3-12 in place of Eq. 3-5 to calculate U_{meas} in the previously outlined parameter estimation technique allows for estimation of the biodegradation kinetic parameters corrected for abiotic removal.

Magbanua et al. (1998) express the importance of accurate information about the competent biomass concentration in process simulations. The authors point out the commonly applied assumption that the competent biomass concentration should be directly proportional to the ratio of CODs of the SOCs to the total feed COD.

$$\frac{X_{Ai}}{X_T} = \frac{S_{Oi}}{S_{OT}} \tag{3-13}$$

where X_{Ai} is the active biomass for constituent i, X_T is the total biomass concentration, S_{Oi} is the initial feed concentration of SOC i and S_{OT} is the total initial organic substrate concentration, with S best expressed in terms of chemical oxygen demand, COD. However, as part of their research the authors applied substrate-specific most probable number (MPN) microtechniques to approximate the competent biomass using the following ratio:

$$\frac{X_{Ai}}{X_T} = \frac{MPN_i}{MPN_{R2A}} \tag{3-14}$$

where MPN_i is the MPN value determined from the SOC-specific growth media, and MPN_{R2A} is the MPN value from the non-specific heterotrophic bacteria growth media. From the authors' findings, it was determined that the use of the influent feed ratio often tended to underestimate the percentage of active biomass as compared to the MPN ratios. However the authors concluded that utilizing MPN microtechniques, which requires significant effort and introduces inherent variability, is not a realistic approach for each

www.manaraa.com

system studied. The authors further stated that due to the importance of having accurate biomass concentrations, the use of influent SOC ratios is a more realistic assumption than not having any correction for active biomass. In order to simplify the current work, the commonly applied assumption represented by Eq. 3-13 will be used in this work to approximate the competent biomass.

3.2.2 SBR Kinetic Parameter Estimation

Due to the cyclic nature of SBRs, extracting kinetic parameters should be accomplished by analyzing time-concentration data over the react period. During the react period, there is no discharge and the substrate and biomass concentrations are not steady state. Therefore, the mass balance equations remain as differential equations. For the non-SOC biomass mass balance, Eq. 2-10 reduces to:

$$\frac{d(X)}{dt} = r_g - r_d \tag{3-15}$$

For the substrate mass balance, during the SBR react cycle Eq. 2-11 reduces to:

$$\frac{d(S_s V)}{dt} = -r_{bio} \tag{3-16}$$

However due to the inherent difficulty of time dependent data collection in an SBR over multiple batches, especially in respect to SOC sampling protocols, the data collected for the SBR in this experiment was only based on initial and final values similar to the CMAS data. In order to estimate the kinetic parameters, numerical techniques were used to approximate the final measured concentrations of X and S based on the initial values at the start of the react period. Therefore, obtaining estimates of the kinetic parameters from the collected data required several key assumptions to simplify the estimation

www.manaraa.com

process. Based on the sampling procedures used, effluent and wastage was analyzed to provide solids information, and effluent data was collected regarding COD and SOC concentrations. However, the initial concentrations at the start of the react cycle were not measured. In order to estimate the initial solids concentration, it was assumed that the final biomass concentration, X_f, was constant over two successive react cycles. In other words, the cycle prior to the cycle in which measurements were taken was assumed to have the same final biomass concentration as the cycle in which measurements were taken. This allows for an approximate initial biomass concentration to be calculated based on the following equation.

$$V_O X_O = V_f X_f - V_W X_W - V_e X_e \tag{3-17}$$

where the subscripts o,f,w, and e represent initial, final, wastage, and effluent, respectively. V_O is equal to V_f, which is 15L, and X_f equals X_W, due to the sample wasting at the end of the react cycle.

This same approach can be used to estimate the initial COD concentration by substituting S in the place of X. In considering S, however, two additional assumptions were required. The first was that no additional substrate removal occurred during the settling period, such that the effluent concentration was equal to the concentration at the end of the react cycle. The second assumption was that the fill time was negligible, such that no substrate removal occurred during the fill time.

$$V_O S_O = V_f S_f - V_W S_W - V_e S_e + V_I S_I \tag{3-18}$$

where I represents the influent. Recognizing that based on the first assumption $S_f = S_W = S_e$ and that since half the volume is replaced each cycle then $V_f - V_W - V_e = V_I = ½ V_O$,

www.manaraa.com

at t = 0 the concentration would ultimately be equal to the average of the initial influent concentration and the residual effluent concentration.

Utilizing these assumptions to estimate the initial concentrations, the 4th order Runge-Kutta method was used to numerically integrate the differential mass-balance equations. The kinetic parameter estimates were taken as the values that minimize the objective function based on the errors associated with both substrate and biomass concentration at the end of the react period (Kesavan & Law, 2005):

$$q = \sum_{i=1}^{n}(S_{meas} - S_{calc})^2 + \sum_{j=1}^{n}(X_{meas} - X_{calc})^2 \tag{3-19}$$

Kesavan and Law (2005) suggest that the S and X values should be dimensionless values normalized by a constant of a similar magnitude to S and X, respectively. The authors recommend using the initial concentrations as the normalizing constants but note that the actual value of the constants used do not affect the results. For this research, the average effluent S and wastage X were the constants used. Because S and X are interdependent, the multi-variable 4th-order Runge-Kutta was used as outlined below:

$$a_{j,n} = f_j(x_{1,n}, x_{2,n}, \ldots, x_{m,n}) \tag{3-20}$$

$$b_{j,n} = f_j\left((x_{1,n} + \tfrac{h}{2}a_{1,n}), (x_{2,n} + \tfrac{h}{2}a_{2,n}), \ldots, (x_{m,n} + \tfrac{h}{2}a_{m,n})\right) \tag{3-21}$$

$$c_{j,n} = f_j\left((x_{1,n} + \tfrac{h}{2}b_{1,n}), (x_{2,n} + \tfrac{h}{2}b_{2,n}), \ldots, (x_{m,n} + \tfrac{h}{2}b_{m,n})\right) \tag{3-22}$$

$$d_{j,n} = f_j\left((x_{1,n} + hc_{1,n}), (x_{2,n} + hc_{2,n}), \ldots, (x_{m,n} + hc_{m,n})\right) \tag{3-23}$$

$$x_{j,n+1} = x_{j,n} + \tfrac{h}{6}(a_{j,n} + 2b_{j,n} + 2c_{j,n} + d_{j,n}) \tag{3-24}$$

with the above equations applied to each variable j = 1,…,m. The time step, h, was selected to be 0.25 min, and the numerical integration was applied for t = 0 min to t = 300

www.manaraa.com

min to represent one full 5 h react cycle. This method was used to provide an estimate of the kinetic parameters when no SOCs were present.

When SOCs are incorporated into the system, the loss due to volatilization and adsorption must be considered for the mass balance of individual SOCs. It should be noted that since no wastage occurs until the end of the react cycle, it can be assumed that the S is sufficiently low as to reduce the loss due to adsorption to a negligible percentage. However, chemicals that adsorb to the biomass will ultimately affect the rate of biodegradation, because over the react cycle the total amount of substrate in the system is not available in solution. In order to track the total mass of SOC present in the reactor, the mass can be approximated as:

$$M_{SOC} = S_{SOC}V + k_P S_{SOC} X_T V \tag{3-25}$$

where M_{SOC} is the total mass of a specific SOC in the reactor. Differentiating this equation gives:

$$\frac{d}{dt}\frac{M_{SOC}}{V} = \frac{dS_{SOC}}{dt} + k_P\left(X_T\frac{dS_{SOC}}{dt} + S_{SOC}\frac{dX_T}{dt}\right) \tag{3-26}$$

In order to fully track the mass balance of the SOCs in the react phase of the SBR, the right side of Eq. 3-26 should be set equal to the right side of Eq. 3-16 with the volatilization term added back and the right side divided by the reactor volume to have consistent units.

$$\frac{dS_{SOC}}{dt} + k_P\left(X_T\frac{dS_{SOC}}{dt} + S_{SOC}\frac{dX_T}{dt}\right) = -\frac{r_{bio}}{V} - \frac{r_{vol}}{V} \tag{3-27}$$

Due to the limited data collected, specifically having only the effluent and wastage data, the ability to track the time-dependent processes in multiple phases over the

www.manaraa.com

react cycle presents a significant challenge. In order to simplify the process and enable estimation of the biodegradation kinetic parameters, several assumptions are required. Due to the more complex nature of the SBR kinetics, it was assumed that the total biomass concentration remained constant and was taken to be the total MLVSS measured in the wastage. Although this assumption does not take into account biomass growth over the react period, the biomass concentration in the wastage is likely at or near the maximum concentration reached during the react period, which allows for a conservative approximation of the kinetic parameters. This simplifies Eq. 3-27 to:

$$\frac{dS_{SOC}}{dt} = -\frac{1}{V(1+k_P X_T)}(r_{bio} + r_{vol}) \tag{3-28}$$

This equation incorporates the biodegradation rate expressed using Monod kinetics, but Kovarova-Kovar and Elgi (1998) report the use of a first order parameter fit in situations when the substrate concentration is low, which is the case with the SOCs in this experiment. The authors point out that any combination of μ_m and K_S will fit equally well and ultimately only the ratio of μ_m:K_S is significant at low substrate concentrations in a batch system. Therefore, the r_{bio} was assumed to be first order in respect to S and a rate constant, k_b, was the selected parameter for the SOC data analysis in the SBR.

$$r_{bio} = -k_b S X_a V \tag{3-29}$$

Another important assumption used to estimate the SOC specific kinetic parameters in the SBR was that the active biomass concentration, X_a, was constant over the react cycle. This is based on the noted condition from Goudar and Ellis (2001) which suggests that when the ratio of substrate to biomass is relatively low then cell growth is minimized. The active biomass concentration was estimated based on the wastage

www.manaraa.com

MLVSS concentration and was assumed directly proportional to the influent feed ratio as indicated in Eq. 3-13. When the appropriate equations for r_{bio} and r_{vol} are then substituted into Eq. 3-28, using the assumed constant X_a, the equation reduces to a first order approximation which can be integrated and solved analytically:

$$S_{SOC} = S_O e^{-K \cdot t} \tag{3-30}$$

where

$$K = \frac{k_b X_a + K_L a}{1 + k_p X_T} \tag{3-31}$$

Using Eq. 3-30, the SOC concentration in the SBR can be estimated as a function of time, and the effluent SOC concentration may be approximated by solving for t = 300 min. The kinetic parameter, k_b, was selected such that objective function was minimized. Since biomass was assumed constant, only the substrate terms in Eq. 3-19 were used.

3.2.3 Experimental K_La Determinations

In order to estimate the removal of SOCs due to volatilization, the K_La for oxygen transfer had to be experimentally approximated for each reactor to allow the use of Eq. 2-14 to determine the K_La for SOC volatilization. This determination was based on the rate of oxygen transfer using the dissolved oxygen balance presented by Mineta el al. (2011):

$$\frac{dC}{dt} = OTR - OUR \tag{3-32}$$

or

$$\frac{dC}{dt} = K_L a(C^* - C) - r_{O2} \tag{3-33}$$

www.manaraa.com

where OTR is the oxygen transfer rate and OUR is the oxygen uptake rate by the biomass, represented by r_{O2} . C^* is the saturated DO concentration, which is primarily a function of temperature, pressure, salinity and specific conductance of the water. Rearranging and integrating Eq. 3-33 results in the following derivations:

$$\int_{C_o}^{C} \frac{dC}{\left(C - C^* + \frac{r_{O2}}{K_L a}\right)} = (-K_L a)\int_0^t dt \tag{3-34}$$

$$\ln\left(\frac{C - C^* + \frac{r_{O2}}{K_L a}}{C_O - C^* + \frac{r_{O2}}{K_L a}}\right) = (-K_L a)t \tag{3-35}$$

$$C = C^* + \frac{r_{O2}}{K_L a} + (C_O - C^* + \frac{r_{O2}}{K_L a})e^{(-K_L a)t} \tag{3-36}$$

$$C = (C^* - \frac{r_{O2}}{K_L a})(1 - e^{(-K_L a)t}) + C_O e^{(-K_L a)t} \tag{3-37}$$

Using Eq. 3-37, the DO concentration is a function of time. In order to approximate $K_L a$ in the CMAS, the DO concentration was monitored as a function of time using a DO meter (Yellow Springs Instruments, Ohio) interfaced with a laboratory computer to record the DO concentration every 15 s. However, if the feed was allowed to pump every 30 min as originally set up the dissolved oxygen would present a cyclic profile due to the increased OUR as a result of the influent COD, as the representative DO profile from the CMAS in Figure 3.9 indicates.

www.manaraa.com

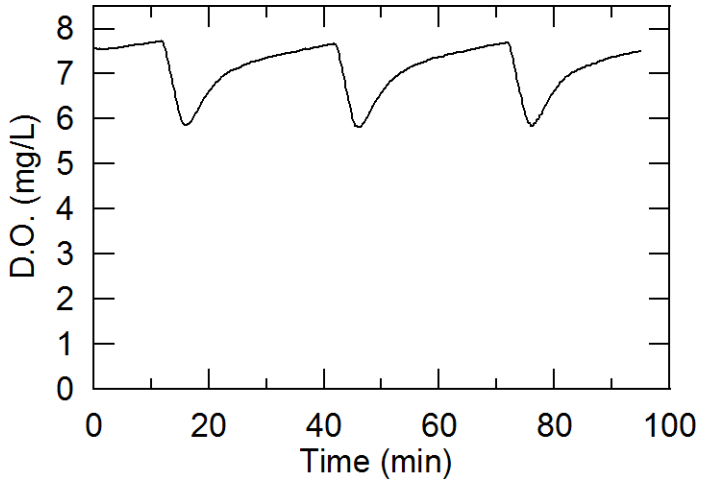

Figure 3.9 Representative dissolved oxygen profile with intermittent feed cycle in the CMAS reactor.

Therefore in order to perform K_La determination tests in the CMAS, the feed and all wastage were discontinued to allow the DO to approach a constant value. Once the DO was stable, the aeration equipment was shut down and the mixing was turned down to a minimal amount required to maintain the solids in suspension. Under these conditions, the OTR is assumed to be zero and thus Eq. 3-33 reduces to a first order equation.

$$\frac{dC}{dt} = -r_{O2} \tag{3-38}$$

If r_{O2} is assumed to be constant over this short time period, then the straight line equation presented as Eq. 3-39 can be best-fit to the measured DO data to determine a value for r_{O2}.

$$C = C_O - r_{O2}t \tag{3-39}$$

Linear regression was performed on the CMAS DO data over the time when aeration was discontinued to estimate r_{O2}. With a value for r_{O2}, the aeration equipment was returned to

www.manaraa.com

normal operational settings and Eq. 3-37 was used to determine a K_La value. This was done with a Solver routine in Excel, in which K_La and C^* were selected to minimize the sum of the residual error between the measured DO concentrations and the calculated DO concentrations. Figure 3.10 provides a representative curve fit for the determination of K_La.

In the SBR reactor, a similar method was used to determine K_La. However, since the SBR DO concentration would not reach a steady-state value until near the end of the react period, as indicated by the representative SBR DO profile in Figure 3.11, an adjustment in the data was required to approximate K_La for the SBR.

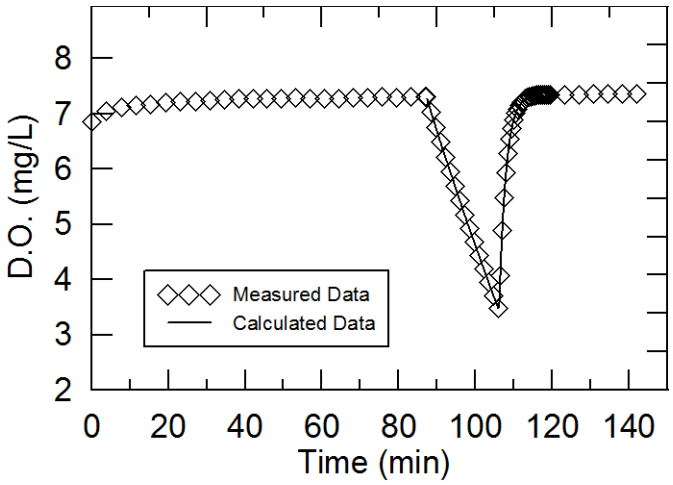

Figure 3.10 Curve fit for K_La estimation in the CMAS reactor.

www.manaraa.com

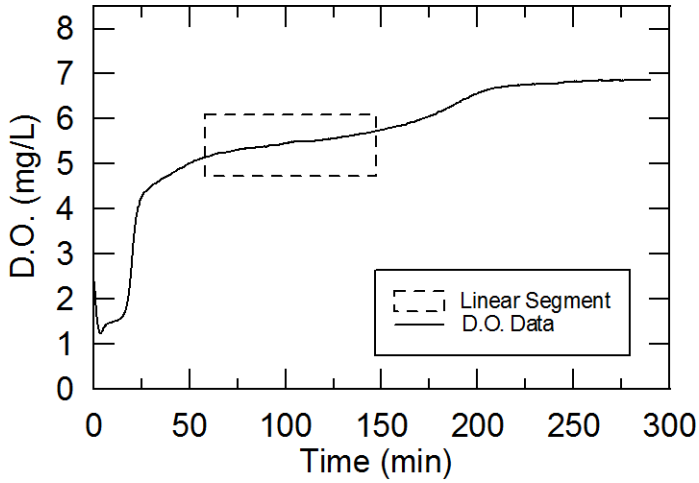

Figure 3.11 Dissolved oxygen profile in the SBR.

As Figure 3.11 indicates, the region outlined as the linear segment is a period during the react cycle when the rate of change in the DO approaches a constant value, and although OTR does not equal OUR, OTR minus OUR is approximately constant. Over multiple evaluations of the SBR reactor, this linear region would consistently occur in the range of approximately 60 to 150 min, which would allow ample time to conduct the K_La determination. In order to perform the K_La approximations, the DO data over this range was normalized to the rate of change, such that a horizontal DO profile was generated, and the curve fit was conducted on the slope-corrected DO data as indicated in Figure 3.12.

www.manaraa.com

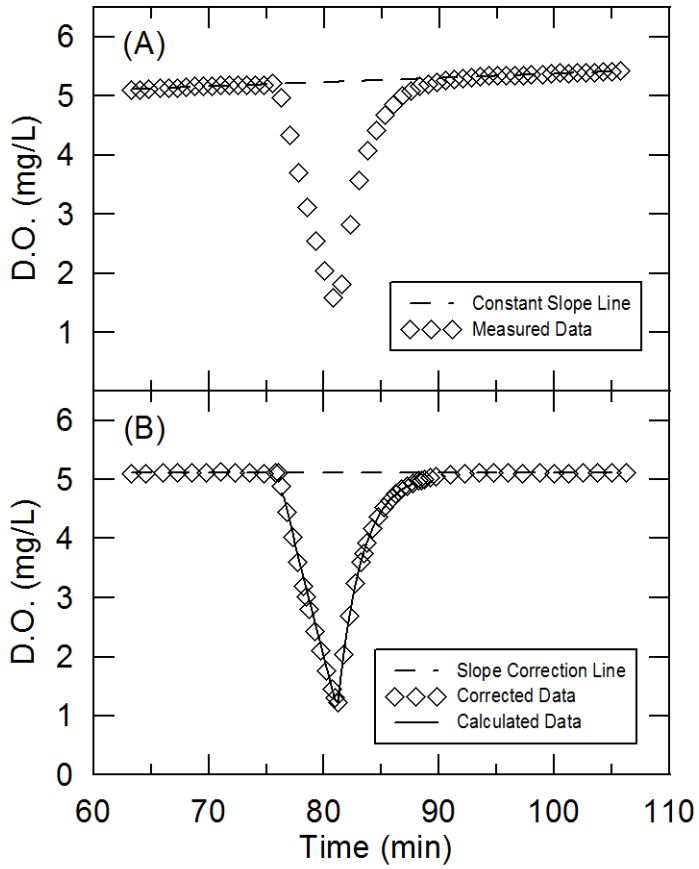

Figure 3.12 (A) Representative plot of measured SBR DO profile with constant slope. (B) Representative plot of slope-corrected data and K_La estimation curve-fit.

www.manaraa.com

With these approximations for K_La for oxygen transfer in both the CMAS and the SBR, the K_La for specific SOCs was then approximated based on the ratio of diffusion coefficients using Eq. 2-14. The diffusion coefficients, D, were estimated using the correlation developed by Wilke and Chang (1955):

$$D = 7.4\times10^{-8}\frac{(xM)^{0.5}T}{\eta V_m^{0.6}} \tag{3-40}$$

where D is in $cm^2\cdot s^{-1}$, x is the association parameter for the solvent presented by Wilke and Chang to be 2.6 for water, M is the molecular weight of the solvent in $g\cdot mol^{-1}$, T is temperature in Kelvin, η is the viscosity of the solvent in centipoise, and V_m is the molar volume of the solute at normal boiling point in $cm^3\cdot mole^{-1}$. Inputting the parameters for water as the solvent and the given experimental conditions, the equation is simplified to a function of molar volume of the solute:

$$D = \frac{1.593\times10^{-4}}{V_m^{0.6}} \tag{3-41}$$

From this equation, the diffusivities of the SOCs were calculated, and the resulting ratios where used in Eq. 2-14 to determine the specific SOC K_La values used in the parameter estimation. V_m for oxygen was taken as 25.6 (Wilke & Chang, 1955). The V_m for each of the SOCs was determined from the ideal gas law:

$$\frac{(V_m)_1}{(V_m)_2} = \frac{T_1}{T_2} \tag{3-42}$$

where $(V_m)_2$ is the molar volume at the normal boiling point, T_2 in Kelvin, and $(V_m)_1$ is the molar volume at standard temperature, T_1 = 293.16 K. Therefore, $(V_m)_1$ was taken as the manufacturer reported molecular weight divided by the density for each SOC.

www.manaraa.com

3.3 Molecular Analysis

A major focus of this study is to determine how the AS community transitions as a function of the specific SOCs that are incorporated into the influent waste stream and as the operational treatment strategies are varied. Molecular techniques are a primary tool used in this study to assess the variations of the bacterial populations in response to changing reactor conditions. Direct DNA extraction from the AS community coupled with PCR amplification and direct gradient gel electrophoresis should be a viable method of comparing the genetic fingerprints of the microbial population as changes to the treatment system operations are introduced.

3.3.1 DNA Extraction

Several researchers have demonstrated that direct extraction from the microbial sample allows for a less selective extraction which elutes more than 90% of the species present in the environmental sample (Watanabe et al., 1998; Widada et al., 2002). In order to extract the DNA from our AS reactors, we utilized the UltraClean™ microbial DNA isolation kit (Mo Bio Laboratories, Inc., Carlsbad, California). Due to the larger sediment content and floc aggregation of the AS samples, lower than expected yields were extracted following the kit's original protocol, shown in Appendix A; therefore, the protocol was modified. In the modified protocol, also presented in Appendix A, the sample was initially concentrated to generate an initial sludge mass between 2 and 5 grams. This was done by taking two 2-mL samples from each reactor, centrifuging, removing the excess supernautant, and combining the sludges from the same reactor into one microfuge tube. This range was experimentally determined to yield enough DNA

www.manaraa.com

(>100 $ng \cdot mL^{-1}$) while not over-concentrating the sample such that processing was too challenging during the phase-separation steps due to the high solids content. Over the course of running the reactors, however, the sludge concentrations occasionally would exceed 2.5 $g \cdot L^{-1}$ and would require taking one 2-mL sample as opposed to taking two and concentrating them in the initial step. The other modifications include inverting the samples instead of vortexing to maintain the length of the DNA strands and increase yield, and instead of using a horizontal vortex adaptor during the lysis phase, the samples were processed using the Disruptor Genie™ cell disruptor (Scientific Industries, Inc., Bohemia, New York). The Mo Bio kit primarily uses microspin filters to trap the genetic material once the cells are lysed, and the DNA was washed to remove proteins and other impurities. Finally, the DNA was eluted from the filter with the appropriate buffer solution, labeled MD5 in the kit. After the DNA was extracted, it was quantified in $ng \cdot \mu L^{-1}$ using the NanoDrop® ND-1000 spectrophotometer (NanoDrop Technologies, Inc., Wilmington, Delaware). The DNA was then stored at -20 °C for downstream processing.

3.3.2 Polymerase Chain Reactions

Polymerase chain reaction (PCR) technology is an important part of the molecular analysis process. PCR is used to selectively amplify a sequence of interest from the extracted DNA so that the bands would be visible on the DGGE gel. PCR-DGGE of ribosomal DNA from environmental samples without the use of selective enrichment cultures was introduced by Muyzer et al. (1993). Since that time, it has become a well-established investigative technique for analyzing the diversity of a microbial population

www.manaraa.com

from numerous environments and is often used to determine the community dynamics in response to environmental variations (Ercolini, 2004). For PCR to be successful, an appropriate primer must be selected and the PCR conditions must be optimal for the given region.

When amplifying via PCR, an appropriate genetic region must be selected that is similar across a range of bacteria, but also has unique sequences within the region that allow for differentiating between species. As indicated previously in Table 2.2, several studies have been conducted using PCR amplification of environmental populations, including AS communities. The fragments used in this study will be derived from the amplification of 16S rDNA genes from genomic DNA extracted directly from the activated sludge (Muyzer et al., 1993). The primers used in this study will also incorporate a GC-clamp which is commonly used to insure that the DNA fragment will remain partially double-stranded and the region being screened is part of the lowest melting domain (Ercolini, 2004). The primers that were ultimately selected are presented in Table 3.2 which is adapted from a compilation of primers presented by Nakatsu et al. (2000). The primers were synthesized by Integrated DNA Technologies (Coralville, Iowa).

www.manaraa.com

Table 3.2

PCR primers for specific amplification of 16S rDNA genes.

Primer	16S rDNA target (base number)[a]	Primer Sequence
PRBA338F	Bacteria V3 Region (338-358)	5' [b]AC TCC TAC GGG AGG CAG CAG 3'
PRUN518F	Universal V3 Region (534-518)	5' ATT ACC GCG GCT GCT GG 3'
PRBA968F	Bacteria V6 Region (968-983)	5' [b]AA CGC GAA GAA CCT TAC 3'
PRBA1406R	Bacteria V6 Region (1406-1392)	5' ACG GGC GGT GTG TAC
PARCH340F	Archea V3 Region (340-358)	5' [b]CC TAC GGG GC/TG CAG/C CAG 3'
PARCH519R	Archaea V3 Region (534-519)	5' TTA CCG CGG CG/TG CTG 3'

[a]Bases numbered relative to E. coli 16S rRNA sequence.
[b]GC clamp added to the 5' end of the primer,
5' CGC CCG CCG CGC GCG GCG GGC GGG GCG GGG GCA CGG CGG G 3'

The amplification mixture in this study had a final volume of 50 µL and contained 25 pmol each of forward and reverse primer, 200 µM of each dNTP, 2.5 units of Taq HS polymerase, 5 µL 10X PCR buffer (dNTPs, Taq, and buffer supplied by Takara Bio Inc., Otsu, Shiga, Japan). The PCR buffer consists of 100 mM Tris-HCl (pH 8.3), 500 mM KCl, and 15 mM $MgCl_2$. The amount of template varied due to the variance in the extracted DNA yield, however it was diluted to approximately 50 ng of template per reaction. The PCR reaction was performed in an Eppendorf Mastercycler® (Eppendorf North America, Westbury, New York), with an initial denaturation step at 94 °C for 9 min, followed by 30 cycles of 94 °C for 30 sec, 55 °C annealing for 30 sec, 72 °C extension for 30 sec, and a final extension at 72 °C for 7 min. Presence of PCR products

www.manaraa.com

was confirmed by electrophoresis on a 2%-agarose gel stained with ethidium bromide. The gel was run for 1 hr at 100V.

3.3.3 Direct Gradient Gel Electrophoresis

Perpendicular DGGE was performed using the D-Code Universal Detection System (Bio-Rad Laboratories, Hercules, California). A 7.5 % polyacrylamide gel was cast using the Bio-Rad gradient delivery system and it contained a gradient of denaturant from 35 % to 75 % (100 % denaturant is 7 M urea and 40 % deionized formamide). DGGE was run at 100 V for 17 hours at 60 °C in 0.5X TAE electrophoresis buffer. The gel was stained for 15 min with EtBr and destained for 30 min with DI water. Gel images were captured and stored using the Syngene GeneGenius Bio Imaging System and associated GeneSnap software (Synoptics, Inc., Frederick, Maryland). Statistical analysis of the gels was conducted using additional Syngene software, including GeneTools and GeneDirectory. In order to compare across multiple DGGE gels, standard lanes, which should form the same banding patterns under consistent DGGE conditions, were run in parallel to the samples (Van der Gucht et al., 2001). Using GeneDirectory, dendrograms were obtained by unweighted pair group method average (UPGMA) based on the Dice similarity coefficient of the banding patterns. A 1% tolerance was used.

3.3.4 Diversity Indices

In addition to comparison of the DGGE community profiles, multiple diversity indices were used to describe and compare between individual samples. The Shannon

www.manaraa.com

(H), Simpson (D), and Evenness (E) indices were used, which are calculated as follows:

$$H = -\sum_{i=1}^{n} p_i \ln(p_i) \tag{3-43}$$

$$D = \sum_{i=1}^{n} p_i^2 \tag{3-44}$$

$$E = \frac{\sum_{i=1}^{n} p_i \ln(p_i)}{\ln(S)} = \frac{H}{H_{MAX}} \tag{3-45}$$

where p_i is the relative intensity of the i^{th} band and S is the species richness, or total number of bands in a given lane, which is also used as an indicator of diversity between samples. The Simpson index is reported as D′ = 1/D, such that D′ and H will increase with an increase in diversity. E, a measure of community variation, is constrained between 0 and 1 with a higher E indicating less variation within the community. The diversity indices were included in additional statistical analysis using SAS 9.2 for Windows (SAS Institute Inc., Cary, NC). The GLM procedure was used with the MEANS procedure and the Tukey-Kramer method to determine if there were statistically significant differences ($\alpha < 0.05$) in the diversity values and other measured reactor performance parameters based on the three class variables: (1) reactor configuration, (2) presence of SOCs, and (3) SRT. Spearman's rank correlation method was used to evaluate the correlation between the diversity indices and the selected treatment performance parameters.

3.4 Microscopic Floc Analysis

Microscopic image analysis of the floc morphology was another key focus of this research to determine if variations in the specified floc parameters exhibited statistically

www.manaraa.com

significant correlation with the incorporation of SOCs and other induced reactor operational changes. Microscopic image analysis (IA) is a tool that has been used recently in analyzing the AS community structure and in modeling the settleability of AS flocs (Araya-Kroff et al., 2004; Contreras et al., 2004; Grijspeerdt & Verstraete, 1997). Particles with a homogenous, regular shape can be specified using a single dimension, such as the diameter of a sphere or the side of a cube. Most particles, however, including AS floc particles, are often irregular and have an infinite number of linear dimensions (Allen, 1997). Consequently, comparisons must be based on relevant shape factors or size equivalents. In AS cultures with biomass concentrations between 0.5 – 4 $g \cdot L^{-1}$, the equivalent diameter (De), form factor (FF), aspect ratio (AR), and roundness (RD) exhibited a significant and reproducible correlation with the SVI and settling efficiency (Grijspeerdt and Verstraete, 1997).

3.4.1 Sample Preparation and Image Capture

Samples for microscopic IA were collected directly from the reactors by pipetting 100 µL of mixed liquor onto a 75 x 51 mm microscope slide and covering with a 45 x 50 mm cover slip. The samples were collected using an adjustable-volume, single channel pipette with a disposable tip that had been trimmed to create a larger mouth, since it is critical when conducting IA to maintain floc integrity and avoid disrupting floc morphology during sampling (Araya-Kroff et al., 2004). The large slide and cover slip were used because, on a standard slide, a large portion of the flocs would be pushed to the edges of the cover glass, artificially creating larger flocs. The larger slide also provided sufficient room such that sample dilution was not necessary. Previous research

www.manaraa.com

showed that a minimum of 150 objects are required to achieve statistically relevant results (Grijspeerdt & Verstraete, 1997). In this work, it was determined that 120 images would easily exceed this minimum quantity of objects and would allow for good coverage of the single slide without replication. Images were viewed using a phase-contrast microscope at a 40X total magnification with an accompanying CCD camera. Live images were transferred to the computer via a USB connection and were saved as bitmapped files for further processing.

3.4.2 Software development

Developing the software for image processing was an essential component to this research which allowed for automated analysis of a large quantity of floc images. Although the image capture was performed manually, the IA program made it possible to process the large number of floc images and efficiently evaluate the geometric properties of the flocs. Initially, manual processing took close to 1 h per sample, but with practice and increased proficiency, the typical processing time for each sample was reduced to less than 30 min. The program had to rapidly iterate several tasks for typically 120 to 130 image files per sample: access the file, convert the grey-scale image to a binary image, then calculate the geometric properties of each floc. The IA program was written in MATLAB (The MathWorks, Natick, MA) and called several functions from the MATLAB image processing toolbox. The program closely followed algorithms described in previous research (Contreras et al., 2004), in that it first determined a threshold grey level to differentiate the flocs from the background and generate a monochrome image which was then subjected to further processing.

www.manaraa.com

The original program that we attempted to use was created by Peter Rush, an undergraduate student in the Computer Science Department. This program, presented in Appendix B, utilized the bottomhat function in MATLAB and was helpful in analyzing individual images, but required user manipulation for each image depending on the contrast and connectivity of the image. However, the nature of our work required that multiple images be processed in rapid succession in order to give a representative estimate of a complete slide which could be more than 150 images. In order to process multiple images, a more standardized image processing program had to be written that would not require user input for each individual image. The new program would utilize the greythresh function in MATLAB to calculate the appropriate value within each image that would most effectively differentiate between the background and the flocs.

During the image processing program, several successive functions are called which manipulate the image into a format that can be used for final calculations of the AS flocs' shape and size. Then, the processing program is included into a loop function that is called for each image and stores the calculated values in an appropriate array. For an individual image the steps are outlined in Table 3.3. Floc morphology was assessed based on size and shape descriptors identified in previous research (Grijspeerdt & Verstraete, 1997). Floc size was quantified as the projected area (A) and the D_e. The IA program discretized flocs based on groups of connected pixels and counted the number of pixels in each floc. The individual pixel area was found to be 0.53 μm^2 by using an objective micrometer, and A was determined by multiplying the pixel area by the number of pixels in each floc. D_e was calculated from A using Eq. 2-17, shown previously. The FF, AR, and RD, described previously, were used as shape descriptors. The FF varies

www.manaraa.com

between 0 and 1, with a circle having FF = 1 and an infinitely thin line approaching zero. AR is minimum (=1) for an object that can be contained within a circle and increases as the object is elongated. RD is primarily influenced by the elongation, while the FF is influenced both by elongation and by the roughness of the perimeter. Similar to the DGGE analysis, the GLM procedure was used with the MEANS procedure and the Tukey-Kramer method to determine if there were statistically significant differences ($\alpha < 0.05$) in the measured variables based on the three class variables: (1) reactor configuration, (2) SRT, and (3) presence of SOCs. Spearman's rank correlation method was used to evaluate the correlation between the size and shape parameters and the performance parameters. The modified MATLAB code for floc image analysis is presented in Appendix B.

www.manaraa.com

Table 3.3

List of select MATLAB functions for image processing.

Action	MATLAB Command
Read image file into an array	I = imread('Filename')
Calculate an appropriate threshold to convert to a binary image	X = graythresh(I)
Convert to black and white image	Im = im2bw(I , X)
Define an appropriate structural element for image dialation	SE = strel('<shape>','<size>')
Dilate the pixels in the image to close any spaces	Im = imdialate(Im, SE)
Fill the any voids within a given floc	Im = imfill(Im , 'holes')
Erode the image edge back to original size	Im = imerode(Im, '<SE>')
Remove small debris and background noise	Im = bwareaopen(Im, '<size>')
Label and count individual images	(Im2 , Num) = bwlabel(Im)
Calculate the physical properties desired	Stats = regionprops('<desired>')

www.manaraa.com

The original image is captured using the video camera package attached to the microscope. The image is stored and converted into a numerical representation using MATLAB's imread function. Figure 3.13 is a sample image after being stored.

Figure 3.13 Original captured image.

Once the image is read into MATLAB, the graythresh function is used to compute a global threshold for the image so that it can be converted to a black and white image. Once the threshold level is computed, the image is converted to black and white using MATLAB's im2bw function which results in an image in which all pixels are given a value of either 1 (white) or 0 (black). Figure 3.14 is shows the image after the conversion to black and white.

www.manaraa.com

Figure 3.14 Image after conversion to black and white.

After the image is converted to black and white, an artificial border is placed around the image to remove the boundary lines on the original image and to make sure that any flocs that contact the boundary of the image are disconnected. Then, the pixel values are reversed (0 = 1 and 1 = 0) to improve the downstream dilation, filling, and erosion functions. Figure 3.15 illustrates the same image after inversion of the pixels. The individual white pixels are then dilated using an elongated structuring element to connect the pixels that are part of the same floc and to foster a more solid perimeter to aid in the filling process, as shown in Figure 3.16. Next, in Figure 3.17, the image is filled to encompass the projected surface area of each floc. The erosion function, imerode, is used to make the edges less rounded and more representative of the original floc shape (Figure 3.18).

www.manaraa.com

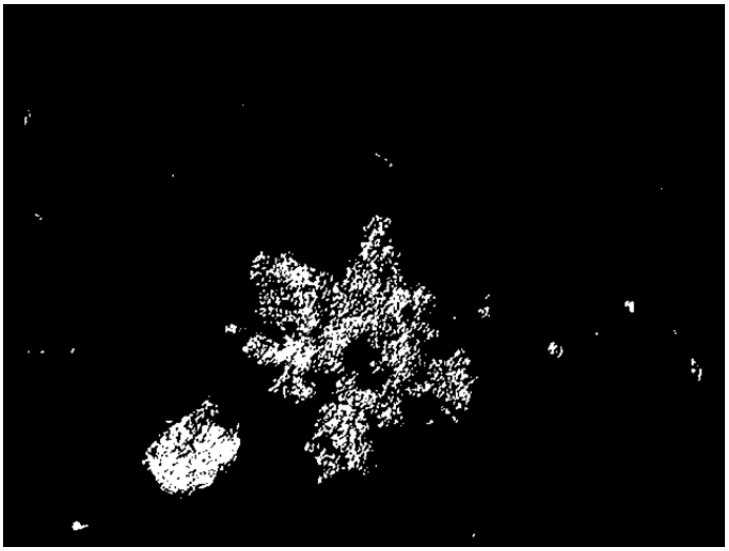

Figure 3.15 Image after addition of border and inversion of pixels.

Figure 3.16 Image after pixel dilation.

www.manaraa.com

Figure 3.17 Image after filling.

Figure 3.18 Image after erosion.

www.manaraa.com

Finally, the smaller particles are removed so that debris and broken floc matter does not skew the data towards smaller flocs. The final image now gives a black and white representation of the original image. This black and white image can be read into other MATLAB functions and the white pixels can be used to give a quantitative measurement for each individual floc. The pixels and their orientation within the image array can be used to calculate physical properties of the flocs. Ultimately, this image data can be statistically correlated to other reactor parameters and treatment capabilities. Figure 3.19 provides a comparison of the final image to the original image.

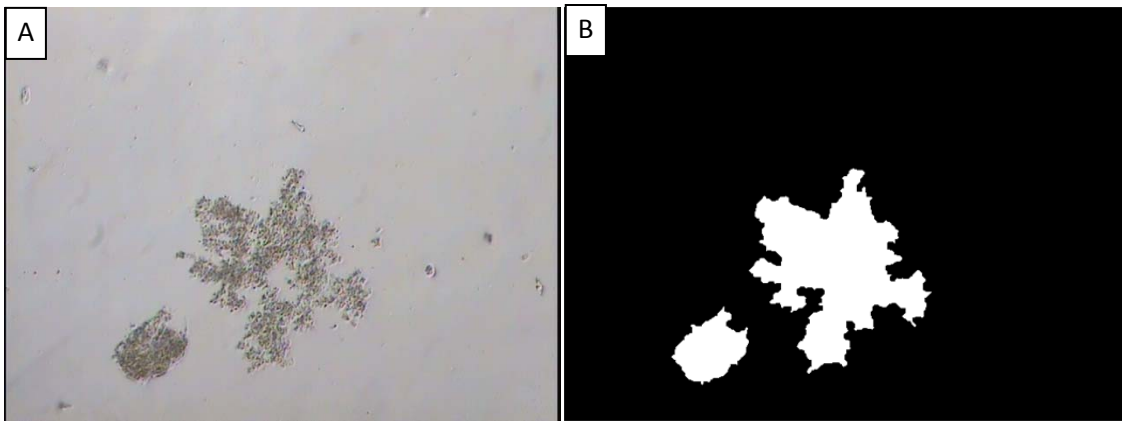

Figure 3.19 Representative sample of an original gray-scale image prior to image analysis (A) and monochromatic representation (B) used to determine size and shape parameters of the AS flocs.

www.manaraa.com

CHAPTER IV

RESULTS AND DISCUSSION

4.1 Reactor Performance

The lab-scale reactors were subjected to variations in operational conditions to assess the effects of these changes on the AS community. At start-up the reactors were operated with a 5 d SRT and no SOCs. Although the reactors had been in operation for several months prior, Day 0 was taken to be the day that all testing procedures were standardized and the reactors were online and functioning consistently. From this date, the SOCs were introduced on Day 72, the SRT was changed from 5 d to 10 d on Day 147, and the tests were concluded on Day 218. Period 1 (P1) refers to days 0 to 72, Period 2 (P2) refers to days 73 to 147, and Period 3 (P3) refers to days 148 to 218. Values of selected performance parameters for each reactor are presented in Table 4.1. Overall, both reactors were effective at utilizing soluble COD attaining average soluble COD removals of 95 % and 93 % for the SBR and the CMAS, respectively, when corrected for the effluent VSS contribution. When VSS is included in the effluent COD, removals were 89 % and 77 % for the SBR and the CMAS, respectively. The CMAS reactor, however, was not equipped with a weir or scum removal system so that any floating material was released in the effluent and would degrade the lab-scale performance vis-à-vis field performance. In contrast, wastage and effluent from the SBR

www.manaraa.com

were pumped from well below the surface and consequently excluded any floating material. Another important difference between the reactors was the provision of a separate clarifier for the CMAS. While both the SBR and the CMAS had identical reaction tanks, with a surface area of approximately 780 mm^2, the clarifier in the CMAS was only 380 mm^2.

It should be noted that the differences in effluent solids concentrations between the CMAS and SBR and their overall settling performance could possibly be attributed to the variations in the laboratory clarification processes of each reactor. The SBR was allowed to settle for approximately 1 hr prior to decanting the effluent. The CMAS settling time was controlled by the flow rate and sizing of the clarifier. The CMAS clarifier was 3 L, and although the flow through the clarifier varied slightly based on wastage flows drawn from the reactor, it averaged 27.4 $L \cdot d^{-1}$. This results in an average hydraulic residence time of 2.6 h in the clarifier. However, when you correct for the fact that the pumps only ran for approximately 14 $min \cdot h^{-1}$, the resulting peak flow rate is approximately 115.7 $L \cdot d^{-1}$ and the hydraulic residence time during periods of flow then becomes 0.6 h. The significantly higher flow rates through the CMAS clarifier and the resulting lower hydraulic residence times could have been a significant factor in the development of floc structures different than those of the SBR. In effect, the overflow rate of the clarifier was much higher than from the SBR. These factors could potentially explain, in part the difference in effluent VSS and total effluent COD between the two reactor configurations.

www.manaraa.com

المنارة للاستشارات

Table 4.1

Reactor performance parameters.

Reactor	Parameter	Units	Period 1	Period 2	Period 3	Overall	Significant Difference[a]
SBR	MLVSS	$mg \cdot L^{-1}$	2749 ± 522	3165 ± 335	4480 ± 982	3475 ± 1026	2,3; Y1,Y2,Y3; +
	VSS_{eff}	$mg \cdot L^{-1}$	42 ± 47	23 ± 7	31 ± 17	33 ± 31	Y2,Y3; +
	COD Removal	%	94 ± 1	95 ± 1	97 ± 2	95 ± 2	2,3;Y3; +
	SVI	$mL \cdot g^{-1}$	66 ± 20	104 ± 28	84 ± 24	83 ± 27	1,2; Y1,Y2,Y3; +
	ISV	$m \cdot s^{-1}$	0.00094 ± 0.00043	0.00032 ± 0.00018	0.00024 ± 0.00013	0.00053 ± 0.00043	1,2; Y1,Y2,Y3; +
CMAS	MLVSS	$mg \cdot L^{-1}$	2027 ± 248	1970 ± 359	2840 ± 517	2301 ± 557	2,3; Y1,Y2,Y3; +
	VSS_{eff}	$mg \cdot L^{-1}$	82 ± 45	88 ± 17	72 ± 21	80 ± 31	Y2,Y3; +
	COD Removal	%	94 ± 2	93 ± 2	92 ± 2	93 ± 2	Y2; +
	SVI	$mL \cdot g^{-1}$	34 ± 8	38 ± 5	56 ± 14	43 ± 14	2; Y1,Y2,Y3; +
	ISV	$m \cdot s^{-1}$	0.00172 ± 0.00012	0.00147 ± 0.00024	0.00109 ± 0.00040	0.00143 ± 0.00039	2,3; Y1,Y2,Y3; +

[a] 1, 2, and 3 indicate a statistically significant difference ($\alpha < 0.05$) between P1 and P2, P1 and P3, and P2 and P3, respectively. Y1, Y2, and Y3 indicate a significant difference between the two reactors for P1, P2 and P3, respectively. + indicates a significant difference in the overall averages between the two reactors during the experiment.

www.manaraa.com

Although the SRT was the same for both reactors, the MLVSS in the SBR was significantly higher than in the CMAS over the duration of the project (Figure 4.1). Throughout the project, the CMAS had a lower SVI and higher ISV compared to the SBR (Figure 4.2); these differences between the reactors were statistically significant in all three operational periods (Table 4.1). It is also evident that the SBR and CMAS respond differently to the variations in the reactor operational parameters. For the SBR, the ISV dropped rapidly after it entered P2, and then it remained somewhat consistent throughout the remainder of the experiment. Hence, the ISV during P2 and P3 did not differ significantly from one another, but were both significantly lower than in P1. The CMAS did exhibit an apparent trend towards lower ISV as the project progressed, however the change was much less pronounced and only showed a significant difference after the SRT was changed to 10 d. In reviewing the SVI data, the SBR has a higher SVI once the SOCs are incorporated, while the CMAS displayed a more consistent SVI for the duration of the project. The effluent VSS did not exhibit a statistically significant difference as a result of the variations in operational conditions of either reactor but did differ between reactors once SOCs were introduced. The only significant change in soluble COD removal occurred when the SRT was increased to 10 d, which resulted in a decreased effluent COD concentration from the SBR (Figure 4.1).

www.manaraa.com

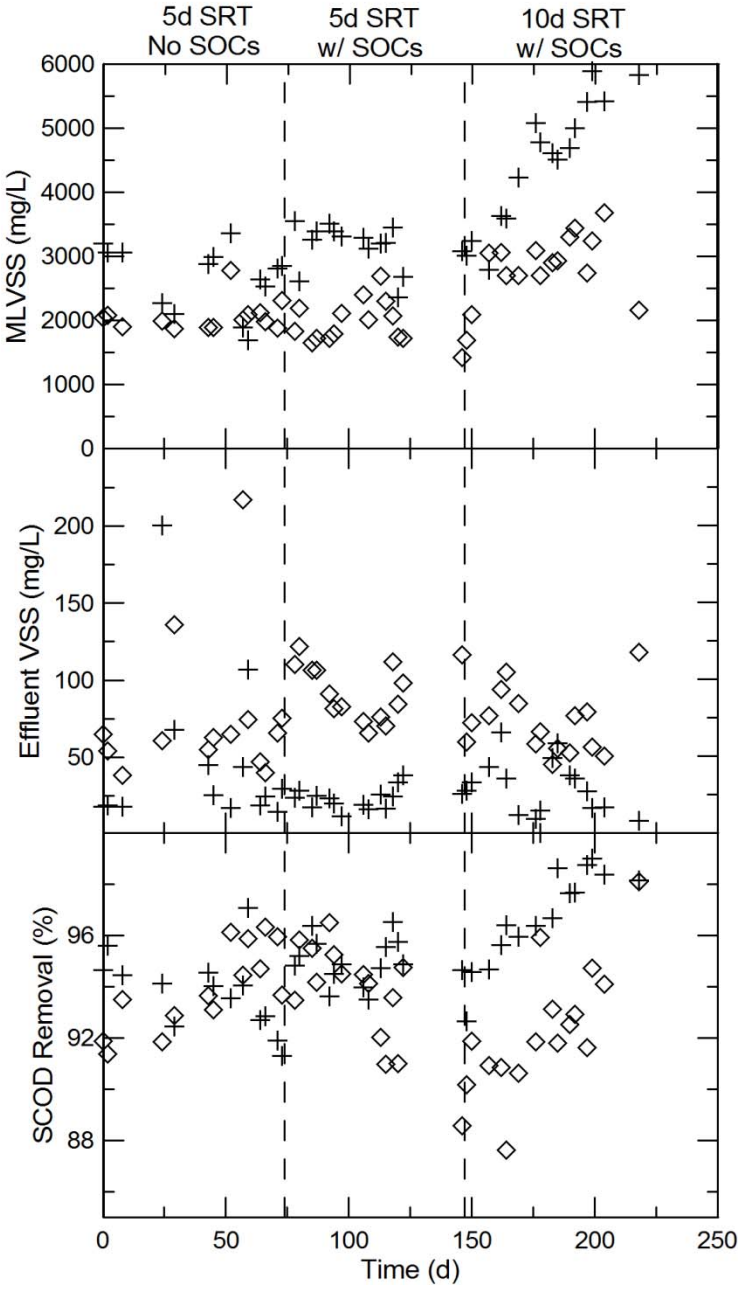

Figure 4.1 Solids concentrations and soluble COD removal percentage as a function of time and separated by reactor type. SBR = +, CMAS = ◊.

www.manaraa.com

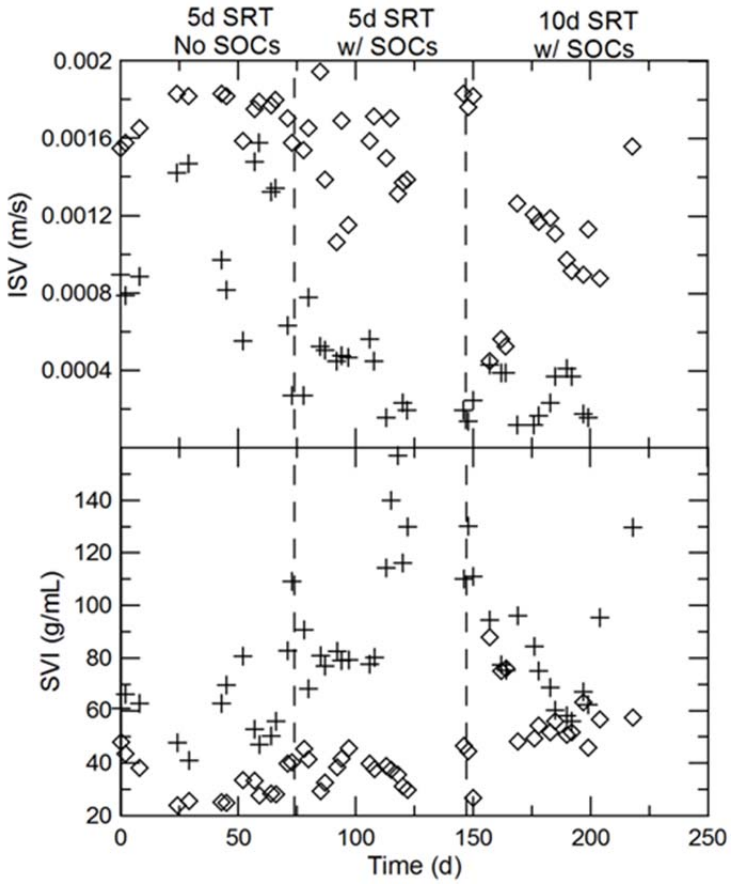

Figure 4.2 Settling parameters as a function of time and separated by reactor. SBR = +, CMAS = ◊.

www.manaraa.com

The effluent SOC concentrations are presented in Figure 4.3. The effluent results for acrylonitrile, chlorobenzene, and phenol were compared to the daily maximum limits for each. These limits were 242 $\mu g \cdot L^{-1}$, 28 $\mu g \cdot L^{-1}$, and 26 $\mu g \cdot L^{-1}$ for acrylonitrile, chlorobenzene, and phenol, respectively, as presented in 40 CFR 414 based on the best available technology (BAT) limits. The USEPA currently does not provide effluent regulations for MTBE, but numerous states have effluent guidelines that are in the 10^1-10^2 $\mu g \cdot L^{-1}$ range. For this comparison, a value of 100 $\mu g \cdot L^{-1}$ was taken as an acceptable level of treatment to evaluate the removal of MTBE. As Figure 4.3 indicates, phenol was effectively removed from both reactors, below the detection limit, after approximately 2 SRTs. The other SOCs had varying degrees of removal. Chlorobenzene was removed to levels below the BAT limit in the SBR in 97% of the samples taken and in all samples taken during P3. In the CMAS, chlorobenzene was removed below the BAT limit in only 71% of the samples taken, however in P3 the removal was below the BAT limit in all but one sample which was taken during the first week of the transition from 5d to 10d SRT. Acrylonitrile was not effectively removed by CMAS with only 16% of samples tested showing removal below the BAT limit. The SBR was moderately successful in the removal of acrylonitrile, providing removal below the BAT limit in 61% of the samples analyzed. Additionally, the SBR showed improved removal capabilities when the SRT was increased to 10d. MTBE was not removed successfully by either reactor configuration, with the effluent concentrations being below the established limit in only 6% and 25% of the samples tested for the CMAS and SBR, respectively. In the case of all chemicals, the SBR met the established limits more often than the CMAS.

www.manaraa.com

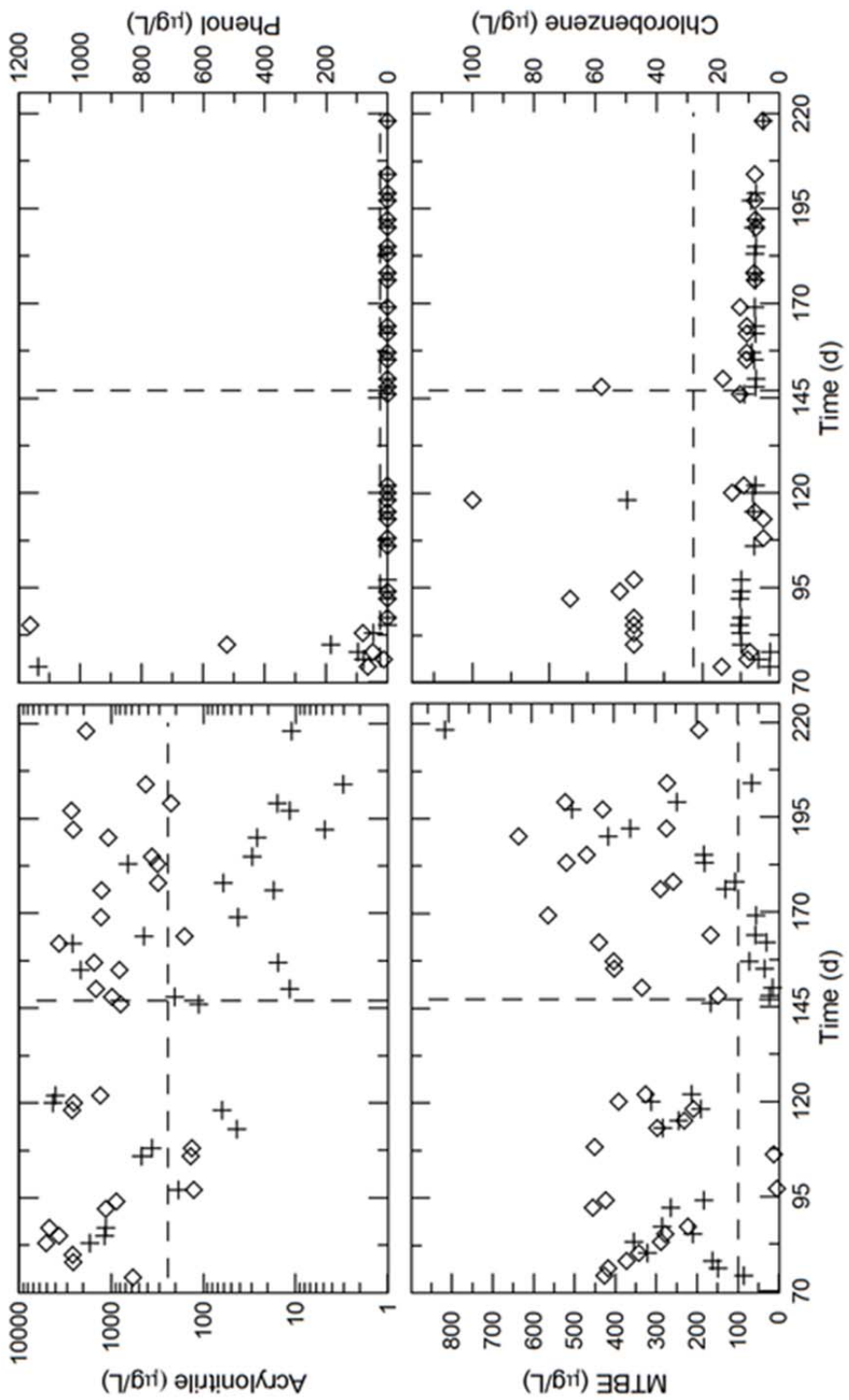

Figure 4.3 Effluent SOC concentrations. Vertical dashed line represents transition from 5d to 10d SRT. Horizontal dashed line represents the treatment limit applied to determine the effectiveness of treatment. SBR = +, CMAS = ◊.

www.manaraa.com

The effluent concentration data does indicate that the increase in SRT did result in more consistent removal of the SOCs, however this was more evident in the SBR than the CMAS. This reliance on a higher retention time for removal could suggest that the higher sludge age is required to promote the growth of slower-growing organisms responsible for SOC removal, which is similar to the proven effects of SRT on the growth of autotrophic organisms in ammonia nitrification processes. However, in the case of MTBE, the concentration originally decreased and then begin to rise back to the 5d SRT concentration levels. This phenomenon could possibly be explained by sorption equilibrium processes. The increased MLVSS available in the reactor with a 10d SRT would initially would facilitate additional sorption, but over time the newly available sorption surface area would become saturated causing the excess MTBE to remain in solution.

4.2 Determination of Kinetic Parameters for Biogenic Substrate

For the biogenic substrates, the kinetic parameters of the typical Monod model were estimated using the aforementioned methodology for each reactor, primarily consisting of linear regression for the CMAS reactor and numerical approximation using 4^{th} order Runge-Kutta for the SBR. For the CMAS, the resulting plot of the inverse of the SRT versus the measured utilization rate is presented in Figure 4.4. The linear regression of this plot results in an estimated yield coefficient of 0.265 $mgX \cdot mgS^{-1}$ and a decay coefficient of -0.0052 d^{-1} for the CMAS reactor. The fit of the data resulted in a coefficient of determination of 0.69.

www.manaraa.com

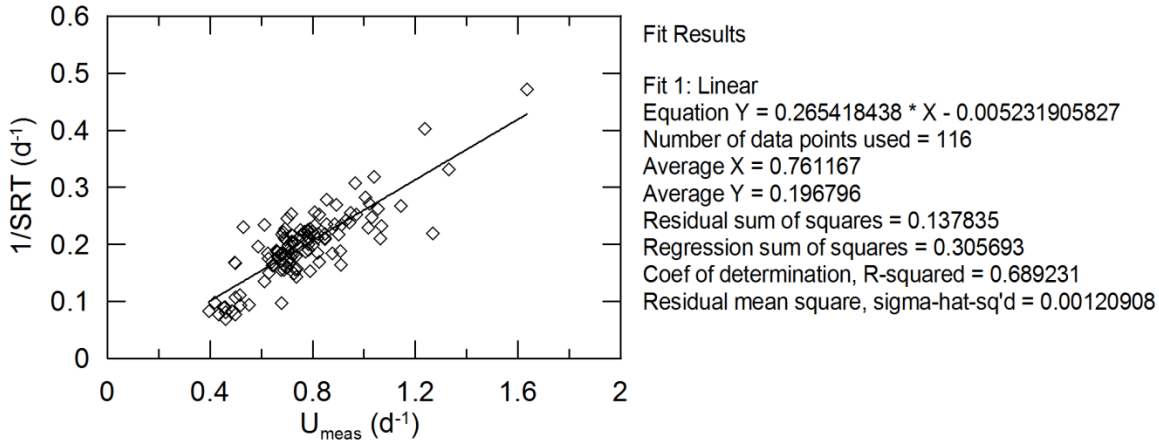

Figure 4.4 Determination of yield coefficient and decay coefficient for CMAS.

Once the Y and b were determined, the inverse of U_{meas} versus the inverse of the effluent COD concentration was plotted to approximate the remaining kinetic parameters, μ_m and K_s. Figure 4.5 illustrates the results of this plot. Since the COD removal for the CMAS was fairly consistent with a standard deviation of 2 percent, the plot in Figure 4.5 resulted in clustering of the data over a small range. Therefore, the resulting R^2 value for the linear fit was 0.01. From the curve-fit, k was found to be 0.764 $mg \cdot (mg \cdot d)^{-1}$, which when multiplied by Y gives a μ_m value of 0.20 d^{-1}. Multiplying the slope of the line by the k value gives an approximation of K_s of 3.41 $mg \cdot L^{-1}$. In an attempt to produce a better fit of the data a histogram was generated from the COD effluent data in bins of 10 $mg \cdot L^{-1}$ effluent COD (Figure 4.6). Once the data was grouped, the average effluent COD and average U_{meas} were calculated for each bin. The inverse of the resulting data was replotted and linear regression was again applied. As the results in Figure 4.7 indicate, the fit is improved with an R^2 of 0.40 with minimal changes in the values of μ_m and K_s, 0.22 d^{-1} and 3.58 $mg \cdot L^{-1}$, respectively.

www.manaraa.com

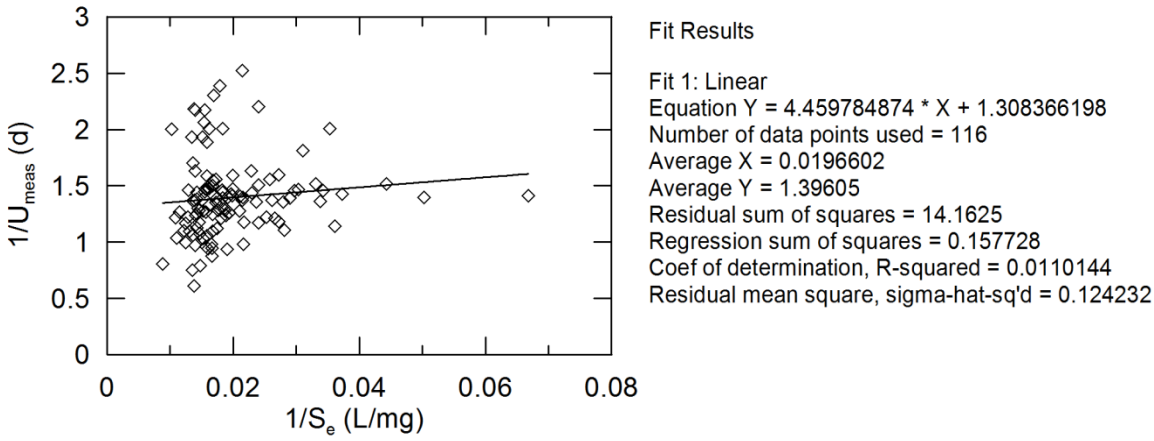

Figure 4.5 Plot used to determine μ_m and K_s using the full data set.

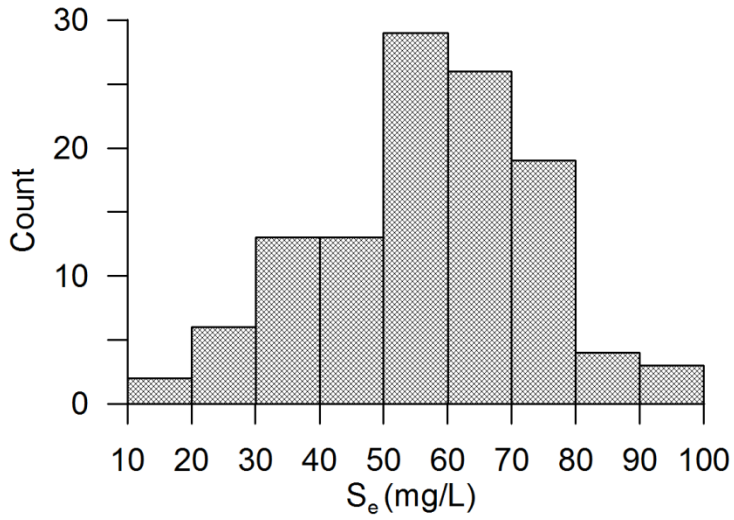

Figure 4.6 Histogram of effluent COD data with 10 $mg \cdot L^{-1}$ bins.

www.manaraa.com

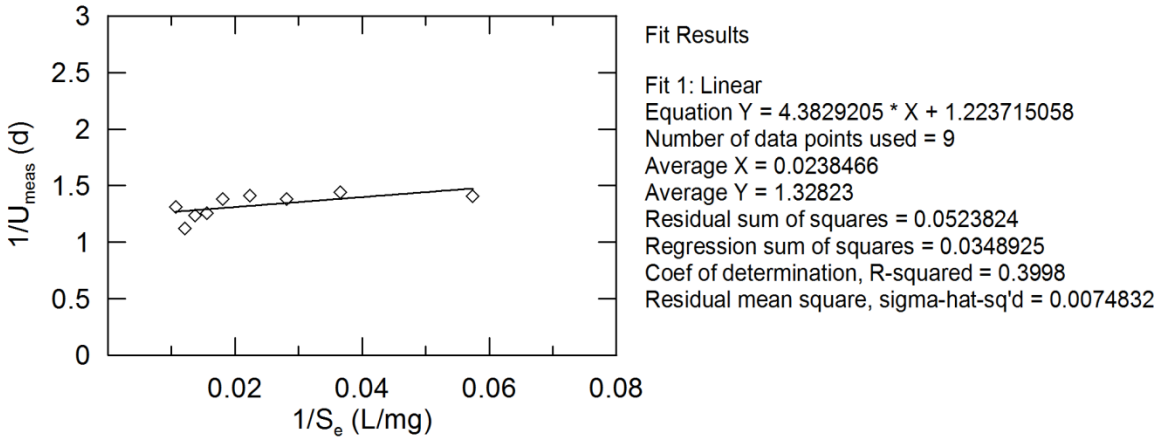

Figure 4.7 Plot used to determine μ_m and K_s using the average of the histogram bins.

As indicated in the methodology, in order to estimate the kinetic parameters associated with the biogenic substrate removal in the SBR the 4th order Runge-Kutta method was used to minimize the objective function presented as Eq. 3-19. A total of 158 data sets were used in this analysis. Although there were numerous data sets used, the lack of time-concentration data throughout the process does present cause for caution in utilizing kinetic parameter estimates developed with this method, in that other combinations of the parameters could potentially result in a similar fit to the data when only an initial and final value are used. However, using the given methodology does allow for the estimation of descriptive parameters specific to this reactor to serve as a basis for comparison to the CMAS system. For the SBR, the yield coefficient was found to be 0.414 mgX·mgS^{-1}, the decay coefficient was estimated to be 0.0364 d^{-1}, μ_m was 4.5 d^{-1}, and the half saturation constant, K_s, was estimated to be 1906 mg·L^{-1}. The evaluation of the fit of the data was estimated using the following calculations based on the given objective function:

www.manaraa.com

$$SS_{tot-X} = \sum_{i=1}^{n} \frac{(X_{meas} - X_{avg})^2}{X_{avg}^2} \quad (4\text{-}1)$$

$$SS_{err-X} = \sum_{i=1}^{n} \frac{(X_{calc} - X_{meas})^2}{X_{avg}^2} \quad (4\text{-}2)$$

$$SS_{tot-S} = \sum_{i=1}^{n} \frac{(S_{meas} - S_{avg})^2}{S_{avg}^2} \quad (4\text{-}3)$$

$$SS_{err-S} = \sum_{i=1}^{n} \frac{(S_{calc} - S_{meas})^2}{S_{avg}^2} \quad (4\text{-}4)$$

$$R^2 = 1 - \frac{(SS_{err-X} + SS_{err-S})}{(SS_{tot-X} + SS_{tot-S})} \quad (4\text{-}5)$$

Using this approach, the R^2 was calculated to be 0.066 which indicates a relatively poor approximation. For the individual components, the calculated R^2-values were determined to be 0.998 and -0.776, for X and S respectively. Since this goodness of fit is based on a comparison of model predictions to measured data with a non-linear model, the negative R^2 value is possible but indicates that the average of the S data potentially gives a better approximation than the predictions of the model. The average difference between X_{meas} and X_{calc} over the 158 data sets was approximately 27 $mg \cdot L^{-1}$ while the average difference for the effluent COD was 18 $mg \cdot L^{-1}$ which further illustrates the better fit of the biomass data compared to the COD data when considering the order of magnitude difference between measured S and X data. However, as Figure 4.8 indicates, the model does have the potential to provide a reasonable prediction of the measured data with selected data sets, such as this example with X_{meas} = 2177 $mg \cdot L^{-1}$ and X_{calc} = 2179 $mg \cdot L^{-1}$, and S_{meas} = 35.3 $mg \cdot L^{-1}$ and S_{calc} = 33.6 $mg \cdot L^{-1}$. Figure 4.9 is

www.manaraa.com

provided to illustrate the fit by comparing the predicted values plotted as a function of the measured values to a perfect fit, indicated by a 45º line. The figure more clearly reveals what is indicated by the calculated r^2 values for S and X individually, i.e. the X-fit is much more accurate than the S-fit for predicting the concentrations following the react period. From these plots it is apparent that although the objective function was normalized based on the averages of each parameter, the fit was still controlled by the biomass concentration.

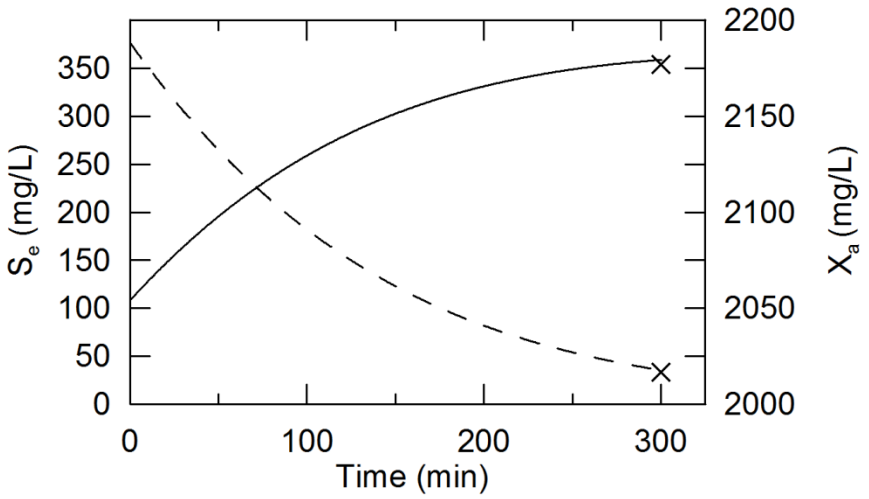

Figure 4.8 Runge-Kutta approximation plotted with measured data points for selected data set. x = measured data, --- = S model, and — = X model.

www.manaraa.com

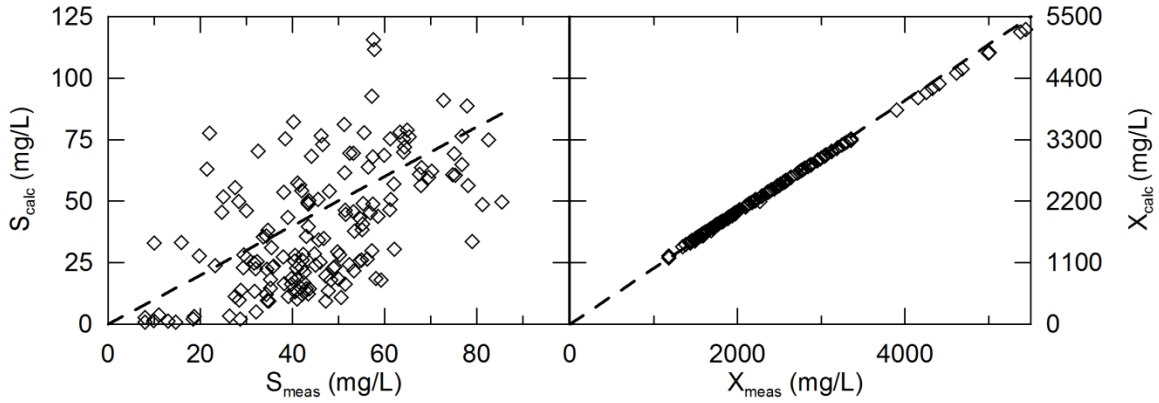

Figure 4.9 Scatter diagrams of measured and predicted concentrations using the Runge-Kutta approximations for biomass and substrate. ◊ = concentrations, --- = perfect fit (1:1 slope).

Table 4.2 presents a recap of the estimated kinetic parameters for both reactor systems. The resulting values indicate a significant difference for the estimated kinetic parameters between reactors. With the exception of the yield coefficient, the kinetic parameters differ between reactors by almost one order of magnitude for the decay coefficient up to nearly three orders of magnitude for the half-saturation constant. The difference of the kinetic parameters between reactors could be a function of the high COD concentration gradient present in the SBR over the react period as compared to the consistently low concentration found in the CMAS, which are inherent to the respective reactor flow regimes. The K_s values for the SBR were significantly higher than those for the CMAS, and although presented under different circumstances, this finding is consistent with those of Magbanua et al. (2003) who, in comparing extant and intrinsic parameter estimates, determined that K_S was generally higher for intrinsic tests in which the biomass are exposed to a much higher substrate concentration than in extant tests. Blok and Struys (1996) similarly found in an investigation of kinetic parameters for

www.manaraa.com

numerous substances that apparent K_S values have a tendency to decrease with lower substrate concentrations.

Table 4.2

Estimated kinetic parameters for biogenic substrate removal.

Parameter	SBR	CMAS
μ_m (d^{-1})	4.5	0.2
K_s ($mg \cdot L^{-1}$)	1906	3.6
Y ($mgX \cdot mgS^{-1}$)	0.414	0.265
b (d^{-1})	0.03640	0.0052

Literature suggests that it is difficult to obtain reliable kinetic parameters in a batch system when the initial substrate is significantly higher than the effective K_S (Kovarova-Kovar & Egli, 1998). These authors claim that in these instances changes in K_S have little impact on the curve fit, and K_S can therefore differ by several orders of magnitude. Grady et al. (1996) recognized the variability in literature reported kinetic parameters and suggest that the history of the biomass is one of the key influences on the kinetic parameter estimates. The authors report that steady-state operation of CMAS reactors can lead to the displacement of low affinity organisms by higher affinity organisms and further postulate that over long periods of continuous reactor performance the K_S and μ_m will decrease. This concept supports the findings of the current research, in that, long-term continuous operation of the CMAS should result in lower kinetic parameters when compared to an SBR that continually experiences a cyclic substrate concentration gradient.

www.manaraa.com

4.3 Determination of Kinetic Parameters for SOCs

The determination of SOC kinetic parameters presents the added difficulty associated with the estimation of substrate removal via abiotic processes, including adsorption and volatilization. The first step was to estimate the important physical properties of the SOCs necessary for calculating the abiotic removal. These include the partition coefficient, k_p, in order to estimate the removal via adsorption and the diffusivity and K_La in order to estimate the removal via volatilization. The K_La values were determined based on the curve fitting methods described in Section 3.2.1.3 for each reactor. The K_La values were estimated from 12 separate DO profiles for the SBR and 11 separate DO profiles for the CMAS over the five month period from October 2008 to February 2009. The K_La for oxygen transfer was found to be 0.41 ± 0.16 min^{-1} in the SBR and 0.62 ± 0.14 min^{-1} in the CMAS. Table 4.3 provides select chemical properties for the SOCs used in this study. Inferring from the provided properties and the K_La values observed in the reactors, it is evident that the SOCs have a greater propensity to volatilize from the CMAS reactor, with acrylonitrile being the most susceptible. From a cursory review of the chemicals selected, chlorobenzene has a significantly higher likelihood to be affected by adsorption to the biomass. One interesting finding from the provided properties is that based on the Henry's Law coefficient chlorobenzene would appear to be the most likely to volatilize from the system, but the diffusivity and resulting K_La for chlorobenzene estimated in this study make it the least likely to be removed via volatilization, primarily due to its higher molar volume.

The appropriate properties of the selected SOCs were used in the CMAS to estimate the α coefficient and the resulting γ coefficient. Since the γ coefficient is a

www.manaraa.com

function of the COD removal, as well as the MLSS concentration, γ varies over the course of the experimental period. Table 4.4 lists the average, standard deviation, and range for the α and γ coefficients for each of the SOCs. However, since phenol was not detected in the effluent, the apparent removal is 100% and as such the γ coefficient for this SOC approaches zero. Therefore, the resulting phenol measurements in the experiment do not allow for the estimation of kinetic parameters for this SOC applying the technique used in this study.

www.manaraa.com

المنارة للاستشارات

Table 4.3

Selected properties of test SOCs.

Analyte	COD ($mg \cdot mg^{-1}$)	K_H ($x10^{-4}$) ($atm \cdot m^3 \cdot mole^{-1}$)	log K_{OW}	MW ($g \cdot mol^{-1}$)	ρ ($g \cdot cm^{-3}$)	BP (ºC)	Vm ($cm^3 \cdot mol^{-1}$)	D ($x10^{-5}$) ($cm^2 \cdot s^{-1}$)	K_La (min^{-1})		k_P ($x10^{-6}$)
									CMAS	SBR	
Acrylonitrile	1.81	1.38	0.25	53.06	0.8044	77.3	78.85	1.159	0.315	0.210	0.59
Chlorobenzene	2.06	31.1	2.84	112.56	1.1048	131.5	140.63	0.819	0.222	0.149	231
MTBE	1.82	5.87	0.94	88.15	0.7404	55.2	133.35	0.846	0.230	0.153	2.91
Phenol	2.38	0.00333	1.46	94.11	1.0555	181.8	138.36	0.827	0.225	0.150	9.63

COD, chemical oxygen demand; K_H, Henry's law coefficient; K_{ow}, ocrtanol-water partition coefficient;MW, molecular weight; ρ, density; BP, boiling point; Vm, molar volume; D, diffusion coefficient; K_La, SOC-specific transfer coefficient for CMAS and SBR, respectively; k_P, sorption coefficient.

www.manaraa.com

Table 4.4

Estimated abiotic removal coefficients for the test SOCs.

		Acrylonitrile	Chlorobenzene	MTBE	Phenol
α_v		226.6	160.1	165.3	161.7
α_s	Avg	1.0×10^{-4}	3.9×10^{-2}	5.0×10^{-4}	1.7×10^{-3}
	Min	3.7×10^{-5}	2.6×10^{-2}	1.8×10^{-4}	6.1×10^{-4}
	Max	1.6×10^{-4}	5.9×10^{-2}	8.0×10^{-4}	2.6×10^{-3}
	std dev	2.9×10^{-5}	1.1×10^{-2}	1.4×10^{-4}	4.6×10^{-4}
α	Avg	226.6	160.1	165.3	161.7
	Min	226.6	160.2	165.3	161.7
	Max	226.6	160.1	165.3	161.7
	std dev	2.9×10^{-5}	1.1×10^{-2}	1.4×10^{-4}	4.6×10^{-4}
γ	Avg	61	0.24	7	N/A
	Min	4	0.17	0.1	N/A
	Max	289	0.41	14	N/A
	std dev	67	0.08	3.3	N/A

www.manaraa.com

As Table 4.4 indicates, the effluent SOC concentrations found in this experiment and alpha values result in gamma values greater than 1 for MTBE and acrylonitrile. For MTBE, only two data points resulted in gamma values less than one, and acrylonitrile had none. The implications of this finding are that the theoretical removal expected by abiotic mechanisms exceeds the measured overall removal achieved by the CMAS system. The ineffectiveness of the CMAS to remove MTBE or acrylonitrile made the given methodology for kinetic parameter estimation unsuitable for the data obtained. Due to the inability to quantify the effluent phenol concentration and the ineffectiveness of MTBE and acrylonitrile removal, of the four SOCs included in this study unfortunately only chlorobenzene had sufficient data available to approximate kinetic parameters using the methodology and setup selected in this research. Although the γ values were either higher than physically permitted or undetermined, it can be inferred from the high α_v:α ratios indicated in Table 4.4 that volatilization accounts for the majority of the abiotic removal, greater than 99.9%, of the SOCs in this study. This finding is consistent with other researchers who found that the ratio of removal via volatilization to adsorption was high for volatile and semi-volatile SOCs (Grady et al., 1997).

For the estimation of chlorobenzene kinetic parameters, the appropriate variables are plotted in Figure 4.10. Through linear regression of the given plot, Y and b are estimated to be 1.21 $mgX_a \cdot mgS_{chloro}^{-1}$ and -0.14 d^{-1}, respectively, for the removal of chlorobenzene. The r^2 value was found to be 0.76. However, this yield coefficient appears to be unpractical in that it suggests that the competent biomass increase is greater than the amount of substrate being metabolized. Although this could stem from numerous sources of error, one possibility is an inaccurate estimation of the competent

www.manaraa.com

biomass. It could also potentially be related to the SRT calculations which assume that the fraction of competent biomass is constant throughout the system, including the wastage and effluent streams.

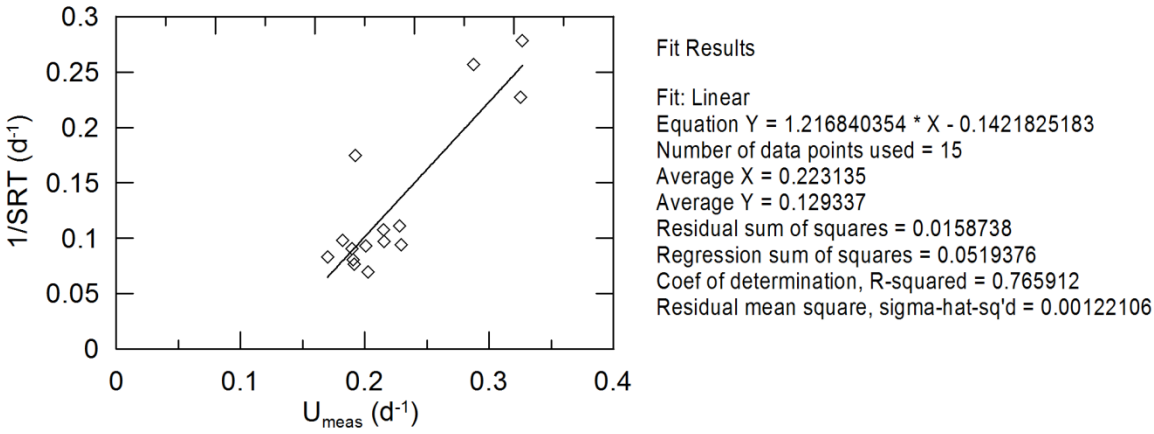

Figure 4.10 Plot used to determine Y and b for chlorobenzene.

Figure 4.11 illustrates the experimental relationship between the inverse of U_{meas} and the inverse of the effluent chlorobenzene concentration in the CMAS reactor. The resulting figure reveals a r^2 value for the chlorobenzene data of 0.07. Since the yield coefficient did not appear to be realistic, this suggests the data does not fully support the estimation of the kinetic parameters specific to chlorobenzene. Using Figure 4.11 and completing the exercise, however, provides an estimate of .32 d^{-1} and 2 $\mu g \cdot L^{-1}$, for μ_m and K_S respectively. Ultimately, from this analysis it becomes evident that the data collected for the SOC specific kinetic parameter estimations was insufficient in the CMAS reactor for determination of realistic values for any of the test SOCs used in this study.

www.manaraa.com

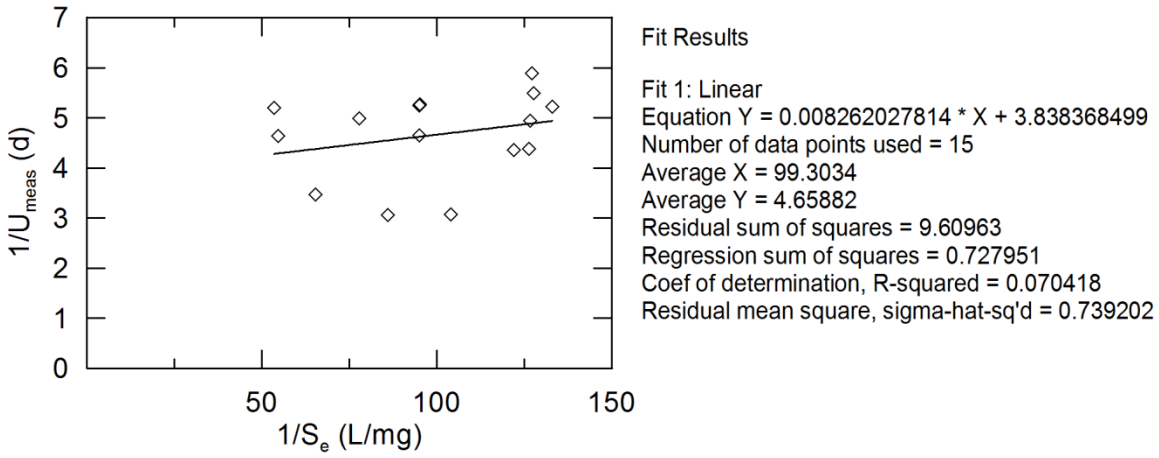

Figure 4.11 Plot used to determine μ_m and K_S for chlorobenzene.

Due to the problems encountered in the estimation of kinetic parameters for the SOCs in the CMAS reactor, the first step in the estimation of SBR kinetic parameters was to determine if the effluent SOC data would support parameter estimation with the calculated K_La values for the SOCs, i.e. is the effluent SOC data low enough that the theoretical removal via abiotic processes is less than the overall removal measured in the SBR. In order to test this condition, the biodegradation was assumed to be zero thus Eq. 3-28 reduces to a first order equation, Eq. 4-6, with respect to S:

$$\frac{dS_{SOC}}{dt} = -\frac{1}{V(1+k_P X_T)} r_{vol} \tag{4-6}$$

This equation can further be reduced and solved analytically resulting in Eq. 4-7:

$$S = S_O e^{-\frac{1}{(1+k_P X_T)} K_L a \cdot t} \tag{4-7}$$

With the assumed constant X_T and the calculated K_La and k_P values, the theoretical SOC concentration can be determined as a function of time when assuming only abiotic removal occurs. Similar to the results from the CMAS reactor, the resulting data for the

www.manaraa.com

SBR suggests that the theoretical abiotic removal rates are significant when compared to the measured overall removal rates for the reactor. For all SOCs in the study, when only considering abiotic removal, the resulting theoretical SOC concentrations after the 300 min react period were approaching zero, ranging from 10^{-7} mg·L^{-1} for chlorobenzene to 10^{-27} mg·L^{-1} for acrylonitrile. As with the CMAS reactor, this indicates that the measured effluent concentrations are higher than the concentrations expected to remain if no microbial conversion occurred. Thus, it is not possible to estimate the biological removal component with the given effluent concentration data. In the case of both the CMAS and the SBR, for any reasonable estimates of SOC-specific kinetic parameters to be obtained appropriate time-concentration data are required as opposed to steady-state or effluent only data.

4.4 Effects of Reactor Conditions on Floc Morphology

The mean morphological parameters are presented in Table 4.5. The size parameters (Figure 4.12) and the shape parameters of the AS flocs (Figure 4.13) responded differently to the changes imparted on the system. For the SBR, the size parameters increased significantly once the SOCs were incorporated into the feed but returned to near their original values when the SRT was increased to 10 d. One possible reason for this increase in size could be an attempt by the AS flocs to protect themselves from the harmful SOCs by creating a sacrificial exterior buffer to reduce transfer of the SOCs into the interior protected interior region. The CMAS, however, exhibited no significant variation in size parameters over the duration of the project. The CMAS did undergo significant changes in the shape parameters after the SRT was increased to 10 d.

www.manaraa.com

The shape parameters in the CMAS during P3 became more similar to those in the SBR, which remained stable throughout the project. In comparing the overall values between the two reactors over the duration of the project, the SBR and CMAS presented a significant difference in size and shape parameters (Table 4.5).

Each reactor responded differently when SOCs were added as indicated through comparing period means in Table 4.1 and Table 4.5. In further analyzing the effects by correlating the size and shape parameters to the specific effluent SOC concentrations, Table 4.6 reveals that both reactors demonstrated some correlations with the effluent chemical concentrations. Phenol was omitted from the statistical analysis in both reactors due to the limited effluent data. The effluent concentration of both acrylonitrile and chlorobenzene displayed a significant positive correlation with the size parameters in the SBR, while chlorobenzene had a significant positive correlation with the FF and RD and a negative correlation with the AR in the CMAS. This suggests the presence of the selected SOCs resulted in larger flocs in the SBR which demonstrated flocculent settling during visual observation of the settling test, and the particles in the CMAS, which experienced more discrete settling, approached more circular particle shapes with increased SOC concentrations. The reactor performance was also affected by the presence of the SOCs. Both reactors showed a negative correlation between the SRT and the effluent concentration of chlorobenzene and acrylonitrile suggesting that an increased SRT may result in better removal of the toxic SOCs; however, the correlation was only statistically significant in the SBR reactor. This could also be indicated by the overall increase in soluble COD removal when the SRT was increased in P3, as demonstrated by the significant difference between P3 and the other periods in Table 4.1 for the SBR.

www.manaraa.com

المنارة للاستشارات

Table 4.5

Floc morphology parameters.

Reactor	Parameter	Units	Period 1	Period 2	Period 3	Overall	Significant Difference[a]
SBR	A	μm^2	6191 ± 4005	14293 ± 4819	6353 ± 2738	8409 ± 5203	1,3; Y2,Y3; +
	D_e	µm	85 ± 27	133 ± 23	88 ± 19	99 ± 31	1,3; Y2,Y3; +
	FF	-	0.29 ± 0.04	0.29 ± 0.02	0.30 ± 0.03	0.29 ± 0.03	Y1,Y2; +
	AR	-	2.12 ± 0.13	2.08 ± 0.14	2.14 ± 0.05	2.12 ± 0.11	Y1,Y2; +
	RD	-	0.46 ± 0.03	0.49 ± 0.03	0.46 ± 0.01	0.47 ± 0.03	Y1,Y2; +
CMAS	A	μm^2	2274 ± 594	1633 ± 297	2615 ± 1229	2224 ± 904	Y2,Y3; +
	D_e	µm	53 ± 7	45 ± 4	56 ± 12	52 ± 10	Y2,Y3; +
	FF	-	0.40 ± 0.07	0.42 ± 0.04	0.32 ± 0.03	0.38 ± 0.06	2,3; Y1,Y2; +
	AR	-	1.89 ± 0.09	1.92 ± 0.10	2.15 ± 0.07	1.99 ± 0.15	2,3; Y1,Y2; +
	RD	-	0.55 ± 0.04	0.54 ± 0.04	0.46 ± 0.01	0.51 ± 0.05	2,3; Y1,Y2; +

* 1, 2, and 3 indicate a statistically significant difference ($\alpha < 0.05$) between P1 and P2, P1 and P3, and P2 and P3, respectively. Y1, Y2, and Y3 indicate a significant difference between the two reactors for P1, P2 and P3, respectively. + indicates a significant difference for the full experimental period.

www.manaraa.com

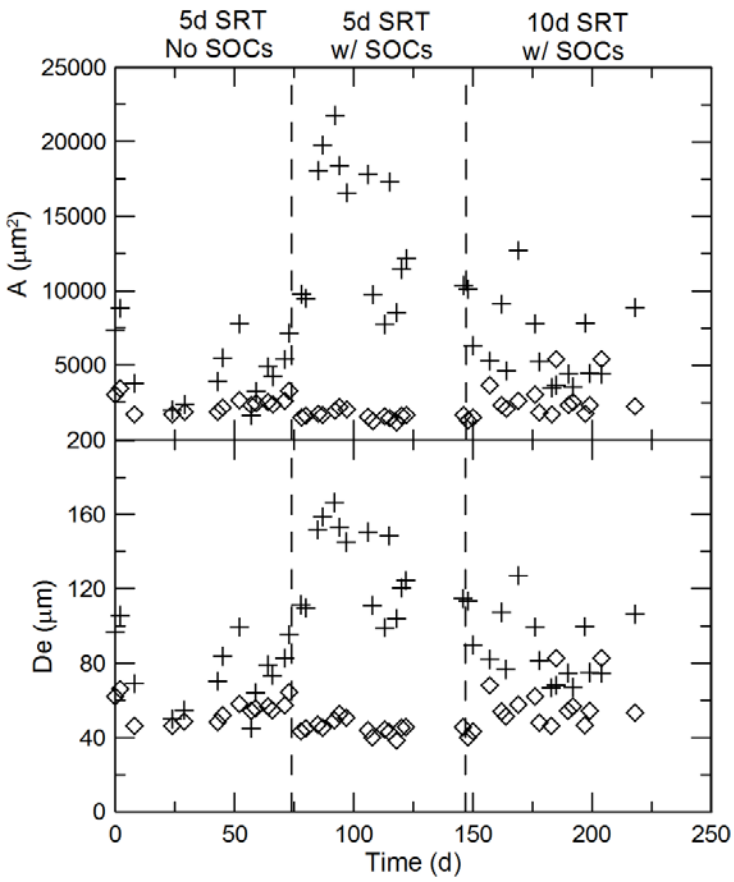

Figure 4.12 Size parameters as a function of time. SBR = +, CMAS = ◊.

www.manaraa.com

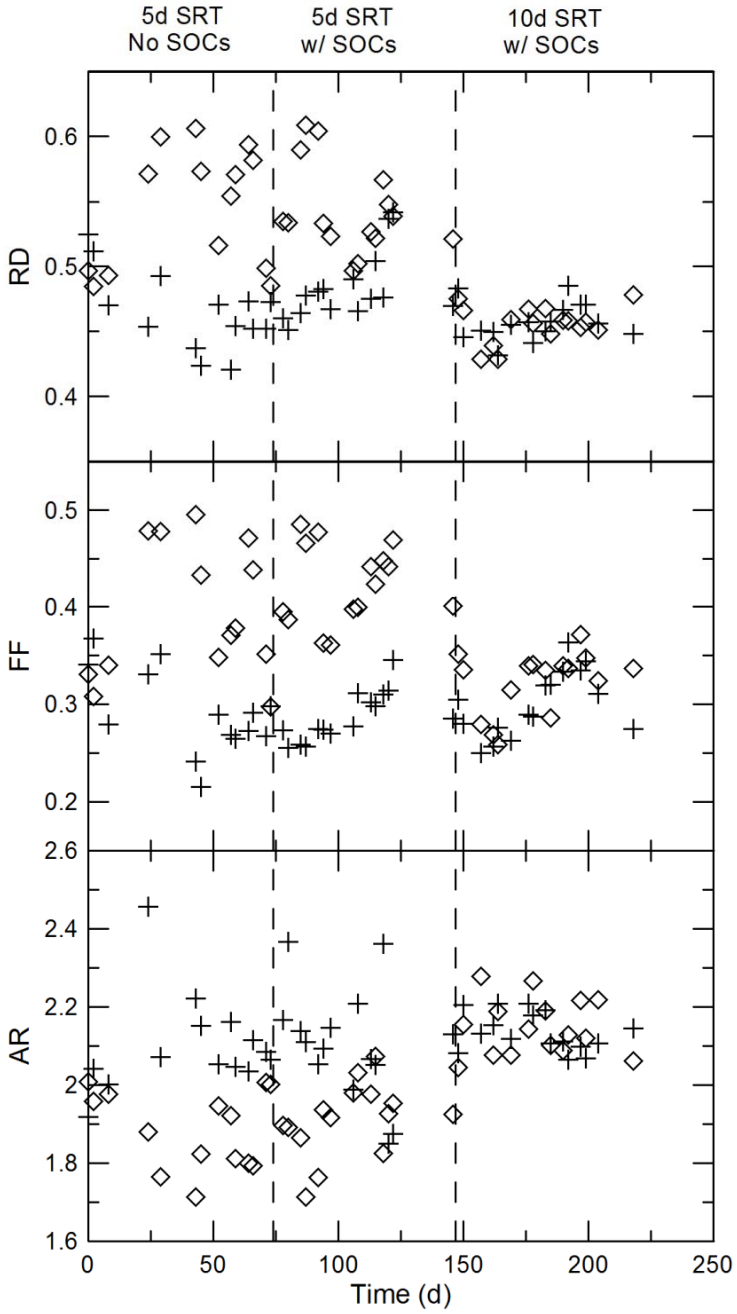

Figure 4.13 Shape parameters as a function of time. SBR = +,CMAS = ◊.

www.manaraa.com

Table 4.6

SOC concentration correlation data.

	SBR			CMAS		
	Acrylonitrile	Chlorobenzene	MTBE	Acrylonitrile	Chlorobenzene	MTBE
A	0.54^{+}	0.47^{+}	-0.001	-0.16	-0.31	0.30
D_e	0.55^{+}	0.44^{+}	-0.05	-0.16	-0.31	0.30
FF	-0.18	-0.29	0.46	0.28	0.39^{+}	-0.19
AR	-0.002	0.18	-0.41	-0.30	-0.58^{++}	0.16
RD	0.24	0.22	0.48^{+}	0.24	0.55^{++}	-0.22
MLVSS	-0.64^{++}	-0.45^{+}	0.30	-0.21	-0.65^{+++}	0.29
VSS_{eff}	0.28	0.02	-0.10	0.60^{++}	0.53^{++}	-0.31
SRT	-0.74^{+++}	-0.53^{+}	-0.07	-0.35	-0.44	0.22
SVI	0.21	0.07	-0.26	-0.15	-0.50^{+}	0.11
ISV	0.33	0.35	0.03	0.06	0.32	-0.21

$+ p < 0.05$; $++ < 0.005$; $+++ p < 0.0001$.

www.manaraa.com

Additionally, this research demonstrated that the MLVSS increased significantly in both reactors when the SRT transitioned from 5 d to 10 d, which corroborates other research conclusions that the suspended solids concentration typically increases with increasing SRT (Laera et al., 2007). In the CMAS, although a significant change in mean floc size as a function of SRT was not demonstrated in comparison between the individual periods, the CMAS did exhibit a significant positive correlation between the mean floc size and both the MLVSS and SRT throughout the experiment (Table 4.7). The floc size did not directly correlate in the SBR with either SRT or solids concentration, however the correlation of floc size and MLVSS is further illustrated by the comparison of the SBR to the CMAS. The SBR resulted in a significantly higher MLVSS concentration compared to the CMAS and correspondingly exhibited a larger mean floc size. This correlation has been noted in other works (Chaignon et al., 2002) which reported that floc size linearly correlated with suspended solids content for lower sludge concentrations and concluded that floc coagulation increases significantly with increasing AS concentrations. Other researchers have also concluded that there is a positive linear correlation between suspended solids concentration and mean floc size (Liwarska-Bizukojc & Bizukojc, 2005; Grijspeerdt & Verstraete, 1997).

www.manaraa.com

Table 4.7

Performance parameters – floc morphology correlation results.

	SBR					CMAS				
	MLVSS	VSS_{eff}	SRT	SVI	ISV	MLVSS	VSS_{eff}	SRT	SVI	ISV
A	0.20	-0.41^{++}	-0.06	0.65^{+++}	-0.36^{+}	0.45^{++}	-0.29^{+}	0.45^{++}	0.35^{+}	-0.31^{+}
D_e	0.11	-0.42^{++}	-0.01	0.62^{+++}	-0.27	0.28	-0.29^{+}	0.28	0.11	-0.16
FF	0.16	0.09	0.04	-0.10	-0.25	-0.64^{+++}	0.16	-0.68^{+++}	-0.76^{+++}	0.58^{+++}
AR	0.18	0.11	0.20	0.01	-0.10	0.70^{+++}	-0.19	0.68^{+++}	0.77^{+++}	-0.61^{+++}
RD	-0.07	-0.13	-0.32^{+}	0.17	-0.09	-0.72^{+++}	0.18	-0.74^{+++}	-0.84^{+++}	0.65^{+++}

$+ p < 0.05$; $++ < 0.005$; $+++ p < 0.0001$.

www.manaraa.com

4.5 Correlation of Floc Morphology and Settling Performance

The Spearman coefficient was used on each reactor separately to assess the correlation between morphological parameters and sludge settleability because, due to its non-parametric nature, it is a more robust indicator than the Pearson coefficient of correlation between variables of widely differing magnitudes and scales. The correlation matrices (Table 4.7) indicate that the parameters most strongly correlated to and thus potential predictors of sludge settleability differed between the SBR and the CMAS reactor. For the SBR, the SVI was most significantly correlated with the size parameters A and De, while the CMAS exhibited a stronger correlation between settling performance and the shape parameters.

In order to determine if this observation might be consistent with mechanistic considerations, we considered models for the discrete particle settling. Biofloc particles are likely to undergo flocculent settling and hindered settling, but discrete settling may prevail within the clarification zone of the sedimentation tank. A number of mathematically complex empirically-derived models have been proposed to describe the relationship between size, shape and settling velocity of non-spherical particles in a fluid (Concha & Barrientos, 1986; Halder & Levenespiel, 1989; Swamee & Ojha, 1989; Bernhardt, 2004), but Crites and Tchobanoglous (1998) provide a relatively simple formulation, valid when $N_{Re} < 10^4$:

$$v^2 = \frac{4g(s-1)D}{3C_D} \tag{4-8}$$

$$C_D = \frac{24}{N_{\mathrm{Re}}} + \frac{3}{N_{\mathrm{Re}}^{1/2}} + 0.34 \tag{4-9}$$

www.manaraa.com

$$N_{Re} = \frac{Dv\varphi}{\nu} \tag{4-10}$$

where v is the terminal settling velocity of the particle; g is the gravitational acceleration, 9.8 $m \cdot s^{-2}$, D is the diameter of a sphere with the same volume of the particle; s is the specific gravity of the particle; C_D is the drag coefficient; N_{Re} is the Reynolds number calculated at the terminal settling velocity; φ is the sphericity of the particle; and ν is the kinetic viscosity of the fluid. The sphericity is defined as the ratio of the surface area of a sphere of equivalent volume to the surface area of the particle, $0 < \varphi < 1.0$. D and φ could be considered as the three-dimensional analogues of D_e and RD, respectively, quantified from the floc images. Through implicit differentiation, the following sensitivity equations can be obtained:

$$D\frac{\partial v}{\partial D} = v\left[\frac{\frac{48}{N_{Re}} + \frac{9}{2N_{Re}^{1/2}} + 0.34}{\frac{24}{N_{Re}} + \frac{9}{2N_{Re}^{1/2}} + 0.68}\right] \qquad \frac{D}{v}\frac{\partial v}{\partial D} = \frac{\frac{48}{N_{Re}} + \frac{9}{2N_{Re}^{1/2}} + 0.34}{\frac{24}{N_{Re}} + \frac{9}{2N_{Re}^{1/2}} + 0.68} \tag{4-11 a,b}$$

$$\varphi\frac{\partial v}{\partial \varphi} = v\left[\frac{\frac{24}{N_{Re}} + \frac{3}{2N_{Re}^{1/2}}}{\frac{24}{N_{Re}} + \frac{9}{2N_{Re}^{1/2}} + 0.68}\right] \qquad \frac{\varphi}{v}\frac{\partial v}{\partial \varphi} = \frac{\frac{24}{N_{Re}} + \frac{3}{2N_{Re}^{1/2}}}{\frac{24}{N_{Re}} + \frac{9}{2N_{Re}^{1/2}} + 0.68} \tag{4-12 a,b}$$

The sensitivity equations describe how a relative change in particle size ($\partial D/D$) or shape ($\partial\varphi/\varphi$) results in an absolute (∂v, equations 4-11a, 4-12a) or relative ($\partial v/v$), equations 4-11b, 4-12b) change in settling velocity. Solution of these equations (Figure 4.14) under conditions typical of activated sludge (20 ^{o}C, s = 1.04) suggests that this set of equations for the discrete settling of non-spherical particles supports the observation that particle shape becomes a less important factor than particle size as the particle size increases.

www.manaraa.com

Specifically, the lines depicting $D(\partial v/\partial D)$ and $\varphi(\partial v/\partial \varphi)$ are parallel at low particle size and begin to diverge at higher particle size (Figure 4.14b); similar behavior is observed for $(D/v)\cdot(\partial v/\partial D)$ and $(\varphi/v)\cdot(\partial v/\partial \varphi)$ (Figure 4.14c). This divergence between the effects of D and φ occurs at a smaller diameter for particles that are spherical or nearly so, i.e., the effect of shape is greatest for particles that deviate the farthest from a perfect sphere. Furthermore, the divergence appears to occur, regardless of sphericity, at a Reynolds number between 1 and 10, the lower range of the transition region ($1 < N_{Re} < 2000$) between laminar and fully turbulent settling. In the case of spherical particles, the divergence occurs at the extreme upper range of equivalent diameters observed in the floc images.

The foregoing model, it should be recognized, applies to particles that undergo discrete settling and does not take into account the acceleration of the settling velocity if particle flocculation occurs; neither does the model consider the reduction in hydrodynamic drag due to floc permeability (Lee et al., 1996). Nevertheless, the model was qualitatively consistent with observed settling behavior. The flocs in the SBR were significantly larger than in the CMAS, which resulted in the settling performance of the SBR being more dependent on size and correlating poorly with the shape parameters. The smaller CMAS particles exhibited a strong correlation between the settling performance and the shape parameters. Although the CMAS particles were significantly smaller, they actually exhibited a higher settling velocity and a lower SVI, due to their more spherical shape.

www.manaraa.com

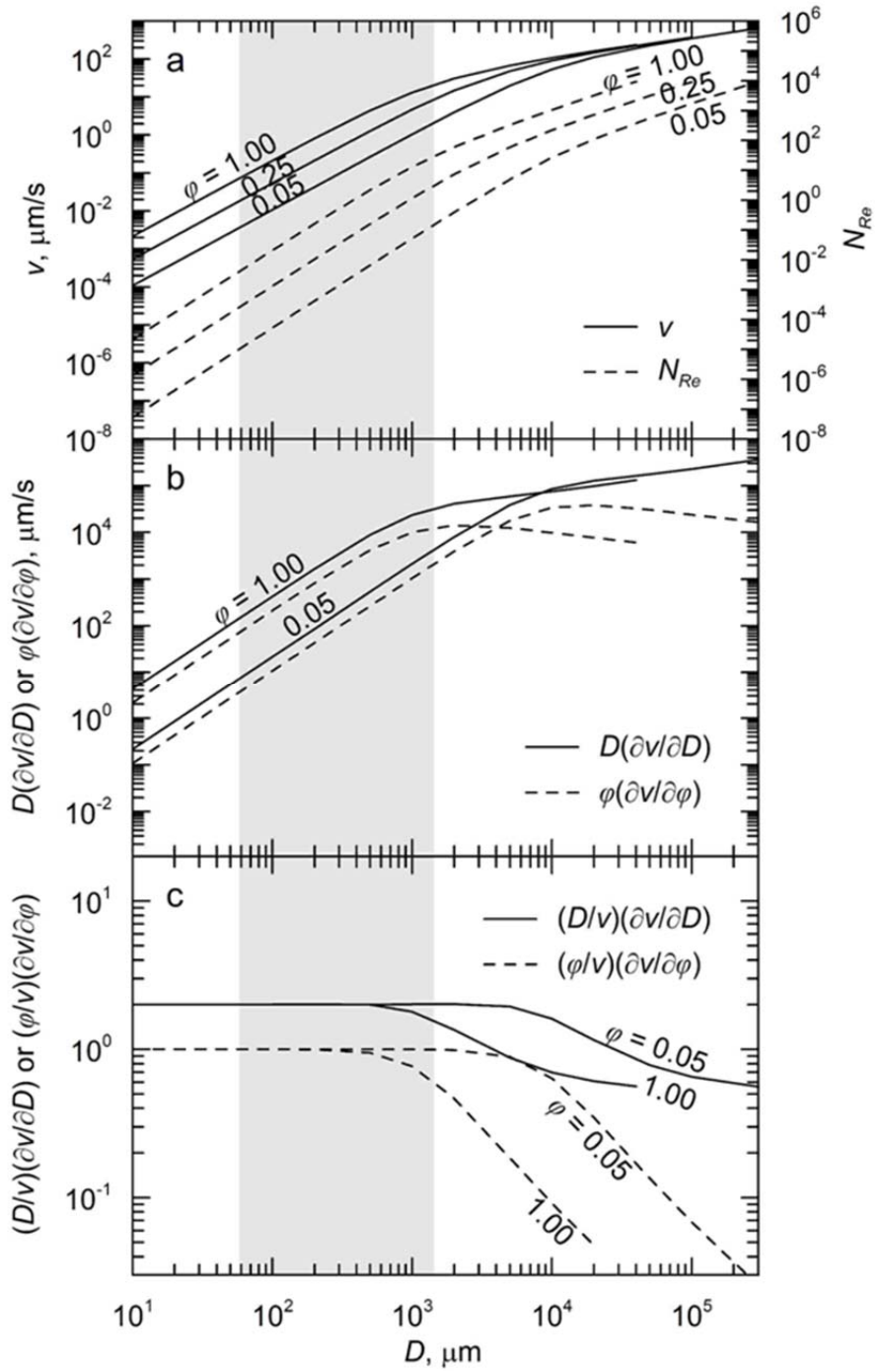

Figure 4.14 Discrete settling behavior for non-spherical particles: (a) terminal settling velocity and Reynolds number; and (b) absolute and (c) relative sensitivity of terminal settling velocity to particle diameter and sphericity, as a function of the particle diameter. The shaded area corresponds to the observed range of equivalent diameters of activated sludge floc particles.

www.manaraa.com

Contrary to the indications of the SVI, the amount of VSS lost in the CMAS was much higher than that of the SBR. The SBR demonstrated a significant negative correlation between the mean floc size and the effluent VSS. From direct laboratory observations, including the photomicrographic images and visual examination of the sludge during the SVI analysis, this was most likely due to the fact that the CMAS sludge had more of a granular appearance and would settle more discretely leaving a more turbid supernatant, while the SBR sludge behaved more consistently with zone settling. Thus, the SBR sludge would create a blanket effect, trapping particles as it settled. This blanket effect could be the primary factor that resulted in the larger sizes, while the more discrete particles of the CMAS resulted in the more spherical shape values. As a result, the shape parameters would better correlate with the SVI for the CMAS, while the size parameters showed stronger correlations for the SBR, which is also supported by the particle settling theory analysis.

4.6 Genetic Diversity Analysis Results

Some of the molecular techniques were established slightly before the standardization of the photomicrographic analysis techniques, and some samples taken prior to Day 0 of the settleability analysis were used in this evaluation. Therefore, Day 0 for the genetic diversity analysis is taken as the time when all required tests for this analysis were standardized. As such, Period 1 (P1) actually includes 108 days prior to the incorporation of SOCs, Period 2 (P2) refers to days 109 to 182 when SOCs were present, and Period 3 (P3) refers to days 182 to 240 when the SRT was changed from 5d to 10d. Prior to DGGE analysis, an agarose gel was run to confirm the presence of PCR

www.manaraa.com

products. Figure 4.15 provides a representative agarose gel image. DGGE gels were then created and processed per the prescribed methods outlined previously. Figure 4.16 provides a representative DGGE gel image.

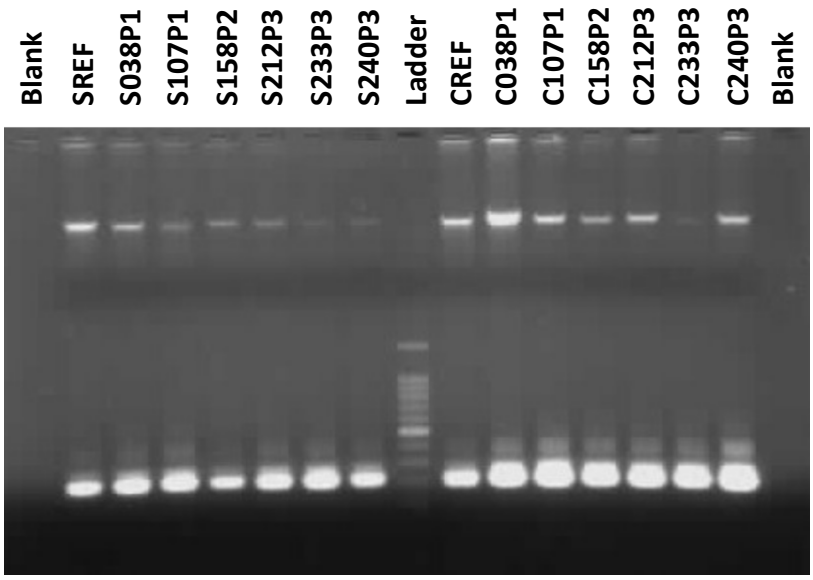

Figure 4.15 Sample agarose gel image. S and C indicate samples taken from the SBR or CMAS reactor, respectively. The following number indicates the sample day and the P1, P2, and P3 correspond to reactor periods 1, 2 and 3, respectively. The SREF and CREF are the reference samples that were used for standardizing the DGGE gels.

www.manaraa.com

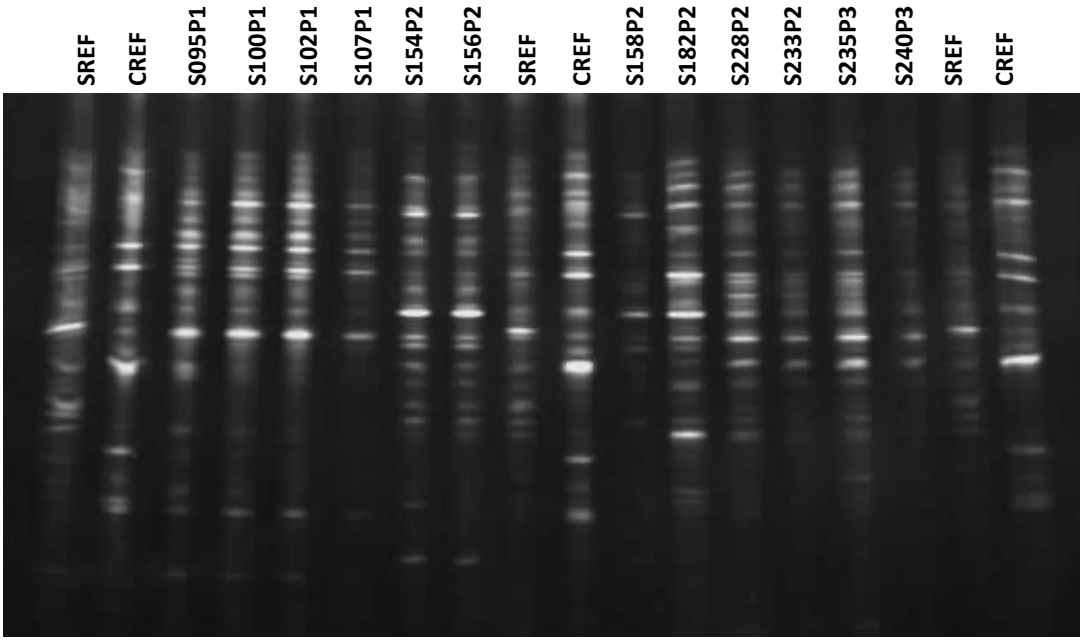

Figure 4.16 Sample DGGE gel image. S indicates samples taken from the SBR. The following number indicates the sample day and the P1, P2, and P3 correspond to reactor periods 1, 2 and 3, respectively. The SREF and CREF are the reference samples that were used for standardizing the DGGE gels.

The different reactor configurations as well as the variations in the operational conditions of the individual reactors resulted in variations in the genetic composition of the AS communities. Dendrograms were generated from three DGGE gels for each reactor, standardized to the reference lanes. The composite dendrograms from the individual reactors show that in both reactors the profiles primarily group into two larger subsets that correlate to the presence and absence of SOCs in the feed stream (Figure 4.17 and Figure 4.18 for the SBR and CMAS, respectively). The grouping of the samples taken with SOCs present is then subdivided into 5 d SRT and 10 d SRT. These subgroupings indicate that the structure of the AS community changes in response to

www.manaraa.com

changes in the reactor operational conditions. In Figure 4.18, sample C114P2 was taken with SOCs present but grouped with the 5d samples without SOCs. This anomaly was taken early in P2 when the community could have potentially been in a state of flux while acclimating to the presence of SOCs.

The resulting cluster analysis combining all six gels is presented in Figure 4.19. Although the combined dendrogram does not result in the same defined hierarchy illustrated by the individual reactor dendrograms, it does indicate that reactor configuration and reactor conditions both resulted in sub-clustering. The separation between the sub-clusters is more defined during P1. The hierarchy of the clustering indicates that the CMAS prior to the incorporation of SOCs is most unique and differentiated from the SBR and the other CMAS periods. The SBR during P1 is also a primary sub-cluster that is separated from the samples taken with the SOCs present. Once the SOCs are incorporated, the samples from the SBR during P2 and P3 are sub-grouped under the P3 CMAS samples, which are subsequently sub-grouped under the P2 CMAS samples. Samples C128P2 and C130P2 clustered within the SBR samples. As the feed is modified, the AS community does undergo a transition and inter-reactor relationships appear to begin to develop.

www.manaraa.com

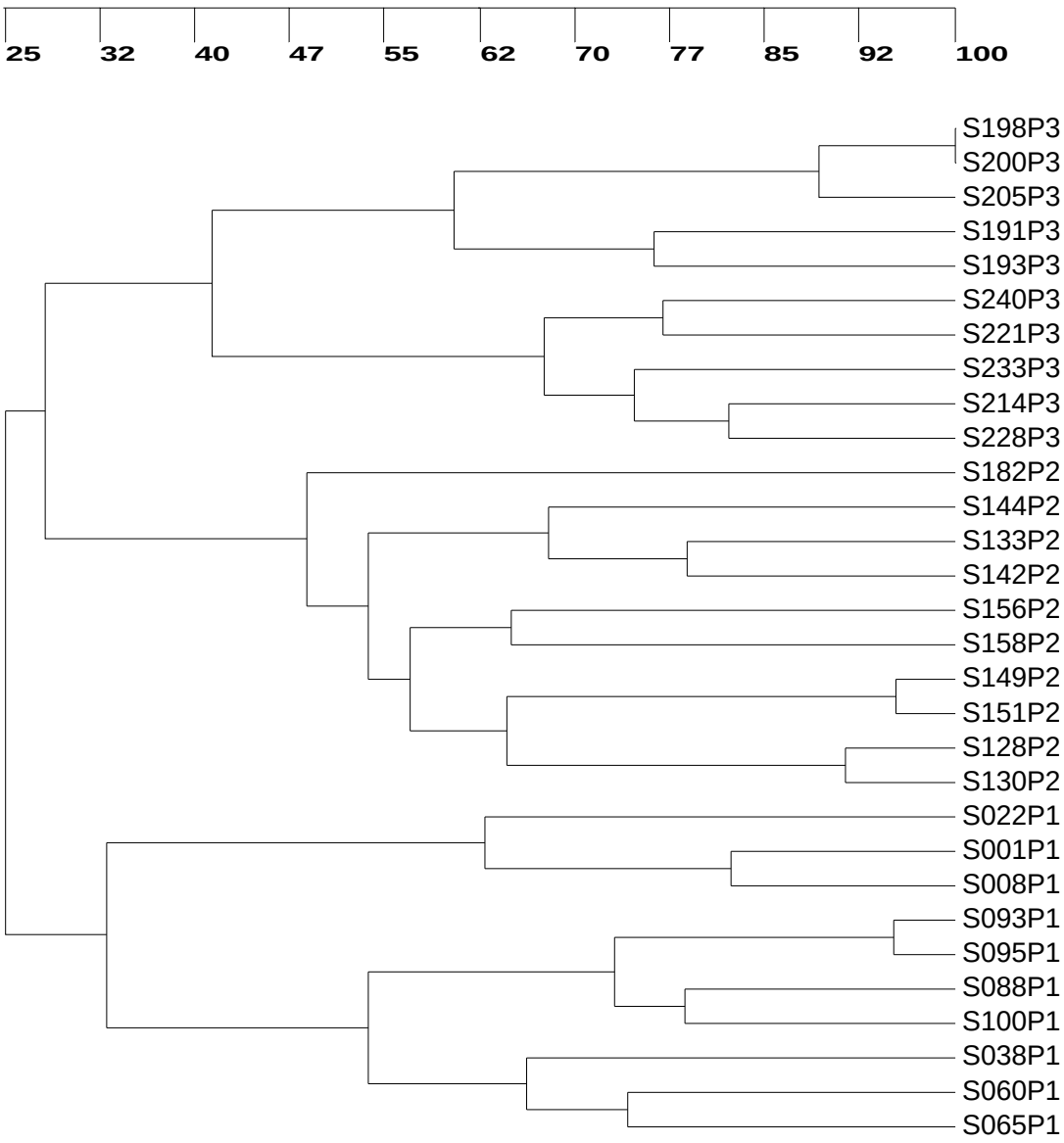

Figure 4.17 SBR dendrogram. S indicates samples taken from the SBR. The following number indicates the sample day and the P1, P2, and P3 correspond to reactor periods 1, 2 and 3, respectively.

www.manaraa.com

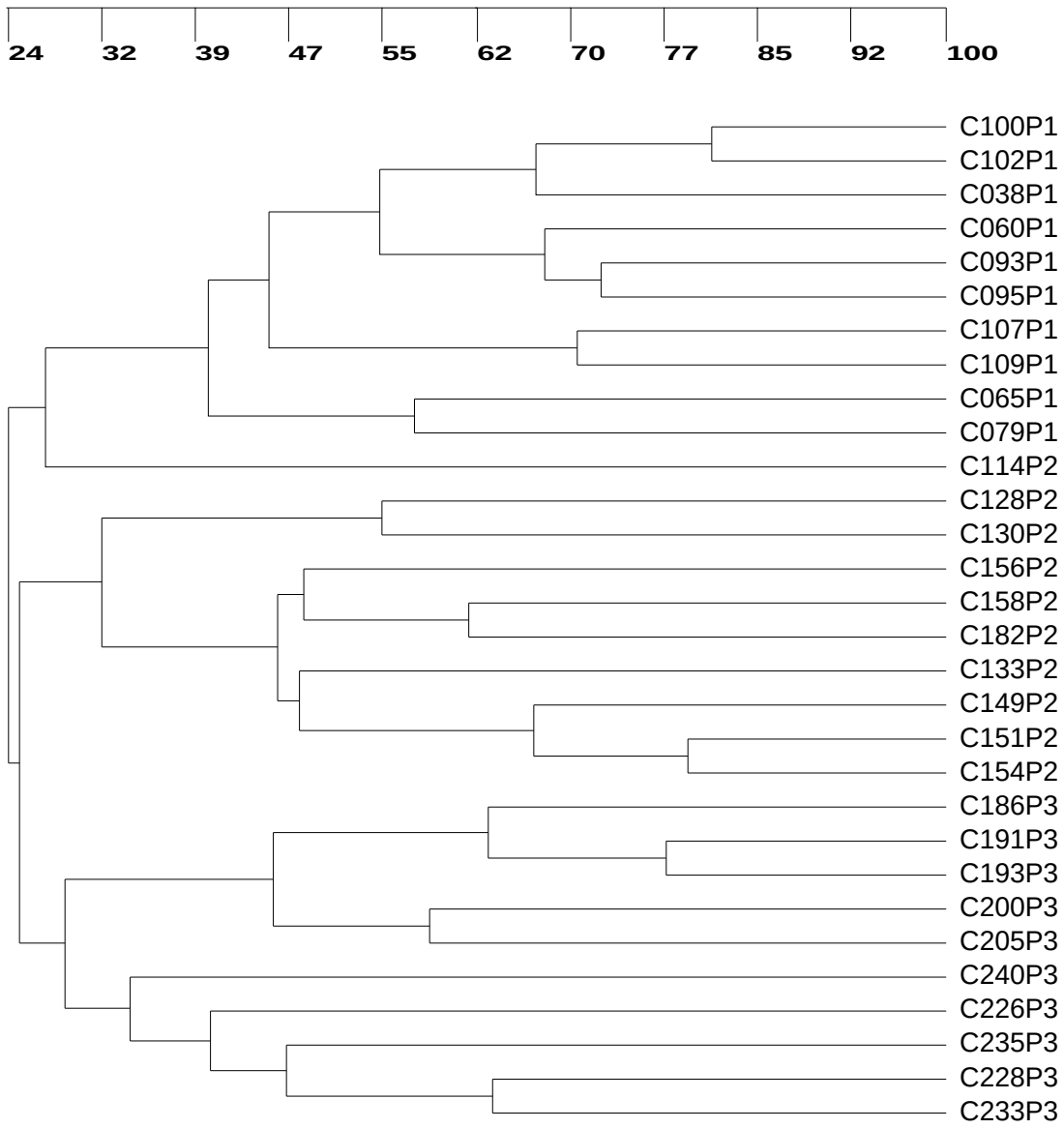

Figure 4.18 CMAS dendrogram. C indicates samples taken from the CMAS. The following number indicates the sample day and the P1, P2, and P3 correspond to reactor periods 1, 2 and 3, respectively.

www.manaraa.com

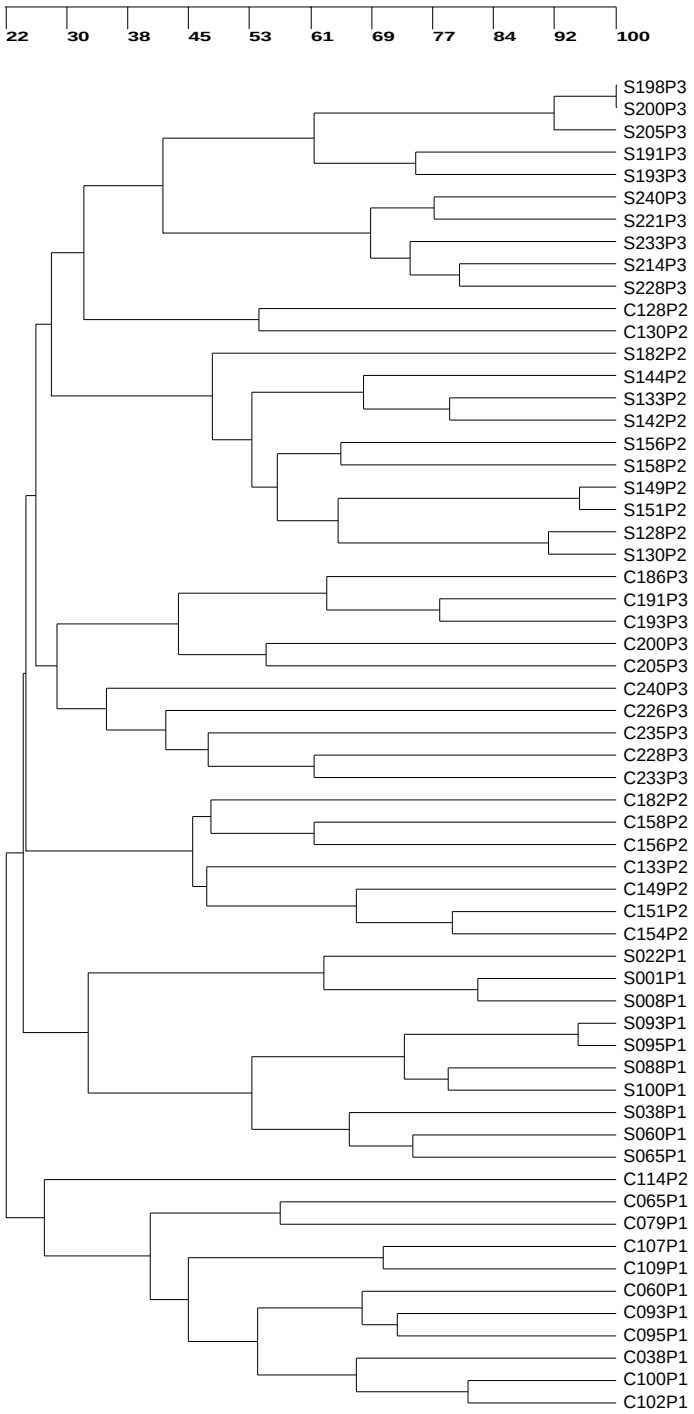

Figure 4.19 Combined 6-gel dendrogram. C and S indicate samples taken from the CMAS and SBR, respectively. The following number indicates the sample day and the P1, P2, and P3 correspond to reactor periods 1, 2, and 3, respectively.

www.manaraa.com

To potentially reduce any bias caused by standardizing across six separate gels, composite gels were run for each reactor. The composite gels included four samples from each reactor period taken just prior to transitioning to the next set of operational conditions, with the assumption that enough time had been provided for the AS community structure to stabilize. Standardization was then performed on the two gels and the composite dendrogram produced (Figure 4.20). The analysis of two combined gels indicates that the samples group primarily based on reactor configuration, but, similar to the findings with the six-gel dendrogram, both reactor configuration and operational conditions resulted in defined sub-clusters. The samples from each reactor taken during P1 were the two clearest sub-groups, containing all four samples. Additionally, all four samples from P2 in the SBR grouped together. However, the other samples taken with SOCs present showed several instances of crossover between the reactors. Several samples from the SBR and the CMAS during P3 where closely linked in the hierarchal structure of the dendrogram, while samples from the CMAS during P2 were split with two samples segregated with other CMAS samples while two samples appeared to be more closely associated with the SBR samples. These anomalies indicate the transient nature of the AS community structure in response to external stimuli. Interestingly, in all the dendrograms produced, very few samples exhibited a significantly high similarity coefficient (> 95). Even in some instances with samples taken as close as two days apart, the resulting similarity coefficient was very low, such as S233P3 and S235P3 in the 2-gel composite with a coefficient of approximately 30. This further illustrates the dynamic, transient condition exhibited by AS communities, as pointed out by other researchers (Saikaly et al., 2005).

www.manaraa.com

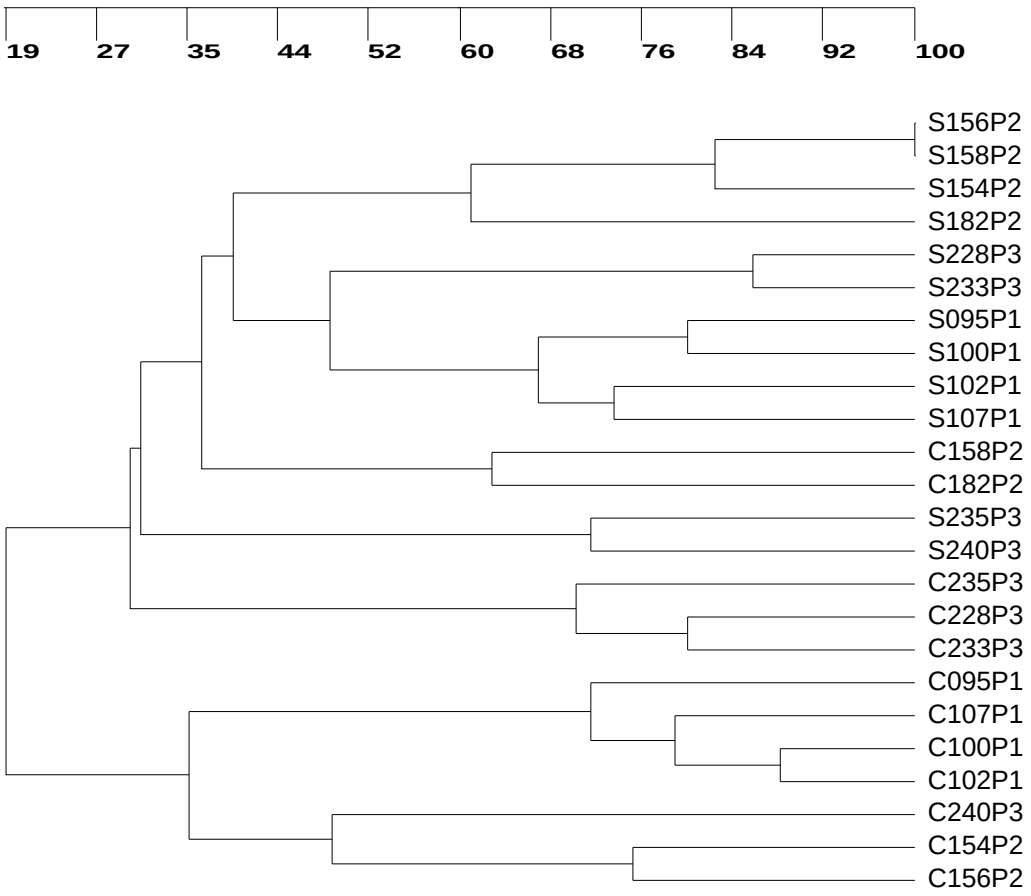

Figure 4.20 Composite 2-gel dendrogram. C and S indicate samples taken from the CMAS and SBR, respectively. The following number indicates the sample day and the P1, P2, and P3 correspond to reactor periods 1, 2, and 3, respectively.

www.manaraa.com

Additional analysis was performed using the diversity index calculated for each lane in the six individual gels. Diversity indices allow for quantitative analysis because a single numerical value can be derived for each sample, which can be correlated to other quantitative results. In the case of this study, diversity indices were analyzed for each reactor period and compared to determine if there is a significant change in community diversity as a result of variations in the reactor operation. Table 4.8 presents the averages and standard deviations of the diversity indices for each reactor. In reviewing the resulting richness values, the CMAS community richness increased significantly after SOCs were incorporated into the feed. The SBR responded similarly, however, the transition did not prove to be statistically significant. The response of the Shannon and Simpson indices varied based on the reactor type, but the two variables behaved similarly to each other for a given reactor. For the CMAS, both diversity indicators significantly increased, corresponding to an increase in genetic diversity in the reactor, from P1 to P2 with the addition of SOCs, however they returned to pre-SOC levels once the SRT was increased to 10 d. Diversity in the SBR did not change significantly until the SRT was increased to 10 d, at which time the diversity was significantly higher than the 5 d SRT with no SOCs present.

www.manaraa.com

المنارة للاستشارات

Table 4.8

Reactor diversity results.

Reactor	Parameter	Period 1	Period 2	Period 3	Overall	Significant Difference[a]
SBR	Richness (S)	15.3 ± 1.9	17.6 ± 2.6	17.2 ± 3.3	16.8 ± 2.8	Y2,Y3; +
	Shannon (H)	2.36 ± 0.13	2.51 ± 0.14	2.57 ± 0.20	2.49 ± 0.18	2; Y1,Y2; +
	Simpson (D')	8.8 ± 1.4	9.9 ± 1.6	11.5 ± 2.3	10.2 ± 2.1	2; Y2; +
	Evenness (E)	0.86 ± 0.03	0.88 ± 0.03	0.90 ± 0.02	0.88 ± 0.03	2,3; Y1,Y2; +
CMAS	Richness (S)	17.0 ± 1.6	20.7 ± 2.7	20.2 ± 2.6	19.5 ± 2.7	1,2; Y2,Y3; +
	Shannon (H)	2.55 ± 0.13	2.76 ± 0.16	2.65 ± 0.19	2.65 ± 0.18	1; Y1,Y2; +
	Simpson (D')	10.8 ± 1.8	13.4 ± 2.3	12.2 ± 2.4	12.1 ± 2.4	1; Y2; +
	Evenness (E)	0.89 ± 0.02	0.91 ± 0.02	0.88 ± 0.03	0.89 ± 0.03	3; Y1, Y2; +

[a] 1, 2, and 3 indicate a statistically significant difference ($\alpha < 0.05$) between P1 and P2, P1 and P3, and P2 and P3, respectively. Y1, Y2, and Y3 indicate a significant difference between the two reactors for P1, P2, and P3, respectively. + indicates a significant difference for the full experimental period.

www.manaraa.com

In both reactors, if diversity is analyzed as a function only of presence or absence of SOCs, with no differentiation between 5 d and 10 d SRT, the diversity, as represented by both the Shannon and Simpson indices, is significantly higher after the addition of SOCs. This is contrary to the finding of Bayle et al. (2009) who found that high mass loading of VOCs resulted in decreased bacterial diversity, which is the expected response of bacterial communities to toxic compounds. High concentrations of recalcitrant toxic compounds are expected to inhibit populations unable to tolerate the chemicals and select populations capable of acclimating to the presence of the SOCs, which would result in a less diverse community. However, in the study by Bayle et al. (2009) lower concentrations of SOCs resulted in an increase in diversity, and the authors suggest a critical concentration could exist, below which there is a potential for the enhancement of some select populations without significant detriment to the remaining populations. Another potential explanation of this increase in diversity accompanying the incorporation of SOCs could be that the inhibitory effects may be greatest on the organisms with the highest affinity for COD utilization, allowing for a more diverse community of slower growth organisms to develop.

In reviewing the evenness results, the reactor communities responded differently to the operational variations. Based on the evenness values, the structure of the AS community in the SBR had a more even distribution of abundant populations at higher SRT, demonstrated by the significantly higher evenness in P3 with the 10 d SRT than either P1 or P2 with the 5 d SRT. Other researchers have demonstrated varying results in the effects of SRT on community diversity. Akarsubasi et al. (2009), utilizing similar DGGE methods, determined that sludge age had no effect on the evenness or richness of

www.manaraa.com

the AS community. Utilizing T-RFLP methods, the findings of Saikaly et al. (2005) are contrary to the SBR findings in the current study as they reported that a lower SRT resulted in greater evenness, as well as significantly higher Shannon and inverse Simpson diversity indices. This result, although counterintuitive, is supported by the statistically significant decrease in the evenness of the CMAS between P2 and P3. Other researchers have investigated the impact of SRT on activated sludge diversity and have presented a theory of oscillating population dominance among the AS community at lower SRTs, but competitive dominance becomes apparent at higher SRTs (Saikaly & Oerther, 2004). Although both reactors in the current study were controlled to maintain a specific SRT, the effective SRT in the SBR is actually lower than the CMAS when considering the amount of active reaction time in the react period. In a 24 h period, the CMAS has 24 h of reactor operation, while the SBR has 20 h of reactor operation and 4 h of settling. In comparison between the reactors for the full experimental period, the CMAS exhibited a significantly more diverse microbial community than the SBR when statistically comparing the Shannon and Simpson indices. From an effective SRT standpoint, this follows popular environmental theory of competitive exclusion as SRT is increased (Saikaly & Oerther, 2004), but this finding is contrary to the results of Pholchan et al. (2010) who found the banding patterns for an SBR to be more diverse than for a CMAS.

Additional analysis was conducted to determine if correlations exist between the reactor performance parameters and the diversity indices using the Spearman rank coefficient. The resulting correlation matrix is presented in Table 4.9. The correlation matrices for each reactor differed in the parameters that showed significant correlation.

www.manaraa.com

Table 4.9

Spearman correlation matrices.

	CMAS				SBR			
Parameter	H	D'	E	S	H	D'	E	S
MLVSS	-0.06	-0.04	-0.27	0.16	0.37^{+}	0.41^{+}	0.50^{++}	0.20
COD Removal	-0.26	-0.34^{+}	-0.06	-0.36^{+}	0.15	0.14	0.23	0.06
SVI	0.18	0.18	-0.10	0.37^{+}	0.34^{+}	0.24	-0.02	0.47^{++}
MTBE	-0.11	-0.06	-0.17	0.00	-0.30	A	-0.26	-0.12
Acrylonitrile	-0.14	-0.10	-0.03	-0.19	-0.03	0.01	0.07	-0.04
Chlorobenzene	0.10	0.01	0.04	0.06	-0.28	-0.25	-0.07	-0.26

$+p < 0.05$, $++p < 0.005$.

The CMAS reactor exhibited a significant negative correlation between the COD removal and both the Simpson inverse and the richness. This would indicate that the COD removal results were better, i.e. less COD released in the effluent, when the community was less diverse. This finding supports the previously stated theory that SOCs allow for the growth of organisms with less affinity for COD utilization, and thus the greater diversity resulted in lower COD removals. The SBR correlation results showed that a strong positive correlation existed between the mixed liquor suspended solids and all three diversity indices, which would suggest that a larger quantity of activated sludge results in a more diverse floc. However, this relationship was not exhibited in the CMAS reactor. The only result common to both reactors was the significant positive correlation between the SVI and the species richness. A higher SVI, which is indicative of a poorer settling sludge, correlated to a more rich genetic profile. Phenol was omitted from the correlation analysis due to limited effluent data. Of the

www.manaraa.com

other three chemicals incorporated, only one correlation was found to be significant, which was a negative correlation between the inverse Simpson and the effluent MTBE concentration in the SBR.

www.manaraa.com

CHAPTER V

CONCLUSIONS

The primary focus of this study was to determine the effects of toxic SOCs on the AS community in different lab scale reactor configurations. An additional modification during the experiment was an adjustment of the SRT, with the SOCs present, to monitor the response of the AS communities. In an attempt to find a more real-time approach to assess the state of the AS community, a combination of microscopic and molecular analysis techniques were used, which are not typically applied to the wastewater treatment process. IA has the potential to become a beneficial tool for assessing the performance of AS reactors. This research demonstrated that IA of AS samples could provide valuable information about the size and shape of the AS flocs. Floc size parameters appeared to be better predictors of settling performance in the sequencing batch reactor, whereas shape descriptors were more strongly correlated to the sludge settleability in the completely mixed system. It was evident that floc morphology varied as a function of operational conditions and reactor configurations. The type of manual IA demonstrated in this work was effective and could be completed in an equal or slightly shorter time period than the standard SVI, and it could reveal changes occurring at a microscopic level within the AS community. As demonstrated, IA could also be utilized

www.manaraa.com

to assess the effects of external factors on the AS community, such as the influence of SOCs in this study.

In practical applications, it would be much more effective to use an automated, inline sampling device that would capture and process the images on a more frequent or even a real-time basis, and then periodically collect and examine samples manually to verify the results. Da Motta et al. (2001) reported the use of automated IA to detect filamentous bulking at a large scale municipal treatment plant and to detect pin flocs in an industrial treatment application. The multiple morphological parameters obtained through IA provide much more physical information of the sludge and the AS flocs than the SVI and other standard sludge settleability analysis which could aid the evaluation of the condition of the AS. Additionally, the correlation between the floc morphology descriptors and sludge settleability parameters suggests that IA has the potential to substitute for typical settling tests. Mesquita et al. (2009) effectively utilized information obtained from IA to predict gross SVI values.

DGGE analysis is a useful tool in quantifying the community structure of activated sludge flocs. Dendrograms generated through this study indicated a shift in the activated sludge community as a result of adjusting the operational conditions of the reactor. During the initial period with no variations, the banding patterns of samples from a particular reactor associated more closely to other samples from that reactor. Variations in operational conditions led to transient population dynamics within the system. Although some of the findings in this study differed in many respects to the results of other researchers, this research does corroborate many of the core conclusions found by others, specifically that the microbial community structure varies as a function

www.manaraa.com

of reactor configuration and as a result of operational changes, but these relationships are not yet fully understood and the diversity of the microbial community and corresponding performance cannot be systematically controlled with the current level of understanding. However, further research in this area could provide possibilities for more advanced control of biological treatment systems that are systematically engineered to promote the growth of microbial populations specific to the removal of a particular contaminant or to perform to a specified level for a given treatment parameter of interest, or possibly to develop a diverse community capable of handling an array of influent constituents or operational conditions.

www.manaraa.com

CHAPTER VI

RECOMMENDATIONS AND FUTURE RESEARCH

The results of this study demonstrate the transient nature of the AS communities and further evidence the more in-depth understanding required to establish and control the desired engineered bioreactor conditions. Both IA and DGGE analysis are technologies that have the capability of providing additional information about the AS floc conditions that could allow for more advanced process control. IA has the potential for real-time analysis, but the process would need to be simplified and automated to allow for less sophisticated operator requirements. Before IA could make the transition from a strict laboratory-based protocol to a more routine automated monitoring system, additional research in this area is needed to better define the relationships between floc morphology and performance and to establish the specific sample criteria necessary to provide the required floc information. As aggregation dynamics continue to be a focus of research efforts to better understand complicated AS flocculation properties, physical AS floc properties obtained through microscopic image analysis should be incorporated to determine future applicability.

Unlike IA, DGGE analysis is already a proven technology for assessing the diversity of microbiological communities. The process has direct applications to the study of the AS community's response to variations in conditions. In this study, the

www.manaraa.com

primary focus was on the overall community response which was assessed via diversity indices and dendrograms comparing the presence/absence and relative concentration of populations within the community. DNA technology allows for more advanced study beyond the focus of this report that has the potential to provide more specific information about the bacteria directly involved in the degradation of the SOCs. Excising and sequencing of select bands from the DGGE gels can provide specific phylogenetic information about the populations within the AS community. Selecting and sequencing bands that exhibit noticeable variations in intensity, or bands that appear or disappear, in response to external stimuli could provide for identification of the bacterial species that play a significant role in the removal of specific constituents or identify those populations more resistant or more susceptible to the toxicity of SOCs.

Another DNA analysis technology that could be incorporated into future research is catabolic gene diversity analysis. Catabolic gene diversity studies are the logical next step in evaluating the response of the AS community to toxic SOCs in the influent feed. As part of the SOC selection process used in this study, the biodegradation pathways were evaluated to determine specific enzymes involved in the removal of the SOCs. This information could be utilized in future research to develop primers that will target the bacteria responsible for the biodegradation of the SOCs. Using these SOC-specific primers, the catabolic gene diversity could be analyzed before and after the SOCs are incorporated into the feed. Therefore, catabolic gene studies could potentially be applied to the samples taken during this experiment to validate and expound on the results of this study. Analyzing the variations in the catabolic genes responsible for SOC degradation

www.manaraa.com

could provide valuable information about the establishment of SOC-specific populations and the transformations that occur within the AS community due to external variations.

More advanced monitoring capabilities of environmentally significant constituents in effluent waters typically leads to tightening limits on specific contaminants. As the national, and even worldwide, trends continue in which effluent requirements become increasingly stringent, more advanced control of the biological treatment processes is necessary to achieve the level of treatment mandated by regulatory agencies. Biological treatment processes are often more economical than physical/chemical processes, but when treating toxic compounds, these systems have an inherent risk of upsets and potential failure, especially in regards to removal of the toxic SOCs which could inhibit their own biodegradation. Future research in this area is needed to provide a better understanding of the capabilities of biological processes for SOC removal.

www.manaraa.com

REFERENCES

Afonso P., Cunha M. (2002). "Assessing parameter indentifiability of activated sludge model number 1". *Journal of Environmental Engineering*, 128(8), 748-754

Akarsubasi A., Eyice O., Miskin I., Head I., Curtis T. (2009). "Effect of sludge age on the bacterial diversity of bench scale sequencing batch reactors". *Environmental Science & Technology*, 43(8), 2950-2956

Alagappan G., Cowan R. (2001). "Biokinetic models of representing the complete inhibition of microbial activity at high substrate concentrations". *Biotechnology & Bioengineering*, 75(4), 393-405

Allen T. (1997). "Particle Size Measurement. Volume I. Powder Sampling and Particle Size Measurement". Fifth Ed., Chapman & Hall, 2-6 Boundary Row, London

Amann R., Ludwig W., Schleiffer K. (1995). "Phylogenic identification and in suti detection of individual microbial cells without cultivation". *Microbiological Reviews*, 59(1), 143-169

American Cynamide Company (ACC), Petrochemicals Department (1959). "The Chemistry of Acrylonitrile". 2nd Ed., New York

American Public Health Association, American Water Works Association, Water Environment Federation (APHA et al.) (2005). "Standard Methods for the Examination of Water and Wastewater". 21st Ed., Washington, DC

Andrews J. (1968). "A mathematical model for the continuous culture of microorganisms utilizing inhibitory substrates". *Biotechnology & Bioengineering*, 10, 707-723

Araya-Kroff P., Amaral A., Neves L., Ferreira E., Pons M.-N., Mota M., Alves M. (2004). "Development of image analysis techniques as a tool to detect and quantify morphological changes in anaerobic sludge: I. Application to a granulation process". *Biotechnology & Bioengineering*, 87(2), 184-193

Bayle S., Malhautier L., Degrange V., Godon J., Fanlo J. (2009). "Investigation of the acclimatization period: example of the microbial aerobic degradation of volatile organic compounds (VOCs)". *Water Science & Technology*, 60(9), 2217-2225

www.manaraa.com

Bernhardt C. (2004). "Sedimentation of nonspherical particles". *Particle and Particle Systems Characterization*, 8, 209-214

Bielefeldt A., Stensel D. (1999). "Treating VOC-contaminated gases in activated sludge: mechanistic model to evaluate design and performance". *Environmental Science & Technology*, 33(18), 3234-3240

Bisogni J. Jr., Lawrence A. (1971). "Relationships between biological solids retention time and settling characteristics of activated sludge". *Water Research*, 5, 753-763

Bloeman H., Burn J. Eds. (1993). "Chemistry and Analysis of Volatile Organic Compounds in the Environment". Chapman & Hall, Blackie Academic & Professional, Glasgow

Blok J., Struys J. (1996). "Measurement and validation of kinetic parameter values for prediction of biodegradation rates in sewage treatment". *Ecotoxicology and Environmental Safety*, 33(3), 217-227

Bourrain M., Achouak W., Urbain V., Heulin T. (1999). "DNA extraction from activated sludges". *Current Microbiology*, 38, 315-319

Campos J., Sánchez M., Mosquera-Corral A., Méndez R. Lema J. (2003). "Coupled BAS and anoxic USB system to remove urea and formaldehyde from wastewater". *Water Research*, 37(14), 3445-3451

Caballa M., Fink G., Omil F., Lema J., Ternes T. (2008). "Determination of the solid-water distribution coefficient (K_d) for pharmaceuticals, estrogens, and musk fragrances in digested sludge". *Water Research*, 42(1-2), 287-295

Chaignon V., Lartiges B., El Samrani A., Mustin C. (2002). "Evolution of size distribution and transfer of mineral particles between flocs in activated sludges: An insight into floc exchange dynamics". *Water Research*, 36(3), 676-684

Chao K., Ong S., Huang M. (2007). "Mass transfer of VOCs in laboratory-scale air sparging tank". *Journal of Hazardous Materials*, 152, 1098-1107

Chaudhuri S., Patanayak A., Thakur A. (2006). "Microbial DNA extraction from samples of varied origin". *Current Science*, 91(12), 1697-1700

Concha F., Barrientos A. (1986). "Settling velocities of particulate system, 4. Settling of nonspherical particles". *International Journal of Mineral Processing*, 18, 297-308

Contreras E., Bertola N., Zaritzky N. (2001). "The application of different techniques to determine activated sludge kinetic parameters in a food industry wastewater". *Water SA*, 27(2), 169-176

www.manaraa.com

Contreras E., Giannuzzi L., Zaritzky N. (2004). "Use of image analysis in the study of competition between filamentous and non-filamentous bacteria". *Water Research*, 38, 2621-2630

Crites R., Tchobanoglous G. (1998). "Small and Decentralized Wastewater Management Systems". McGraw-Hill, Boston

Crittenden J., Trussell R., Hand D., Howe K., Tchobanoglous G. (2005). "Water Treatment Principles and Design". Second Ed., John Wiley & Sons, Inc., New Jersey

Da Motta M., Pons M., Roche N., Vivier H. (2001). "Characterisation of activated sludge by automated image analysis". *Biochemical Engineering Journal*, 9,165-173

Datta S., Datta S. (2003). "Comparisons and validation of statistical clustering techniques for microarray gene expression data". *Bioinformatics*, 19(4), 459-466

Diaz A., Drogos D. (2002). "Oxygenates in Gasoline: Environmental Aspects". American Chemical Society, Washington, D.C.

Eisen M., Spellman P., Brown P., Bolstein D. (1998). "Cluster analysis and display of genome-wide expression patterns". *Proceedings of the National Academy of Sciences of the USA*, 95(25), 14863-14868

Ercolini D. (2004). "PCR-DGGE fingerprinting: novel strategies for detection of microbes in food". *Journal of Microbiological Methods*, 56, 297-314

Felske A., Engelen B., Nubel U., Backhaus H. (1996). "Direct ribosomal isolation from soil to extract bacterial rRNA for community analysis". *Applied and Environmental Microbiology*, 62(11), 4162-4167

Ferris M., Muyzer G., Ward D. (1996). "Denaturing gradient gel electrophoresis profiles of 16S rRNA-defined populations inhabiting a hot spring microbial mat community". *Applied and Environmental Microbiology*, 62(2), 340-346

Forster C. (1985a). "Factors involved in the settlement of activated sludge-I: nutrients and surface polymers". *Water Research*, 19(10), 1259-1264

Forster C. (1985b). "Factors involved in the settlement of activated sludge-II: the binding of polyvalent metals". *Water Research*, 19(10), 1265-1271

Fouad M., Bhargava R. (2005). "Mathematical model for the biofilm-activated sludge reactor". *Journal of Environmental Engineering*, 131(4), 557-562

www.manaraa.com

Fromin N., Hamelin J., Tarnawski S., Roesti D., Jourdain-Miserez K., Forestier N., Teyssier-Cuvelle S., Gilet F., Aragno M., Rossi P. (2002). "Statistical analysis of denaturing gel electrophoresis (DGE) fingerprinting patterns". *Environmental Microbiology*, 4(11), 634-643

Gillan D., Speksnijder A., Zwart G., De Ridder C. (1998). "Genetic diversity of the biofilm covering *Montacuta ferruginosa* (Mollusca, Bivalvia) as evaluated by denaturing gradient gel electrophoresis analysis and cloning of PCR-amplified gene fragments coding for 16S rRNA". *Applied and Environmental Microbiology*, 64(9), 3464-3472

Goodwin J., Forster C. (1985). "A further examination into the composition of activated sludge surfaces in relation to their settlement characteristics". *Water Research*, 19(4), 527-533

Goudar C., Ellis T. (2001). "Explicit oxygen concentration expression for estimating extant biodegradation kinetics from respirometric experiments". *Biotechnology and Bioengineering*, 75(1), 74-81

Grady C. Jr., Magbanua B. Jr., Brau S., Sanders R. (1997). "A simple technique for estimating the contribution of abiotic mechanisms to the removal of synthetic organic chemicals by completely mixed activated sludge". *Water Environment Research*, 69(7), 1232-1237

Grady C. Jr., Smets B., Barbeau D. (1996). "Variability in kinetic parameter estimates: A review of possible causes and a proposed terminology". *Water Research*, 30(3), 742-748

Grijspeerdt K., Verstraete W. (1997). "Image analysis to estimate the settleability and concentration of activated sludge". *Water Research*, 31(5), 1126-1134

Guan J., Waite T., Rose A. (1998). "Rapid structure characterization of bacterial aggregates". *Environmental Science and Technology*, 32, 3735-3742

Gujer W., Henze M., Mino T., Van Loosdrecht M. (1999). "Activated sludge model No. 3". *Water Science and Technology*, 39(1), 183-193

Halder A., Levenspiel O. (1989). "Drag coefficient and terminal velocity of spherical and nonspherical particles". *Powder Technology*, 58, 63-70

Håkansson K., Welander U., Mattiasson B. (2005). "Degradation of acetonitrile through a sequence of microbial reactors". *Water Research*, 39, 648-654

www.manaraa.com

Henckel T., Jackel U., Schnell S., Conrad R. (2000). "Molecular analysis of novel methanotropic communities in forest soil that oxidize atmospheric methane". *Applied and Environmental Microbiology*, 66(5), 1801-1808

Henze M., Grady C. Jr., Gujer W., Marais G., Matsuo T. (1987). "A general model for single-sludge wastewater treatment systems". *Water Research*, 21, 505-515

Henze M., Gujer W., Mino T., Matsuo T., Wentzel M., Marais G., Van Loosdrecht M. (1999). "Activated sludge model No. 2D, ASM2D". *Water Science and Technology*, 39(1), 165-182

Hsieh C. (2000). "Removal mechanisms of VOCs in an activated sludge process". *Journal of Hazardous Materials*, B79, 173-187

Hu Z., Ferraina R., Ericson J., MacKay A., Smets B. (2005). "Biomass characteristics in three sequencing batch reactors treating a wastewater containing synthetic organic chemicals". *Water Research*, 39, 710-720

Jacobs J., Guertin J., Herron C. (2001). "MTBE: Effects on Soil and Groundwater Resources". Lewis Publishers, CRC Press LLC, Boca Raton, FL

Jeong J., Yoon J. (2004). "Dual roles of $CO_2^{-\bullet}$ for degrading synthetic organic chemicals in the photo/ferrioxalate system". *Water Research*, 38, 3531-3540

Jin B., Wilén B., Lant P. (2004). "Impacts of morphological, physical and chemical properties of sludge flocs on dewaterability of activated sludge". *Chemical Engineering Journal*, 98, 115-126

Jorand F., Zartarian F., Thomas F., Block J., Bottero J., Villemin G., Urbain V., Manem J. (1995). "Chemical and structural (2D) linkage between bacteria within activated sludge flocs". *Water Research*, 29(7), 1639-1647

Junca H., Pieper D. (2004). "Functional gene diversity analysis in BTEX contaminated soils by means of PCR-SSCP DNA fingerprinting: comparative diversity assessment against bacterial isolates and PCR-DNA clone libraries". *Environmental Microbiology*, 6(2), 95-110

Junca H., Pieper D. (2003). "Amplified functional DNA restriction analysis to determine catechol 2,3-dioxygenase gene diversity in soil bacteria". *Journal of Microbiological Methods*, 55, 697-708

Keith L. (1996). "Compilation of EPA's Sampling and Analysis Methods". Second Edition. Lewis Publishers, A CCR Press Company, Boca Raton, FL

www.manaraa.com

Kesavan P., Law V. (2005). "Practical identifiability of parameters in Monod kinetics and statistical analysis of residuals". *Biochemical Engineering Journal*, 24, 95-104

Kilander J., Blomström S., Rasmuson A. (2006). "Spatial and temporal evolution of floc size distribution in a stirred square tank investigated using PIV and image analysis". *Chemical Engineering Science*, 61, 7651-7667

Klimiuk E., Kulikowsha D. (2004). "Effectiveness of organics and nitrogen removal from municipal landfill leachate in single- and two-stage SBR systems". *Polish Journal of Environmental Studies*, 13(5), 525-532

Kovárová-Kovar K., Elgi T. (1998). "Growth kinetics of suspended microbial cells: From single-substrate-controlled growth to mixed-substrate kinetics". *Microbiology and Molecular Biology Reviews*, 62(3), 646-666

Kümmerer K., Ed. (2004). "Pharmaceuticals in the Environment. Sources, Fate, Effects, and Risks". Second Ed., Springer-Verlag Berlin Heidelberg, Germany

Laera G., Giordano C., Pollice A., Saturno D., Mininni G. (2007). "Membrane bioreactor sludge rheology at different solid retention times". *Water Research*, 41(18), 4197-4203

LaGrega M., Buckingham P., Evans J. (2001). "Hazardous Waste Management and Environmental Resources Management". Second Ed., McGraw-Hill, New York

Lee D., Chen G., Liao Y., Hsieh C. (1996). "On the free-settling test for estimating activated sludge floc density". *Water Research*, 30, 541-550

Lee S., Koopman B., Bode H., Jenkins D. (1983). "Evaluation of alternative sludge settleability indices". *Water Research*, 17(10), 1421-1426

Li D., Ganczarczyk J. (1991). "Size distribution of activated sludge flocs". *Research Journal of the Water Pollution Control Federation*, 63(5), 806-814

Liao B., Allen D., Droppo I., Leppard G., Liss S. (2001). "Surface properties of sludge and their role in bioflocculation and settleability". *Water Research*, 35(2), 339-350

Liao B., Droppo I., Leppard G., Liss S. (2006). "Effect of solids retention time on structure and characteristics of sludge flocs in sequencing batch reactors". *Water Research*, 40, 2583-2591

Liwarska-Bizukojc E., Bizukojc M. (2005). "Digital image analysis to estimate the influence of sodium dodecyl sulphate on activated sludge flocs". *Process Biochemistry*, 40, 2067-2072

www.manaraa.com

Lopez C., Pons M., Morgenroth E. (2005). "Evaluation of micrscopic techniques (epifluorescence microscopy, CLSM, TPE-LSM) as a basis for the quantitative image analysis of activated sludge". *Water Research*, 39, 456-468

Lovett D., Kavanagh B., Herbert L. (1983). "Effect of sludge age and substrate composition on the settling and dewatering characteristics of activated sludge". *Water Research*, 17(11), 1511-1515

Lyautey E., Lacoste B., Ten-Hage L., Rols J., Garabetian F. (2005). "Analysis of bacterial diversity in river biofilms using 16S rDNA PCR-DGGE: methodological settings and fingerprints interpretation". *Water Research*, 39, 380-388

Magbanua B. Jr., Hoover P., Campbell P., Bowers A. (1994). "The effect of cosubstrates on phenol degradation kinetics". *Water Science and Technology*, 30(9), 67-77

Magbanua B. Jr., Poole L., Grady C. Jr. (1998). "Estimation of the competent biomass concentration for the degradation of synthetic organic compounds in an activated sludge culture receiving a multicomponent feed". *Water Science and Technology*, 38(8-9), 55-62

Magbanua B. Jr., Smets B., Bowyer R., Rodieck A., Sanders R., Sowerz W., Stolze S., Grady C. Jr. (2003). "Relative efficacy of intrinsic and extant parameters for modeling biodegradation of synthetic organic compounds in activated sludge: Steady-state systems". *Water Environment Research*, 75, 126-136

Magbanua B. Jr., Stanfill J., Fehniger S., Smets B., Farkas F., Grady C. Jr. (2004). "Relative efficacy of intrinsic and extant parameters for modeling biodegradation of synthetic organic compounds in activated sludge: Dynamic systems". *Water Environment Research*, 76, 256-267

Massé A., Spérandio M., Cabassud C. (2006). "Comparison of sludge characteristics and performance of submerged membrane bioreactor and an activated sludge process at high solids retention time". *Water Research*, 40, 2405-2415

McMurry J. (1984). "Organic Chemistry". Brooks/Cole Publishing Company, Monterey, CA

Mesarch M., Nakatsu C., Nies L. (2000). "Development of catechol 2,3-dioxygenase-specific primers for monitoring bioremediation by competitive quantitative PCR". *Applied and Environmental Microbiology*, 66(2), 678-683

Mesquita D., Dias O., Amaral A., Ferreira E. (2009). "Monitoring of activated sludge settling ability through image analysis: validation on full-scale wastewater treatment plants". *Bioprocess and Biosystems Engineering*, 32(3), 361-367

www.manaraa.com

Metcalf & Eddy, Inc. (2003). "Wastewater Engineering: Treatment and Reuse". Fourth Ed., McGraw-Hill, New York

Mineta R., Salehi Z., Yoshikawa H., Kawase Y. (2011). "Oxygen transfer during aerobic biodegradation of pollutants in a dense activated sludge slurry bubble column: Actual volumetric oxygen uptake rate in p-nitrophenol degradation by acclimated waste activated sludge". *Biochemical Engineering Journal*, 53, 266-274

Monod, J. (1949) The growth of bacterial cultures. *Annual Reviews in Microbiology* 3, 371-394.

Morgan, J., Forster, C., Evison, L. (1990) A comparative study of the nature of biopolymers extracted from anaerobic and activated sludges. *Water Research* 24(6), 743-750.

Murray, A.E., Hollibaugh, J.T., Orrego, C. (1996) Phylogenic compositions of bacterioplankton from two California estuaries compared by denaturing gradient gel electrophoresis of 16S rDNA fragments. *Applied & Environmental Microbiology* 62(7), 2676-2680.

Muyzer, G. (1999) DGGE/TGGE a method for identifying genes from natural ecosystems. *Current Opinion in Microbiology* 2, 317-322.

Muyzer, G., De Waal, E., Uitterlinden, A. (1993) Profiling of complex microbial populations by denaturing gradient gel electrophoresis analysis of polymerase chain reaction-amplified genes coding for 16S rRNA. *Applied & Environmental Microbiology* 59(3), 695-700.

Nakatsu, C., Torsvik, V., Ovreas, L. (2000) Soil community analysis using DGGE of 16S rDNA polymerase chain reaction products. *Soil Science Society of America Journal* 64, 1382-1388.

Nakhla, G., Liu, V., Bassi, A. (2006) Kinetic modeling of aerobic biodegradation of high oil and grease rendering wastewater. *Bioresource Technology* 97, 131-139.

National Center for Biotechnology Information (NCBI) (2007). Accessed online at: www.ncbi.nlm.nih.gov.

Perron, N., Welander, U. (2004) Degradation of phenol and cresols at low temperatures using a suspended-carrier biofilm process. *Chemosphere* 55(1), 45-50.

Pholchan, M., Baptista, J., Davenport, R., Curtis, T. (2010) Systematic study of the effect of operating variables on reactor performance and microbial diversity in laboratory-scale activated sludge reactors. *Water Research* 44(5), 1341-52.

www.manaraa.com

Pons, M., Vivier, H., Rémy, J., Dodds, J. (1993) Morphological characterization of yeast by image analysis. *Biotechnology & Bioengineering* 42(11), 1352-1359.

Reysenbach, A., Giver, L., Wickham, G., Pace, N. (1992) Differential amplification of rRNA genes by polymerase chain reaction. *Applied & Environmental Microbiology* 58(10), 3417-3418.

Rittmann, B., McCarty, P. (2001) *Environmental Biotechnology: Principles and Applications*. McGraw-Hill, New York.

Rudolph, J., Grady, C. Jr. (2002) Catabolic enzyme levels in bacteria grown on binary and ternary substrate mixtures in continuous culture. *Biotechnology & Bioengineering* 79(2), 188-199.

Saikaly, P., Oerther, D. (2004) Bacterial competition in activated sludge: Theoretical analysis of varying solids retention times on diversity. *Microbial Ecology* 48(2), 274-284.

Saikaly, P., Stroot, P., Oerther, D. (2005) Use of 16S rRNA gene terminal restriction fragment analysis to assess the impact of solids retention time on the bacterial diversity of activated sludge. *Applied & Environmental Microbiology* 71(10), 5814-5822.

Schnoor, J. *Ed.* (1992) *Fate of Pesticides and Chemicals in the Environment*. John Wiley & Sons, Inc., New York.

Sponza, D. (2004) Properties of four biological flocs as related to settling. *Journal of Environmental Engineering* 130(11), 1289-1300.

Suzuki, M., Giovannoni, S. (1996) Bias caused by template annealing in the amplification of mixtures of 16S rRNA genes by PCR. *Applied & Environmental Microbiology* 62(2), 625-630.

Swamee PK, Ojha CSP. 1989. Drag coefficient and fall velocity of nonspherical particles. J Hydraul Eng ASCE 117, 660-667.

USEPA (1979a) *Water-Related Environmental Fate of 129 Priority Pollutants*. EPA-440-4-79-029b, Office of Water Planning and Standards, Washington, D.C.

USEPA (1979b) *Status Assessment of Toxic Chemicals: Acrylonitrile.* EPA-600-2-79-210a, Industrial Environmental Research Laboratory, Cincinnati, OH.

USEPA (1994) *Acrylonitrile Fact Sheet: Support Document (CAS No. 107-13-1).* EPA-749-F-95-001a, Office of Pollution Prevention and Toxics, Washington, D.C.

www.manaraa.com

USEPA (1995) *Chlorobenzene Fact Sheet: Support Document (CAS No. 108-90-7).* EPA-749-F-95-007a, Office of Pollution Prevention and Toxics, Washington, D.C.

USEPA (1998) *Ambient Water Quality Criteria for the Protection of Human Health: Acrylonitrile.* EPA-822-R-98-006, Office of Water, Washington, D.C.

USEPA (2002) *Toxicological Review of Phenol*. EPA-635-R-02-006, Office of Solid Waste, Washington, D.C.

USEPA, Syracuse Research Corporation (EPA-SRC) (2007) Estimation Programs Interface (EPI) Suite, Version 3.20. Accessed online at: http://www.epa.gov/oppt/exposure/pubs/episuitedl.htm.

University of Minnesota Biocatalyst/Biodegradation Database (UMBBD) (2007). Accessed online at: http://umbbd.msi.umn.edu/index.html.

Van der Gucht, K., Sabbe, K., De Meester, L., Vloemans, N., Zwart, G., Gillis, M., Vyverman, W. (2001) Contrasting bacterioplankton community composition and seasonal dynamics in two neighbouring hypertrophic freshwater lakes. *Environmental Microbiology* 3(11), 680-690.

Vavilin, V., Lokshina, L. (1996) Modeling of volatile fatty acids degradation kinetics and evaluation of microorganism activity. *Bioresource Technology* 58, 69-80.

Viessman, W., Hammer, M. (2004) *Water Supply and Pollution Control*. Seventh Ed., Prentice Hall, Upper Saddle River, New Jersey.

Watanabe, K., Kodama, Y., Harayama, S. (2001) Design and evaluation of PCR primers to amplify bacterial 16S ribosomal DNA fragments used for community fingerprinting. *Journal of Microbiological Methods* 44, 253-262.

Watanabe, K., Teramoto, M., Futamata, H., Harayama, S. (1998) Molecular detection, isolation, and physiological characterization of functionally dominant phenol-degrading bacteria in activated sludge. *Applied & Environmental Microbiology* 64(11), 4396-4402.

Watts, J., Wu, Q., Schreier, S., May, H., Sowers, K. (2001) Comparative analysis of polychlorinated biphenyl-dechlorinating communities in enrichment cultures using three different molecular screening techniques. *Environmental Microbiology* 3(11), 710-719.

Widada, J., Nojiri, H., Omori, T. (2002) Recent developments in molecular techniques for identification and monitoring of xenobiotic-degrading bacteria and their catabolic genes in bioremediation. *Applied Microbiology & Biotechnology* 60, 45-59.

www.manaraa.com

Wilén, B., Jin, B., Lant, P. (2003) The influence of key chemical constituents in activated sludge on surface and flocculating properties. *Water Research* 37, 2127-2139.

Wilke, C., Chang, P. (1955) Correlation of diffusion coefficients in dilute solutions. *American Institute of Chemical Engineering Journal* 1(2), 264-270.

Xia, S., Shi, Y., Fu, Y., Ma, X. (2005) DGGE analysis of 16S rDNA of ammonia-oxidizing bacteria in chemical-biological flocculation and chemical coagulation systems. *Applied Microbiology & Biotechnology* 69, 99-105.

Zita, A., Hermansson, M. (1997) Effects of bacterial cell surface structure and hydrophobicity on attachment to activated sludge flocs. *Applied & Environmental Microbiology* 63(3), 1168-1170.

www.manaraa.com

APPENDIX A

ORIGINAL AND MOTIFIED DNA EXTRACTION PROTOCOLS

www.manaraa.com

ORIGINAL MOBIO DNA EXTRACTION PROTOCOL:

1. Add 1.8 ml of microbial (bacteria, yeast) culture to a 2 ml Collection Tube and centrifuge at 10,000 x g for 30 seconds at room temperature. Decant the supernatant and spin the tubes at 10,000 x g for 30 seconds at room temperature and completely remove the media supernatant with a pipet tip. NOTE: Based on the type of microbial culture, it may be necessary to centrifuge longer than 30 seconds.

2. Resuspend the cell pellet in 300 µl of MicroBead Solution and gently vortex to mix. Transfer resuspended cells to MicroBead Tube.

3. Add 50 µl of Solution MD1 to the MicroBead Tube.

4. Optional: To increase yields, heat at 65ºC for 10 minutes.

5. Secure bead tubes horizontally using the MO BIO Vortex Adapter tube holder for the vortex (Catalog No. 13000-V1) or secure tubes horizontally on a flat-bed vortex pad with tape. Vortex at maximum speed for 10 minutes.

6. Make sure the 2 ml MicroBead Tubes rotate freely in the centrifuge without rubbing. Centrifuge the tubes at 10,000 x g for 30 seconds at room temperature. CAUTION: Be sure not to exceed 10,000 x g or tubes may break.

7. Transfer the supernatant to a clean 2 ml Collection Tube (provided).

8. NOTE: Expect 300 to 350 µl of supernatant.

9. Add 100 µl of Solution MD2, to the supernatant. Vortex 5 seconds. Then incubate at 4ºC for 5 minutes.

10. Centrifuge the tubes at room temperature for 1 minute at 10,000 x g.

11. Avoiding the pellet, transfer the entire volume of supernatant to a clean 2 ml Collection Tube. Expect approximately 450 µl in volume.

12. Add 900 µl of Solution MD3 to the supernatant and vortex 5 seconds.

13. Load about 700 µl into the Spin Filter and centrifuge at 10,000 x g for 30 seconds at room temperature. Discard the flow through, add the remaining supernatant to the Spin Filter, and centrifuge at 10,000 x g for 30 seconds at room temperature. NOTE: A total of 2 to 3 loads for each sample processed are required. Discard all flow through liquid.

www.manaraa.com

14. Add 300 µl of Solution MD4 and centrifuge at room temperature for 30 seconds at 10,000 x g.
15. Discard the flow through.

16. Centrifuge at room temperature for 1 minute at 10,000 x g.

17. Being careful not to splash liquid on the spin filter basket, place Spin Filter in a new 2 ml Collection Tube.

18. Add 50 µl of Solution MD5 to the center of the white filter membrane.

19. Centrifuge at room temperature for 30 seconds at 10,000 x g.

20. Discard Spin Filter. The DNA in the tube is now ready for any downstream application. Store at -20 ºC.

MODIFIED DNA EXTRACTION PROTOCOL USING MOBIO KIT:

1. Collect two 2 ml samples from activated sludge reactor in Collection Tubes by submerging in reactor and opening tubes.

2. Centrifuge at 10,000 x g for 30 seconds at room temperature. Decant 1.2 ml of supernatant. Resuspend cell pellet with remaining supernatant and combine into single tubes.

3. Centrifuge at 10,000 x g for 30 seconds at room temperature. Decant supernatant and spin the tubes at 10,000 x g for 1 minute. Completely remove the media supernatant with a pipet tip.

4. Resuspend the cell pellet in 300 µl of MicroBead Solution and invert tube 3-5 times to mix. Transfer resuspended cells to MicroBead Tube.

5. Add 50 µl of Solution MD1 to the MicroBead Tube.

6. To increase yield, heat at 65ºC for 10 minutes in water bath.

7. Secure bead tubes in Disrupter Genie and run at maximum speed for 5 minutes.

8. Continue from Step 6 in the original MoBio DNA extraction protocol.

www.manaraa.com

APPENDIX B

ORIGINAL AND MODIFIED MICROSCOPIC IMAGE PROCESSING

MATLAB CODES

www.manaraa.com

ORIGINAL MATLAB CODE:

```
function newImage = Segmentation(I)
%this is a function that will accept a color image as its input
% and perform the object recognition

%below 'im' just stands for 'image'.

%this function displays four images along the course of the segmentation procedure
%to help identify what is occurring along the way.  You can just remove the
%"figure, imshow(im);" lines to prevent this, or add more
%"figure, imshow(im)" lines after each line to see what occurs after every
%single line, if one feels inclined to do that.

%if there are any questions about functions, you can just simply type in
%the function name at the MATLAB help menu, and the help menu will detail
%each function.

%written by Peter Rush
%-----------------------------------------------------------------------%
%begin

im = rgb2gray(I); %converts the color image into a gray-scale image

im = imbothat(im, ones(15));
        %performs a bottom hat transformation with a structuring element of size 15
        %ones(x) is a predefined matlab function that
        %returns a matrix of size x by x, and every
         %value is equal to 1

im = histeq(im); % performs a histogram equalization
im = Threshold(im, IntermeansAlgorithm(im));
        %I wrote the threshold and IntermeansAlgorithm functions
        %they can be found below

im = im2bw(im);
         %this just converts im from gray scale to a logical image
        %this just means the values go from 0-255 (gray scale) to
        %either 0 or 1 (logical). 1 = white, 0 = black

im = ~im;
        %this just reverses the image, i.e. 1 becomes 0, 0 becomes 1
        %the '~' can perform this operation on any logical array/matrix
         %at any point beyond this, you can reverse the image from blac
        %floc with white background to white floc with black background
```


www.manaraa.com

```
        %by using the "im = ~im;" function. However, it must be done
        %before the 'imfill' function below or erratic results occur.

im= imdilate(im, ones(2));
        %performs an image dilation with a structuring element of size 2.
       %this improves the image

figure, imshow(im), title('image after dilation.' );
        %the imshow() function
       %just displays the image

im = ~im;
       %have to reverse it again to perform the 'imfill' function.
       %if you do not perform this line, 'imfill' performs erratically

im = imfill(im, 'holes');
        %fills in holes in the flocs

figure, imshow(im), title('image after imfill.' );

im = imerode(im, ones(3));
       % performs another erosion removing noise
       %NOTE:  the line directly above this one
       %requires human interaction to change the size of the
       %structuring element (which is 'ones(3)' in this
       %case) if the filaments or any other lines are
       %still connected in the image that is shown
       %by the 'imshow' function in the line below. If
       %there are still filaments connected, just
       %increase the size of ones(3) to ones(4) and run
       %the code again. If still unsatisfactory,
       %increase to ones(5), and so forth until
       %satisfactory results occur. The flocs become smaller
       %though as the integer increases; the line
       %im = imdilate(im, ones(2));

       %can be performed to "grow" the function to a larger size.
       %Increase 2 as done above until satisfactory results
       %occur.

       %for example, the image '10x3.bmp' image sent to
       %me requires ones(3) to disconnect all
       %filaments,but '10x4.bmp' requires ones(4).
       %I have to go back and manually increase this
       %each time I change between the two images.
```


www.manaraa.com

```
figure, imshow(im), title('image after erosion');

im = bwareaopen(im, 1000);
          %this just removes all elements from the image
          %that are less than 1000 pixels in size (size
          %here just means the number of connected pixels)

          %You can increase or decrease the 1000, but I
          %find 1000 to be simple and satisfactory

figure, imshow(im), title('after bwareaopen() call');

newImage = im;

%end Segmentation.m
%--------------------------------------------------------------------%

%--------------------------------------------------------------------%
%begin Intermeans Algorithm

function t = IntermeansAlgorithm(originalImage)
          % this function will perform the Intermeans Algorithm
          %it accepts the variable “originalImage”, and returns
          %the integer t, which will be the thresholding value for that specific
          %image that satisfies the Intermeans Algorithm

dimensions = size(originalImage);
          %this returns a 2 element vector into "dimensions",
          %1st being row size, the 2nd being column size

rows = dimensions(1);
          %sets the variable rows to the # of rows in the matrix passed to the function

cols = dimensions(2);
          %sets the variable cols to the # of columns in the matrix passed to the function

H(256) = 0;
          %creates an array of 256 elements that will be used to store the occurrence
          %of each pixel value in the image

for i = 1 :rows
   for j = 1 : cols
      temp = originalImage(i,j) ; %must use temp + 1 since image is from 0-255
      H( temp +1 ) = H(temp + 1) + 1; %but array is from 1-256
   end %ends the for j=1
```


www.manaraa.com

```
end %ends the for i=1

%Now H has the occurence of each pixel value stored in the array index of
%that pixel value + 1

%Need to perform intermeans algorithm
t = median(H); % t is the median value of H
temp = 0; %this is a temporary storage value containing t's value the previous iteration

while(t ~= temp)
   temp = t;
   u1 = 0; u2 = 0; u1_ = 0; u2_ = 0;
         %restores these summation values back to zero
         %after each iteration

   for i=1: t
      %need error handling to make sure H(i) isn't zero
      %so a "divide by zero" warning doesn't occur

          if(H(i) ~= 0)
         u1 = u1 + ((i-1) * H(i) ) ; %first summation of u1 (numerator)
         u1_ = u1_ + H(i); %second summation of u1 (the denominator)
      end %end if
   end %end for

   for i = t+1: 256
     if(H(i) ~= 0)  %again,need error handling to avoid "divide by zero"
         u2 = u2 + ( (i-1) * H(i) );  %first summation of u2 (numerator)
         u2_ = u2_ + H(i);          %second summation of u2 (the denominator)
     end %end if
   end %end for

   if(u1_ ~= 0 && u2_ ~= 0)
      u1 = u1/ u1_ ;
      u2 = u2/ u2_ ;
   end

   %now, need to make t the average of the 2 values, storing t as integer
   t = floor((u1 + u2)/2) ;
end
%end Intermeans Algorithm
%-----------------------------------------------------------------------%

%-----------------------------------------------------------------------%
%begin Threshold
```


www.manaraa.com

```
function newImage = Threshold(originalImage, t)
        % this function will perform a single threshold;
        %it accepts the variable “originalImage” and integer t, and returns the variable
        %newImage, which will be the new image after the algorithm is performed on the
        %original image; all values less than or equal to t become 0, and all those
        %greater become 255

newImage = originalImage;
        %I do this to allocates memory space for newImage
dimensions = size(originalImage);
        %this returns a 2 element vector into "dimensions",
         %1st being row size, the 2nd being column size
rows = dimensions(1);
        %sets the variable rows to the # of rows in the matrix passed to the function
cols = dimensions(2);
        %sets the variable cols to the # of columns in the matrix passed to the function
for i = 1 :rows
   for j = 1 : cols
      if(originalImage(i,j) <= t)
         newImage(i,j) = 0;
      else
         newImage(i,j ) = 255;
      end
   end %ends the for j=1 ...
end %ends the for i=1...

%end Threshold function
%-----------------------------------------------------------------------%
```


www.manaraa.com

MODIFIED MATLAB CODE:

```
function [DataTable] = ImageAnal(foldername,reactortype,a,b,c)
        %Function carries out image analysis on all images in a folder of a given
        %reactor type, and if c is greater than one and b is less than a it will
        %do multiple iterations of a random subset of the data to check for
        %reproducibility of results.
        %Function returns a data table that gives results from a permutation check
        %of the data from the processed images.  The input is foldername = complete
        %folder location, reactortype =  SBR or CMAS, a = number of slides to be
        %processed, b = number of slides per permutation, c = number of iterations
        %to be performed.
%-------------------------------------------------------------------------%
%begin
format long;

 %The following is in order to use on R images
 %where R will be a random permutation of the slides.
  q = 1;
        % q is used to count the total number of flocs (i.e. the number of times through
        %the loop).
  p = 1; % used to store loop number in case choose starting j not equal to 1.
  for j = 1:a
     str = strcat( foldername, reactortype,'4x' , int2str(j),'.bmp');
         %concatenates string name & j & .bmp
        %Currently, folder name is 'Floc images/Month Year/Mo. Day/'

     eval('I=imread(str);'); %performs imread funtion of str into I
     im = Segmentation(I);   %Carries out segmentation program on image I

     [im2,numObjects] = bwlabel(im);
        %labels connected objects  with same and gives total number of objects

     stats = regionprops(im2,'Area','Perimeter','EquivDiameter',
        'MajorAxisLength','MinorAxisLength');
        % finds the desired properties of the images
        % More or less properties can be added, but the way the current code
        % is constructed user must edit the number of columns in array A below, and
        % must change the properties in the storing loop below.
        %loop for storing stats in Array A

       for w = 1:numObjects
           m = p + w -1;
        % Used to set m = 1 if i and j both equal 1.
```


www.manaraa.com

```
        if (m = = 1)
              A = [p w stats(w).Area stats(w).Perimeter stats(w).EquivDiameter
              stats(w).MajorAxisLength stats(w).MinorAxisLength ];
              % Stores info for first time so successive stats can be added in
              % additional rows to the same matrix.
        end %ends if

        if (m > 1)
              A = [A; p w stats(w).Area stats(w).Perimeter stats(w).EquivDiameter
              stats(w).MajorAxisLength stats(w).MinorAxisLength ];
               % Stores data in successive rows for each image/floc.
        end  %ends if

        q = q + 1; %counts number of flocs.
      end %ends for b = 1....
   p = p+1;  %counts loop iterations.
end %ends j = 1...

DataTable{1,1} = 'Iteration';
DataTable{1,2} = 'Total Images';
DataTable{1,3} = 'Total Flocs';
DataTable{1,4} = 'Avg Area';
DataTable{1,5} = 'Area SD';
DataTable{1,6} = 'Area Cu';
DataTable{1,7} = 'Avg Eq. Dia.';
DataTable{1,8} = 'Eq. Dia. SD';
DataTable{1,9} = 'Eq. Dia. Cu';
DataTable{1,10} = 'Avg Form Factor';
DataTable{1,11} = 'FF SD';
DataTable{1,12} = 'FF Cu';
DataTable{1,13} = 'Avg Aspect Ratio';
DataTable{1,14} = 'AR SD';
DataTable{1,15} = 'AR Cu';
DataTable{1,16} = 'Avg Roundness';
DataTable{1,17} = 'RD SD';
DataTable{1,18} = 'RD Cu';
DataTable{1,19} = 'Unused images';

if c>1 %does multiple permutations and iterations if c is greater than one.
  for x=1:c
   check = 1; %set to one to establish first array row
   R = randperm(a);
   for i =1:b %calculations for b subsets
      for k = 1:(q-1); %subset for q flocs
```


www.manaraa.com

```
        if (R(1,i)==A(k,1))&(check~=1)
           Array = [Array; A(k,:)];
           tflocs = tflocs + 1;
        end %ends if

        if (R(1,i)==A(k,1))&(check == 1)
           Array = A(k,:);
           check = 2;
           tflocs = 1; %to count total flocs in the given subset
        end %ends if
      end %ends k = 1....
end %ends i = 1....

Totalflocs = tflocs;

[Aavg, Astd, CuA] = Area(Array, Totalflocs);
   %Calls Area function that manipulates Area data
[EqDavg, EqDstd, CuD] = EquivDia(A,Totalflocs);
    %Calls EquivDia function that manipulates Equivalent Diameter data
[FFavg, FFstd, Cff] = FormFactor(A, Totalflocs);
   %Calls FormFactor function to calculate Form Factor
[ARavg, ARstd, Car] = AspectRatio(A, Totalflocs);
   %Calls function to calculate Aspect Ratio
[RDavg, RDstd, Crd] = Roundness(A, Totalflocs);
   %Calls function to calculate Roundness

for z = 1:(a-b)
  if (z == 1)
    str3 = int2str(R(1,1+b));
  end %ends if

  if z >1
     str2 = int2str(R(1,(z+b)));
     str3 = strcat( str3, ',', str2);
  end
end %ends for z = 1..

  DataTable{x+1,1} = x;
  DataTable{x+1,2} = b;
  DataTable{x+1,3} = Totalflocs;
  DataTable{x+1,4} = Aavg;
  DataTable{x+1,5} = Astd;
  DataTable{x+1,6} = CuA;
  DataTable{x+1,7} = EqDavg;
  DataTable{x+1,8} = EqDstd;
```


www.manaraa.com

```
        DataTable{x+1,9} = CuD;
        DataTable{x+1,10} = FFavg;
        DataTable{x+1,11} = FFstd;
        DataTable{x+1,12} = Cff;
        DataTable{x+1,13} = ARavg;
        DataTable{x+1,14} = ARstd;
        DataTable{x+1,15} = Car;
        DataTable{x+1,16} = RDavg;
        DataTable{x+1,17} = RDstd;
        DataTable{x+1,18} = Crd;
        DataTable{x+1,19} = str3;
      end %ends for x....
   end %ends if c>1

if (c == 1) %if you are only doing a single iteration
      Totalflocs = (q-1);
      [Aavg, Astd, CuA] = Area(A, Totalflocs);
         %Calls function that manipulates Area data
      [EqDavg, EqDstd, CuD] = EquivDia(A,Totalflocs);
         %Calls function that manipulates Equivalent Diameter data
      [FFavg, FFstd, Cff] = FormFactor(A, Totalflocs);
          %Calls function to calculate Form Factor
      [ARavg, ARstd, Car] = AspectRatio(A, Totalflocs);
          %Calls function to calculate Aspect Ratio
      [RDavg, RDstd, Crd] = Roundness(A, Totalflocs);
         %Calls function to calculate Roundness

    x = 1;
        DataTable{x+1,1} = x;
        DataTable{x+1,2} = a;
        DataTable{x+1,3} = Totalflocs;
        DataTable{x+1,4} = Aavg;
        DataTable{x+1,5} = Astd;
        DataTable{x+1,6} = CuA;
        DataTable{x+1,7} = EqDavg;
        DataTable{x+1,8} = EqDstd;
        DataTable{x+1,9} = CuD;
        DataTable{x+1,10} = FFavg;
        DataTable{x+1,11} = FFstd;
        DataTable{x+1,12} = Cff;
        DataTable{x+1,13} = ARavg;
        DataTable{x+1,14} = ARstd;
        DataTable{x+1,15} = Car;
        DataTable{x+1,16} = RDavg;
        DataTable{x+1,17} = RDstd;
```


www.manaraa.com

```
        DataTable{x+1,18} = Crd;
        DataTable{x+1,19} = 0;
    End % ends c = 1.

 %Output variables
DataTable;
A;
end %ends ImageAnal
%--------------------------------------------------------------------------

%--------------------------------------------------------------------------
%begin Segmentation

function newImage = Segmentation(I)
%this is a function that will accept a color image as its input
% and perform the object recognition based on Segmentation program
% developed by Peter Rush of the Computer Science Department at MSU

im = I;
x = graythresh(im);
          % Selects threshold value for determining cutoff value for black and white
          % to allow distinguishing particles from background.

im = im2bw(im,x);
          %this just converts im from gray scale to a logical image
          %this just means the values go from 0-255 (gray scale) to
          %either 0 or 1 (logical). 1 = white, 0 = black

im = ~im;
          %this just reverses the image, i.e. 1 becomes 0, 0 becomes 1

for k=1:6
          %Used to place border around images in order to not completely fill
          %flocs that are in contact with edge.
    im(:,k)= 0;
    im(:,641-k)=0;
    im(k,:)=0;
    im(481-k,:)=0;
end %ends for k=1...

SE = strel('disk', 4);
          %defines structuring element strel('<shape>','<size of element>')
          %a disk of size 4 was subjectively determined to provide the 'best' results
          % through trials of numerous structural elements available in the software.
```


www.manaraa.com

```
im= imdilate(im, SE);
        %performs an image dilation with a structuring element SE.

im = imfill(im, 'holes'); %fills in holes in the flocs

im = bwareaopen(im, 200);
        %this removes all elements from the image
        %that are less than 200 pixels in size (size
        %here just means the number of connected pixels)
        %You can increase or decrease the 200, but I
        %find 200 satisfactory.

im = imerode(im, ones(5));
        % performs erosion removing noise  and making the appearance of the edges
        % of the flocs more reflective of the original images.

newImage = im; %end Segmentation
%-----------------------------------------------------------------------%

%-----------------------------------------------------------------------%
%begin Area function

function [Aavg, Astd, CuA] = Area(A, totalflocs)
%Arranges Area data for histogram plot and D60/D10
%calculations to allow for uniformity coefficient.  Input is A matrix from ImageAnal
%which contains the data for all the flocs and totalflocs which is a count variable for all
%the flocs.

%Clear variables
clear Pval SortedA y Aavg Astd Area bin Dsixty Dten CuA

Area = A(:,3);    %Select area column from array A passed from ImageAnal
Aavg = mean(Area); %Calculates average area from slide
Astd = std(Area); % Calculates standard deviation of area from slide
SortedA = sort(Area, 'descend'); %Sorts area data

bin = 0:1000:max(Area);
        %selects bin size for the histogram of the area data, larger or smaller values
        %ultimately affect sensitivity for smaller flocs.  You need to be able to
        %differentiate enough so that
        %the D10 (particles smaller than 10% of the flocs) and D60 (particles smaller
        %than 60% of flocs can be found.

%Output a histogram of data (if preferred).
%figure, hist(Area,bin), title('Area Histogram')
```


www.manaraa.com

```
%Calculate percentage values for number of flocs
%Using Weibull method for probability calculations
for k = 1:totalflocs
   Pval(k,1) = 100-(k/(totalflocs+1)*100);
end %ends for k = 1...

%Place in single two-column table so that interpolation can be performed.
y = horzcat(Pval, SortedA);

%Interpolation for size of floc at 60% and 10%
Dsixty = interp1(y(:,1),y(:,2),60);
Dten = interp1(y(:,1),y(:,2), 10);

%Output of semilog plot (if desired).
%figure, semilogx(SortedA,Pval), title('Semi-log of Area')
%hold on
%plot(Dsixty,60,'o','MarkerSize', 3)
%plot(Dten, 10, 'o', 'MarkerSize', 3)
%hold off
%set(gca,'XDir','reverse')

%Output uniformity coefficient
CuA = Dsixty/Dten;

%end Area function
%-----------------------------------------------------------------------%

%-----------------------------------------------------------------------%
%begin Equivalent Diameter function

function [EqDavg, EqDstd, CuD] = EquivDia(A,totalflocs)
%Arranges Equivalent diameter data for histogram plot and D60/D10
%calculations to allow for uniformity coefficient.  Input is A matrix from ImageAnal
%which contains the data for all the flocs and totalflocs which is a count variable for all
%the flocs.

%Clear variables
clear EqDia EqDavg EqDstd SortedD binD Pval2 yD Dsixty Dten CuD

EqDia = A(:,5); %Equivalent diameter column selected from Array A
EqDavg = mean(EqDia); %Calculates average
EqDstd = std(EqDia);  % Calculates standard deviation
SortedD = sort(EqDia,'descend'); %Data is sorted from largest to smallest
```


www.manaraa.com

```
binD = 0:10:max(EqDia);
        %bins for diameter histogram are set.  In this case
        %10 is currently used, but should be changed to
        %give a good representation of the data.

%Output histogram (if desired).
%figure, hist(EqDia,binD), title('Equivalent Diameter Histogram')

%Calculate percentage values for number of flocs
%Using Weibull method for probability calculations
for k = 1:totalflocs
   Pval2(k,1) = 100-(k/(totalflocs+1)*100);
end %ends for k = 1...

%Place in single two-column table so that interpolation can be performed.
yD = horzcat(Pval2,SortedD);

%Interpolation for size of floc at 60% and 10%
Dsixty = interp1(yD(:,1),yD(:,2),60);
Dten = interp1(yD(:,1),yD(:,2), 10);

%Output semilog plot (if desired).
%figure, semilogx(SortedD,Pval2), title('Semi-log of Eq. Dia.')
%hold on
%plot(Dsixty,60,'o','MarkerSize', 3)
%plot(Dten, 10, 'o', 'MarkerSize', 3)
%hold off
%set(gca,'XDir','reverse')

%Output uniformity coefficient
CuD = Dsixty/Dten;

%end Equivalent Diameter function
%-----------------------------------------------------------------------%

%-----------------------------------------------------------------------%
%begin Form Factor function

function [FF, FFavg, FFstd, Cff] = FormFactor(A, totalflocs);

%Calculates the form factor for each of the individual flocs and then does
%the weibull method and calculates uniformity coefficient Cff.

%NOTE: the area and perimeter are both given in pixels, however in this
%does impart some error on the process, since the pixel value is actually
```


www.manaraa.com

```
%an area term, and perimeter should be a length term. -A pixel is a square
%(or rectangle) with two side lengths.

%Clear variables
clear Area Perimeter FFavg FFstd SortedFF binFF Pval3 yFF Dsixty Dten Cff

Area = A(:,3); %Assign Area array from passed column from array A

Perimeter = A(:,4); %Assign Perimeter array from passed column from Array A

%Calculate form factor for all flocs
for i = 1:totalflocs
   FF(i,1) = 4*pi*Area(i,1)/(Perimeter(i,1))^2;
         %Calculates form factor = 4*pi*area/perimeter^2
end

FFavg = mean(FF); %Calculate average form factor
FFstd = std(FF); %Calculate standard deviation for form factor
SortedFF = sort(FF, 'descend'); %Sort in descending order
binFF = 0:.05:max(FF); %sets up equal bins from 0 to max in 0.05 intervals.


%Output histogram (if desired)
%figure, hist(FF,binFF), title('Form Factor Histogram')

%Calculate percentage values for number of flocs
%Using Weibull method for probability calculations
for k = 1:totalflocs
   Pval3(k,1) = 100-(k/(totalflocs+1)*100);
end %ends for k = 1...

%Place in single two-column table so that interpolation can be performed.
yFF = horzcat(Pval3,SortedFF);

%Interpolation for size of floc at 60% and 10%
Dsixty = interp1(yFF(:,1),yFF(:,2),60);
Dten = interp1(yFF(:,1),yFF(:,2), 10);

%Output semilog plot (if desired)
%figure, semilogx(SortedFF,Pval3), title('Semi-log of FF')
%hold on
%plot(Dsixty,60,'o','MarkerSize', 3)
%plot(Dten, 10, 'o', 'MarkerSize', 3)
%hold off
%set(gca,'XDir','reverse')
```


www.manaraa.com

```
%Output uniformity coefficient
Cff = Dsixty/Dten;

%end Form Factor function
%-------------------------------------------------------------------%

%-------------------------------------------------------------------%
%begin Aspect Ratio function

function [AR, ARavg, ARstd, Car] = AspectRatio(A, totalflocs);

%Calculates the aspect ratio of the given floc.  Input variables are A =
%floc properties matrix and totalflocs = total number of flocs from
%ImageAnal function

%NOTE: The aspect ratio uses the length and width which are taken as the
%major axis length and minor axis length, repectively. These values are used
%as a pixel count and not in actual length dimensions, which potentially
%imparts error, since the pixels are two-dimensional objects.

%Clear variables
clear Length Widte ARavg ARstd SortedAR binAR Pval4 yAR Dsixty Dten Car
Length = A(:,6); %Set length equal to major axis length
Width = A(:,7); %Set width equal to minor axis length

for i = 1:totalflocs
   AR(i,1) = 1.0 + (4/pi)*((Length(i,1)/Width(i,1))-1.0);
   %Calculates Aspect ratio of the individual flocs
end

ARavg = mean(AR); %Calculates average
ARstd = std(AR); %Calculates standard deviation
SortedAR = sort(AR, 'descend'); %Sort data in descending order

binAR = 0:.05:max(AR); %sets up equal bins from 0 to max in 0.05 intervals.

%Output histogram (if desired)
%figure, hist(AR,binAR), title('Aspect Ratio Histogram')

%Calculate percentage values for number of flocs
%Using Weibull method for probability calculations
for k = 1:totalflocs
   Pval4(k,1) = 100-(k/(totalflocs+1)*100);
end %ends for k = 1...
```


www.manaraa.com

```
%Place in single two-column table so that interpolation can be performed.
yAR = horzcat(Pval4,SortedAR);

%Interpolation for size of floc at 60% and 10%
Dsixty = interp1(yAR(:,1),yAR(:,2),60);
Dten = interp1(yAR(:,1),yAR(:,2), 10);

%Output semilog plot (if desired)
%figure, semilogx(SortedAR,Pval4), title('Semi-log of AR')
%hold on
%plot(Dsixty,60,'o','MarkerSize', 3)
%plot(Dten, 10, 'o', 'MarkerSize', 3)
%hold off
%set(gca,'XDir','reverse')
%Output uniformity coefficient
Car = Dsixty/Dten;

%end Aspect Ration function
%-------------------------------------------------------------------%

%-------------------------------------------------------------------%
%begin Roundness function
function [RD, RDavg, RDstd, Crd] = Roundness(A, totalflocs);

%Calculates the roundness of the given floc.  Input variables are A =
%floc properties matrix and totalflocs = total number of flocs from
%makeloop function.  The roundness varies between 0 and 1 and gives an
%indication of the elongation of an object.  Circle = 1.  Infinitely long
%rectangle approaches 0.

%NOTE: The roundness uses the length which is taken as the
%major axis length.  These values are given in terms
%of pixel count and not as length dimensions.

%Clear variables
clear Length Area RDavg RDstd SortedRD Pval5 yRD Dsixty Dten Crd

Length = A(:,6); %Set length equal to major axis length
Area = A(:,3); %Select Area from array A

for i = 1:totalflocs
   RD(i,1) = (4*Area(i,1))/(pi*(Length(i,1))^2);
   %Calculates Roundness of the individual flocs
end
```


www.manaraa.com

```
RDavg = mean(RD); %Calculate average
RDstd = std(RD); %Calculate standard deviation
SortedRD = sort(RD, 'descend'); %Sort in descending order

%binRD = 0:.05:max(RD); %sets up equal bins from 0 to max in 0.05 intervals.

%Output histogram (if desired)
%figure, hist(RD,binRD), title('Roundness Histogram')

%Calculate percentage values for number of flocs
%Using Weibull method for probability calculations
for k = 1:totalflocs
   Pval5(k,1) = 100-(k/(totalflocs+1)*100);
end %ends for k = 1...
%Place in single two-column table so that interpolation can be performed.
yRD = horzcat(Pval5,SortedRD);

%Interpolation for size of floc at 60% and 10%
Dsixty = interp1(yRD(:,1),yRD(:,2),60);
Dten = interp1(yRD(:,1),yRD(:,2), 10);


%Output semilog plot (if desired)
%figure, semilogx(SortedRD,Pval5), title('Semi-log of RD')
%hold on
%plot(Dsixty,60,'o','MarkerSize', 3)
%plot(Dten, 10, 'o', 'MarkerSize', 3)
%hold off
%set(gca,'XDir','reverse')

%Output uniformity coefficient
Crd = Dsixty/Dten;

%end Roundness function
%-----------------------------------------------------------------------%
```


www.manaraa.com